2017-01-01

Gypsum, Calcite, And Dolomite Caprock Fabrics And Geochemistry From The Gypsum Valley Salt Diapir, Paradox Basin, Southwestern Colorado

Kevin Lerer
University of Texas at El Paso, kevinlerer1886@gmail.com

GYPSUM, CALCITE, AND DOLOMITE CAPROCK FABRICS AND GEOCHEMISTRY FROM THE GYPSUM VALLEY SALT DIAPIR, PARADOX BASIN, SOUTHWESTERN COLORADO

KEVIN LERER

Master's Program in Geology

APPROVED:

Benjamin Brunner, Ph.D., Chair

Katherine Giles, Ph.D.

Jennie McLaren, Ph.D.

Charles Ambler, Ph.D.
Dean of the Graduate School

DEDICATION

To Julia Mae Lerer, my daughter, who has been a constant source of inspiration to me.

Her endless enthusiasm motivated me to pursue my passion for geology.

GYPSUM, CALCITE, AND DOLOMITE CAPROCK FABRICS AND GEOCHEMISTRY FROM THE GYPSUM VALLEY SALT DIAPIR, PARADOX BASIN, SOUTHWESTERN COLORADO

by

KEVIN LERER, B.A.

THESIS

Presented to the Faculty of the Graduate School of
The University of Texas at El Paso
in Partial Fulfillment
of the Requirements
for the Degree of

MASTER OF SCIENCE

Department of Geological Sciences
THE UNIVERSITY OF TEXAS AT EL PASO
December 2017

ACKNOWLEDGEMENTS

First, I would like to thank my parents, Sheila and Richard Lerer and my brother, Joshua Lerer for their encouragement and moral support during my time at the University of Texas at El Paso. Second, I would like to thank my daughter, Julia Mae Lerer, who I found to be a constant source of motivation. She provided me with the perseverance necessary to successfully earn a MSc degree.

The completion of this thesis would not have been possible without the guidance, instruction and support of my graduate advisor, Dr. Benjamin Brunner. Ben encouraged me to exceed my own expectations in the field of geology. Whether involved with field work, lab work, class work or behind a computer screen, Ben has always been willing and able to help me in the pursuit of excellence. I extend a special thank you to Ben for his unmatched patience and understanding in dealing with my occasional hard-headed nature.

Dr. Kate Giles, also played an integral role in the completion of this thesis. Kate's instruction and willingness to indulge my many questions was much appreciated. I also want to thank Kate for the financial support provided to me by the Institute of Tectonic Studies.

I would also like to thank the many exceptional instructors, I was lucky enough to study under at the University of Texas at El Paso. They provided me with the knowledge and understanding necessary to successfully navigate the pursuit of my MSc degree. Most notably, I would like to thank Dr. Gail Arnold, Dr. Richard Langford, Dr. Nicholas Pingitore, Dr. Terry Pavlis, Dr. Jason Rickets, Dr. Jennie McLaren and Dr. Jasper Konter.

ABSTRACT

Caprocks are found on top of or in a lateral position relative to salt diapirs. The caprocks predominantly comprise sulfate minerals such as anhydrite or gypsum, which presumably accreted during the dissolution of salt from evaporite sediments. In some cases, the sulfate minerals are replaced by carbonate minerals, referred to as 'carbonate caprock'. Carbonate caprocks associated with salt diapirs are important because they can act as reservoirs or conduits for hydrocarbons, and because they can be easily misidentified as carbonate lithologies belonging to the stratigraphy of the sedimentary sequences adjacent to the diapir, which can jeopardize the accurate interpretation of seismic profiles. Today's understanding of caprocks is based on observations from salt diapirs found along the US Gulf Coast salt diapir province, home to the famous Spindletop oil field; whereas carbonate caprocks from another salt diapir province in the United States, the Paradox Basin, have been hardly recognized, and in many cases misinterpreted as part of the 'normal stratigraphy'.

At one of the salt walls exposed in Gypsum Valley, Paradox Basin in Southwestern Colorado, abundant and well-exposed carbonate caprock was found in an area referred to as Mary Jane Draw. The carbonate and adjacent gypsum caprock display an amazing richness in lithologies, including micritic calcitic and dolomitic caprocks that are silicified to various degrees, and display an astonishing diversity in caprock fabrics, including massive, brecciated, zebraic, and finely laminated benches. In order to enable caprock identification, and to facilitate communication between caprock researchers, this richness in fabrics calls for a comprehensive caprock classification scheme, and first steps towards such unified nomenclature are reported in this study.

Light carbon isotope signatures of dolomitic and calcitic caprock indicate that hydrocarbon oxidation likely contributed to the formation of either carbonate caprock lithology; whereas the oxygen isotope signature did not provide conclusive evidence for calcite or dolomite as primary or secondary mineral phase. However, the relatively higher abundance of micritic dolomite compared to calcite indicates that dolomite, or a dolomite-precursor, must have been an early mineral phase. The oxidation of the hydrocarbons was likely tied to microbial sulfate reduction. However, all of the classical signatures for this process, such as pyrite, native sulfur or heavy sulfur and oxygen isotope signatures of sulfate associated with carbonate caprock are absent. The only geochemical fingerprint for microbial sulfate reduction is a high content of isotopically light sulfur in organic matter extracted from the carbonate caprock.

These observations can be explained by a carbonate caprock formation at the Gypsum Valley salt diapir as the result of a multi-stage process involving oxidation of hydrocarbons coupled to microbial sulfate reduction in a system that was open to fluid flow. The fluid flow provided magnesium and silica, enabling the precipitation of primary dolomite and silicification, while removing sulfide and sulfate. Waxing and waning supply with fluids may also have triggered phase transitions between anhydrite and gypsum, causing rock deformation, which explains the amazing richness and diversity in caprock fabrics found in Gypsum Valley. As such, the carbonate caprock at Gypsum Valley constitutes the 'open-system' end member of geochemical settings that are conducive to carbonate caprock formation.

TABLE OF CONTENTS

LIST OF TABLES

LIST OF FIGURES

1. INTRODUCTION

1.1 OVERVIEW

This study investigated the role of microbes in the formation of carbonate rocks found in close association with many salt diapirs, being part of a lithological succession referred to as 'caprock'. This unit is often composed of a basal member dominated by sulfate minerals such as anhydrite ($CaSO_4$) and gypsum ($CaSO_4 \cdot 2H_2O$), which is, in some cases, overlain by carbonate rocks – herein referred to as 'carbonate caprock'. Carbonate caprocks can be composed of limestones, containing predominantly the carbonate minerals calcite (trigonal $CaCO_3$) and, to a lesser degree, aragonite (orthorhombic $CaCO_3$), or dolomite rocks (sometimes referred to as dolostones), containing predominately the carbonate mineral dolomite ($CaMg(CO_3)_2$).

1.1.1 Significance

Carbonate caprocks have long been recognized as important targets for oil and gas exploration due to their propensity to act as reservoirs or conduits for hydrocarbons. Famously, the nine days of uncontrolled out-gushing of oil and gas – the Lucas Gusher – at the Spindletop salt dome oil field started when a well hit a carbonate caprock oil reservoir on January 10, 1901, and triggered the Texas oil boom (Figure 1). The Spindletop carbonate caprock consists of porous dolomite and of limestone associated with native sulfur (Figure 2). Today, carbonate caprocks are of minor importance as oil and gas reservoirs, but the identification of carbonate caprocks and the correct interpretation of their genesis remains critical for petroleum exploration in settings where salt, by its sheer presence (as a seal, for example in Pre-salt deposits) or by its movement relative to adjacent strata (salt tectonics), is a central element in the formation of potential hydrocarbon traps.

Correct identification of carbonate caprock is critical for the correlation of stratigraphic units, and the prediction of their presence, or absence, in the subsurface. If an isolated carbonate caprock unit within a salt dome setting is misconstrued as a continuous marine carbonate unit, the projection of the non-existing marine formation into the subsurface can severely skew the interpretation of the interface between salt structures and their neighboring lithologies. The carbonate caprock studied in this project is a prime example for this situation, it was previously mapped as marine limestone of the Pennsylvanian Honaker Trail Formation, but is now reinterpreted as lateral carbonate caprock that formed during passive rise of the salt wall within a limited time interval, a 'caprock event' in the Triassic-age (Giles et al., 2012; this study, Poe et al., 2018a).

Correct interpretation of the genesis of carbonate caprock is critical for the understanding of the temperature and fluid history of a salt dome, and adjacent strata. Carbonate caprock can be considered the culmination and recorder of a series of events, encompassing the formation of gas and oil, the timing of their migration, the dissolution of salt and the replacement of sulfate minerals by carbonates – a process either mediated by thermochemical sulfate reduction (TSR) or sulfate-reducing microbes, (Machel, 2001; Barré et al., 2017; Ghazban and Al-Aasm, 2010; Jiang et al., 2017). The ability to decipher this geochemical archive of the temperature and fluid history of salt structures can provide key insights into the hydrocarbon maturation and migration history of target areas for oil and gas exploration.

1.1.2 Carbonate Caprock Settings and Genesis – the Classic Perspective

A little history – The discovery of oil and gas in the crestal position of at a large number of salt diapirs in the U.S. Gulf Coast region in the early 1900s was followed by the discovery of

hydrocarbons in the flanking position of diapirs, and then at deeper depths, and the expansion into offshore and deep-water settings, such as the Gulf of Mexico, kept and keeps the petroleum industry's interest in salt domes alive. Additionally, geologic interest in salt domes was fueled because they can contain other valuable commodities, such as salt, sulfur, ore minerals and carbonate – all of which have been exploited by various approaches, such as by mining (salt, ore minerals) and quarries (carbonate), or in the case of sulfur, by extraction from the subsurface with the help of hot water (Frasch-process). Moreover, beginning in the 1950s, salt became a target as potential site for the long-term storage of nuclear waste (for a review, see Posey and Kyle, 1988a). The conducted studies resulted in the accumulation of considerable information and insight into the formation of salt domes, and specifically into the formation of caprock, and latest, by 1988, a fairly consistent view on the processes was established. In that year, a special issue on the geochemistry of salt domes was published in the journal Chemical Geology (Fluid-Rock Interactions in the Salt Dome Environment, Volume 74, Issues 1–2, Pages 1-188), based on papers that were presented at the 1987 mid-year meeting of the Society of Economic Paleontologists and Mineralogists (SEPM) in Austin, Texas. In that volume, the guest-editors Harry H. Posey and J. Richard Kyle stated that "Although the contributions in this issue are limited to the U.S. Gulf Coast, the processes discussed should be generally appropriate for fluid-rock interactions in other salt dome terranes and for sedimentary basins dominated by saline formation waters" (Posey and Kyle, 1988a). It could be argued that this assessment was prophetic, as the work presented in that special issue heavily influenced the general view and understanding of the geochemical evolution of salt domes until today.

The classic view – the classical illustration of a salt dome depicts a mushroom/ice cream cone shaped structure that consists of a salt stock overlain by a caprock, which can be subdivided into

an anhydrite cap that sits on top of the salt, followed by gypsum, which is succeeded by carbonates as outermost caprock unit. The carbonate caprock is in contact with the surrounding sedimentary strata, which typically show signs of deformation related to salt diapirism, i.e. the sedimentary strata dip away from the diapir (Figure 3). In the case of the Gulf Coast salt domes, the carbonate caprock can be further subdivided into a lower banded limestone and an upper variegated limestone caprock (Posey and Kyle, 1988a).

Caprock formation on salt diapirs is considered a multi-staged process. In the first stage, as the diapir ascends relative to the adjacent sediments; cross-flowing water that is undersaturated with respect to sodium chloride (NaCl) dissolves halite, while less soluble components of the diapir accrete to the base of the overlying lithology (typically also caprock), a process known as underplating. The lesser components of the diapir include evaporite minerals such as anhydrite (quantitatively most important) and gypsum, but also other lithologies such as carbonates and shales that were part of the layered evaporite sequence that was deposited with the salt in an evaporite basin. It is presumed that the underplating mechanism causes the layering of the anhydrite (Posey and Kyle, 1988b).

The halite dissolution, which condenses the remaining anhydrite can be described by the reaction:

$$CaSO_4(s) + NaCl(s) + 2H_2O(l) \Rightarrow CaSO_4(s) + Na^+(aq) + Cl^-(aq) + 2H_2O(l). \quad \text{Eq. 1}$$

There are two important points to note: First, it is to be expected that not only halite is dissolved, but likely also considerable quantities of calcium sulfate, whereby the ion strength of the saline solution plays a key role (Werner et al., 1988). Secondly, it is important to note that in a caprock environment the presence of water and anhydrite does not automatically result in the conversion to gypsum, according to the reaction:

$CaSO_4(s) + 2H_2O(l) => CaSO_4 \cdot 2H_2O(s)$, Eq. 2

because salinity and temperature can be such that anhydrite persists (Werner et al., 1988). For example, at a temperature of 60°C, relative to gypsum, anhydrite is the stable phase for any sodium chloride concentration; whereas, at a temperature of 40°C, anhydrite is the more stable calcium sulfate mineral phase at concentrations higher than approximately 3mol NaCl/kg H_2O; and, gypsum is the stable phase at concentrations below 3mol NaCl/kg H_2O (Werner et al., 1988). At shallow depth – coinciding with lower temperatures and potentially fresher water – anhydrite is replaced with gypsum.

The second stage of caprock formation, the replacement of sulfate minerals with carbonates, does not take place in all caprocks. Prerequisite for this step is the migration of oil and/or gas into the vicinity of the anhydrite or gypsum caprock. Sulfate-reducing bacteria (SRB) then convert sulfate into sulfide (Feely and Kulp, 1957), thereby using sulfate as an electron acceptor for the oxidation of the reduced carbon from oil or gas to carbonate. It is not specified if the SRB directly oxidize hydrocarbons, or rely on microbial partners. Considering that SRB can operate at temperatures exceeding 100°C (Jørgensen et al., 1992), it is possible that SRB can obtain sulfate directly from anhydrite dissolution, without the need for gypsum; however, not only high temperatures, but also high salinities impose limits to the extent to which anhydrite can serve as a substrate for sulfate reduction. Overall, the oxidation of oil and/or gas in conjunction with sulfate reduction results in the replacement of sulfate minerals with carbonates, according to the reaction:

$CaSO_4 \cdot 2H_2O(s) + C_2H_3O_2^- => H_2S + CaCO_3(s) + HCO_3^- + H_2O$, Eq. 3

and

$CaSO_4 \cdot 2H_2O(s) + CH_4 \Rightarrow H_2S + CaCO_3(s) + 3H_2O,$ Eq. 4

with $C_2H_3O_2^-$ representing a simple carbohydrate, and CH_4 representing methane. The replacement of sulfate minerals by carbonate minerals can be a molecule-by-molecule process, which results in the preservation of anhydrite ghosts and anhydrite layering in the formed carbonate rocks (Posey and Kyle, 1988b; Werner et al., 1988).

The richness in carbonate fabrics (i.e. banded vs. variegated) is considered the result of the progressive top to down replacement of sulfate minerals with carbonates: in an initial stage after hydrocarbons entered the contact between gypsum/anhydrite caprock and adjacent sediment, the early-formed calcite incorporates detritus from nearby sediments. With continued dissolution of gypsum/anhydrite, the calcite-anhydrite interface moves downward, away from the overlying detritus, which means that later-formed carbonate should contain less detritus. Because the replacement of anhydrite or gypsum with calcite results in a decreased volume, it is assumed that there are voids within the formed carbonate. These voids can collapse, and result in brecciation or are infilled by later carbonate phases (Posey and Kyle, 1988b; Prikryl et al., 1988).

For the produced sulfide, there are several possible fates. If suitable metals are available, sulfide minerals can form (Kyle and Agee, 1988), sulfide can be transported away from the location where carbonate caprock forms, and sulfur can be oxidized into native sulfur or sulfate. Many of the Gulf Coast salt domes harbored economical quantities of of native sulfur. Feely and Kulp (1957), who made a convincing argument for the involvement of SRB in the formation of these deposits, proposed that native sulfur was derived from the oxidation of sulfide with sulfate, according to the reaction:

$3H_2S + SO_4^{2-} \Rightarrow 4S^0 + 2H_2O + 2OH^-.$ Eq. 5

This reaction is interesting because it creates a basic environment, which promotes precipitation of carbonate minerals. However, it was shown that this reaction is unlikely to occur at low temperatures, and as an alternative to sulfate as an oxidant for sulfide, molecular oxygen (O_2) was proposed, in conjunction with the conclusion that native sulfur deposits cannot form too far away from the surface (Davis et al., 1970). This explanation is generally accepted (e.g. Machel, 1992), although concerns exist with regards to the large quantities of O_2 that must be supplied to produce large sulfur deposits in the subsurface (Kirkland, 2014).

1.1.3 Carbonate Caprock Settings and Genesis – Emerging New Views

The insights that were reported in the Special Issue of Chemical Geology (Fluid-Rock Interactions in the Salt Dome Environment, Volume 74, Issues 1–2, Pages 1-188) remain valid until today. However, it becomes apparent that the focus on the classic examples of salt domes from the U.S. Gulf Coast may have limited or skewed the view on other settings. A large portion of the data currently available regarding genetic models for diapiric caprock are based on near-surface caprock outcrops and/or drill-hole data found on the peaks of vertical diapirs (Giles, 2012), which may have limited the recognition of caprock that is located in a lateral position relative to the diapir instead of the expected top-salt position. In addition, the interpretation of lateral caprock based on the lessons learned from top-salt position caprock may be inadequate. While the depiction of the salt diapir as the classic mushroom/ice cream cone shaped structure is highly instructive, it gives the impression of a static process, where caprock is formed by an unremitting accretionary process of dissolution by cross-flow of under-saturated waters, with concomitant accretion and sulfate reducing bacteria mediated anhydrite alteration. From this it follows that caprock, once formed, keeps floating on top of the diapir, while continuously gaining in thickness. This concept may be applicable to the U.S. Gulf Coast salt diapirs, where it was shown that the anhydrite caprock at

Winnfield Dome in north Louisiana formed shortly after deposition of the mother salt during the Late Jurassic and Early Cretaceous and is now juxtaposed against Eocene sedimentary rocks that are approximately 100 Myr. younger (Gose et al., 1985; Kyle et al., 1987; Posey and Kyle, 1988b), but may not be valid in other settings.

Field work in a different salt dome province, the Paradox Basin has revealed that carbonate caprock is often found in a lateral position with respect to the salt wall, for example in the Gypsum Valley, CO (Giles et al., 2012, Poe et al., 2018a) and Castle Valley, Utah (Shock, 2012). The encountered lithologies comprise a multitude of fabrics, and dolomite is abundant. Remarkably, dolomite is rarely reported from U.S. Gulf Coast diapirs – despite its role as 'oil rock' at Spindletop (Figure 2). The lateral carbonate caprocks in the Paradox Basin appear to be associated with fluvial lithologies (e.g. the Permian Cutler Formation and Triassic Chinle Fromation). Caprock formation can take place during discrete time slices in which the environmental conditions favored caprock formation, a so-called 'caprock event'. Unlike the scenario proposed for the U.S. Gulf Coast salt diapirs, where once formed, these caprocks remain on top of the diapir, and rise with the passively rising diapir. Instead, together with the adjacent lithologies, they are halokinetically drape-folded off the roof of the diapir into the lateral position in which they are found today (Giles et al., 2012). This implies that in addition to the caprock-type known from the Gulf Coast diapirs, there may be other caprocks that have a distinctly different genetic history. At least at first sight, the U.S. Gulf Coast caprocks are markedly different from the lithologies encountered in Gypsum Valley. Typically, the U.S. Gulf Coast caprock is thick and can be readily divided into a variegated upper section and a banded lower section. The caprock found in association with the diapir in Gypsum Valley is much thinner and composed of many benches that display a variety of different fabrics, colors and textures, that cannot be easily assigned to an upper and lower section.

Finally, microbial sulfate reduction by SRB has become the generally accepted model for carbonate caprock formation. However, it has never been shown that TSR cannot be a viable alternative, and recent literature points to TSR as a potential player in the genesis of carbonate caprocks, but also as a process that may induce additional porosity in carbonates that contain sulfate minerals (Barré et al., 2017; Ghazban and Al-Aasm, 2010; Jiang et al., 2017).

1.2 UNRESOLVED QUESTIONS IN REGARD TO CARBONATE CAPROCK FORMATION

Whereas there is a general consensus that the oxidation process that transforms hydrocarbons to carbonate and concomitant reduction of sulfate from gypsum and anhydrite to sulfide is the trigger for the replacement of gypsum and anhydrite with carbonate caprock, several key aspects of these processes remain unresolved. Particularly, the critical role of sulfate reducing microbes in carbonate caprock formation has not been fully elucidated and the conditions that control the *in situ* formation of different authigenic minerals, such as calcite vs. dolomite or pyrite vs. zero-valent sulfur remain unconstrained. In the following, major unresolved key aspects of carbonate caprock formation are described in more detail.

1.2.1 Role of Sulfate Reducing Microbes in the Formation of Carbonate Caprock and Associated Sulfur-Bearing Minerals

The process of sulfate reduction has long been recognized as an essential process in the formation of carbonate caprock, as shown by Feely and Kulp, 1957. The ubiquity and antiquity of microbial sulfate reducing bacteria in the environment in general (Shen and Buick, 2004) and particularly in hydrocarbon bearing systems, where they can cause massive problems such as oil souring (e.g. Hubert et al., 2009, Gieg et al., 2011) makes it evident that this process must be considered the 'prime suspect' when it comes to the formation of carbonate caprock in a system that provides

both sulfate from gypsum and hydrocarbons. Moreover, within the past 20 years, the hypothesis that microbes, in particular sulfate reducing microbes, directly catalyze carbonate precipitation has become generally accepted (Warthmann et al., 2000; Deng et al., 2010; Sánchez-Román et al., 2009) and it has been shown that sulfate reducing bacteria are involved in carbonate precipitation in systems where other oxidants for reduced carbon, such as oxygen, would be expected to be available (e.g. Heindel et al. 2012; Gischler et al. 2017). This means that any alternative to the dogma that sulfate reducing microbes are involved in the formation of carbonate caprock must not only make a convincing argument regarding the validity of an alternative process, but must also explain why sulfate reducing microbes were not involved. In the framework of this thesis, this guideline is of high importance, because, as will be shown, typical inducators for microbial sulfate reduction, such as pyrite and elemental sulfur are absent in the study area.

While the hypothesis that microbes directly catalyze carbonate precipitation has become generally accepted and salt diapirs that contain sulfate-bearing minerals and that are affected by the migration of hydrocarbons, appear to be a perfect habitat for sulfate reducing microbes that catalyze the genesis of caprock carbonates, it must be acknowledged that at higher temperatures, the same setting also permits thermogenic sulfate reduction, which could also trigger the precipitation of carbonate caprock. Moreover, the origin of the sulfate reducing microbes is not known, microbes that may have been transported with hydrocarbons, may have persisted as a part of the deep biosphere of the salt dome, or may have been transported into the system by meteoric waters from environments close to the Earth's surface. Classically, it is assumed that sulfate reducing microbes produce sulfide (H_2S and HS^-), which can be sequestered as sulfide minerals, organic sulfur, pyrite (FeS_2), or zero valent sulfur (S^0). Such a scenario, where pyrite and zero valent sulfur is formed, would necessitate that the produced sulfide be partially oxidized, requiring

an external oxidant, such as ferric iron (Fe^{3+}) or molecular oxygen (O_2). Alternatively, there is the possibility that some sulfate reducing organisms may form zero valent sulfur instead of sulfide – as appears to be the case for sulfate reduction coupled to the anaerobic oxidation of methane (Milucka et al., 2012) – which would obviate the need for an external oxidant. Finally, it is possible that the sulfate reducing microbes not only catalyze the precipitation of carbonates, but also catalyze the diagenesis (chemical transformation) of carbonates, i.e. their recrystallization and the transition from one mineral to another, such as calcite to dolomite. Thus, the chemical composition (i.e. calcite vs. dolomite) and hydraulic conductivity (e.g. porosity and permeability) of formed carbonate depends on a multitude of interconnected processes (Feely and Kulp, 1957; Dessau et al., 1962; Davis and Kirkland, 1979; Peckmann et al., 1999; Ziegenbalg et al., 2010). Still,

1.2.2 Microcrystalline (Primary?) vs. Secondary Dolomite as Major Constituent of Carbonate Caprock

Dolomitic carbonate caprock, although frequently found in Gypsum Valley, is not found in any notable abundance along the U.S. Gulf Coast salt diapir province. Canonically, dolomite caprocks are presumed to be of secondary origin. The implication is that under favorable thermodynamic and kinetic conditions primary calcium carbonates, i.e. calcite, is replaced by dolomite. The common belief that dolomitization creates 12% porosity is based upon a mole-for-mole equation; however, dolomite rocks inherit porosity and fabric from the precursor limestone and porosity is occluded by overdolomitization. Limestones lose porosity through compaction and cementation; whereas, dolomite rocks resist compaction and retain much of their porosity (Lucia, 2004), which renders the formed dolomite rocks prime hydrocarbon reservoirs. If dolomite caprocks are of primary origin, no replacement of calcium carbonate by dolomite is involved; and there would not be an increase in porosity associated with dolomite rock formation. Petrographic observations

from dolomite caprocks found in the Paradox Basin, in Southwestern Colorado and from many other locations indicate that dolomite caprocks are largely microcrystalline and quite possibly primary in origin (K. Giles, personal communication, 2014). The Giles' hypothesis that dolomitic caprocks may be of primary origin thus challenges the generally accepted view that these rocks must have a high porosity due to their inferred secondary nature. The hypothesis that dolomite caprock can be of primary origin is corroborated by studies on modern primary dolomite formation, where primary dolomite is often found in saline environments, and in settings where microbial sulfate reduction combined to the oxidation of hydrocarbons (i.e. methane) and organic matter plays a dominant role (Russell et al. 1967; Burns et al., 2000; Bontognali et al., 2010; Lindtke et al., 2011; Meister et al., 2011). Furthermore, laboratory experiments with sulfate reducing microbes unambiguously demonstrate that microbial sulfate reduction can induce dolomite formation (Warthmann et al., 2000; Deng et al., 2010; Sánchez-Román et al., 2009). The settings identified as conducive for primary dolomite formation are remarkably similar to the conditions expected for the formation of carbonate caprocks.

1.2.3 Open vs. Closed System: Salt Dome Kinematics and Timing of Hydrocarbon Migration – Impact on Formation and Diagenesis of Carbonate Caprock

Salt dome kinematics, hydrocarbon migration, and the formation and diagenesis of carbonate caprock are thought to be linked, which implies that there must be an order regarding the timing of the processes. This potentially results in a chicken-or-egg problem: to act as a trap for hydrocarbons, carbonate caprock must have been formed and potentially undergone diagenesis. However, the latter two processes may require the migration of hydrocarbons. A scenario where an initial hydrocarbon migration catalyzed carbonate caprock formation and a later hydrocarbon migration phase transported oil into the trap may present a solution for this problem. This example

highlights that fluid flow and caprock formation in diapirs may be rather episodic rather than continuous, with time periods of restricted and times of accelerated fluid flow. Thus, a key parameter affecting the formation and diagenesis of carbonate caprock and associated authigenic minerals is the openness or closed-ness of the system in which this process takes place.

For example:

- A fully closed system limits migration of hydrocarbons, inhibiting the production of carbonates.
- A system that is closed with respect to migration of aerated groundwater would limit supply with molecular oxygen, creating conditions where formed sulfide cannot be oxidized, impeding the sequestration of sulfide into pyrite or zero valent sulfur.
- Conversely, a system that is open to migration of aerated groundwater would cause oxidation of pyrite and zero valent sulfur, creating acidity that may induce carbonate dissolution and recrystallization.
- Moreover, a fully open system that allows for aerated groundwater to intersect with hydrocarbons would favor the aerobic oxidation of hydrocarbons over hydrocarbon oxidation coupled to sulfate reduction, likely inducing carbonate dissolution rather than carbonate formation.
- In the case of either primary or secondary dolomite formation, magnesium (Mg^{2+}) must be available, which requires fluid flow form potential magnesium sources, such as:
    1) Brine from salt dissolution
    2) Intrasalt clasts of black shale and igneous rock
    3) Hydrocarbons

4) Alteration of overlying siliciclastic sediments to the site where carbonate caprock is formed or diagenetically overprinted (i.e. dolomitized).

The diagenesis and formation of carbonates and silicates is intimately linked (e.g. Hobert and Wetzel 1989; Ireland et al., 2010; Mackenzie and Garrels, 1966; Wallmann et al., 2008). Silicate diagenesis can lead to the removal or release of large quantities of magnesium, which has a direct impact on dolomite formation or dissolution (also referred to as dedolomitzation). In all of these cases, primary or secondary dolomite formation necessitates a certain openness of the system; however, in the case of secondary dolomite formation, this openness could occur in a phase of salt dome evolution that postdates the formation of the original carbonate caprock.

1.3 QUESTIONS ADDRESSED IN THIS STUDY

Many of the questions in regard to carbonate caprock formation are closely linked. Timing of salt movements, thermal history, fluid migration, lithological composition of the salt and the overlying strata, presence and activity of hydrocarbon-oxidizing microbes that reduce sulfate are all prerequisites for the formation of carbonate caprock. In turn, the existence, composition and rheology of carbonate caprock may strongly affect parameters such as fluid flow and hydrocarbon migration, providing a feedback on fluid flow in salt diapirs. Understanding these interlinked mechanisms would provide researchers with the ability to more accurately determine the potential for carbonate caprocks to act as hydrocarbon reservoirs or conduits.

In this study, the following questions were addressed:

- Is there a need for a new caprock classification scheme?
- Is there a general carbonate caprock stratigraphy?

- Is there a general thickness of carbonate caprock at the investigated site?
- What was the role of sulfate reducing microbes in the formation of carbonate caprock at the study site, located in the Paradox Basin, Southwestern Colorado?
- Was the occurrence of dolomite linked to the silicification of caprocks?
- Is the dolomite that has been observed at the study site of primary or secondary origin?
- Was the caprock at the study site formed in an open or closed system?

1.4 TASKS AND APPROACHES

- **Is there a need for a new rock classification scheme for caprocks?**

Motivation: It is important to recognize (carbonate) caprocks and not misidentify such caprocks as 'normal' stratigraphy, as has occurred in Gypsum Valley (Honaker Trail FM). Equally important is to be able to communicate findings between various caprock settings. Approaches to tackle these questions included field and microscopic observations.

- **Is there a general carbonate caprock stratigraphy?**

Motivation: There appears to be a general setting for Gulf Coast Carbonate Caprocks with a layered/laminated base, and a variegated top section. Can the same pattern be identified in Gypsum Valley, and could such a stratigraphy provide clues to the process of carbonate caprock formation? The approach to address this question was detailed field observations, measured sections, combined with thin section analyses.

- **Is there a general thickness of carbonate caprock at investigated site?**

Motivation: Over short-scale distances, are differences in thickness observed, and can those differences be attributed to the genesis of caprock, thinning during rotation into lateral position, or other mechanics? The answers to these questions will provide important

information regarding geologic settings in salt shoulders, which may represent significant sites for hydrocarbon accumulation. The chosen approach to address this question was the determination of the carbonate caprock thickness based on the intersect between contour lines and the contacts between carbonate caprock and gypsum, and carbonate caprock and the sandstones from the overlying Chinle Formation, respectively.

- **What was the role of sulfate reducing microbes in the formation of carbonate caprock at the study site, located in the Paradox Basin, Southwestern Colorado?**

Motivation: While a sulfate reduction model provides an explanation, it does not provide definitive proof. This is particularly problematic for the caprock systems in Paradox Basin where there is little evidence in form of minerals (pyrite, or native sulfur). The approaches taken were geochemical analyses, in particular the extraction and isotopic analysis of carbonate associated sulfate (CAS) from limestone and dolomite, as well as the extraction of sulfur from refractory organic matter from these carbonate lithologies for the determination of S/C ratios and sulfur isotope compositions.

- **Was the occurrence of dolomite linked to the silicification of carbonate caprocks?**

Motivation: With regards to the question regarding if dolomite is primary or secondary, it is important to know if there is a link between silicification and the appearance of dolomite. The approach to address this question was thin section analyses, combined with field observations.

- **Is the dolomite that has been observed at the study site of primary or secondary origin?**

Motivation: A key question with regards to the 'Dolomite Problem' is if dolomite, or a dolomite-precursor can form as a primary carbonate phase, or if all dolomite is the results of

the conversion of primary calcite/aragonite into a secondary dolomite. The approaches to address these questions included thin section analyses, $\delta^{13}C$ analyses of dolomite and limestone to compare the relative contribution of organic carbon to the formed carbonate mineral, and $\delta^{18}O$ isotopes of dolomite and limestone to assess oxygen isotope composition of water during mineral formation, which provides insight into influence of meteoric diagenesis.

- **Was the caprock at the study site formed in a closed or open system?**

Motivation: Open or closed systems determine the caprock's potential to act as a trap or conduit for hydrocarbons, and provide a model on how the carbonate caprocks formed. To answer this question, several approaches are combined and analyzed. The carbon isotope mass balance, assessed the mixing of organic with inorganic carbon based on isotope mass balance for carbon from residual organic matter (trapped dead oil) and an estimate for the marine carbon end-member provided information on the openness or closedness of the system with respect to carbonate, whereas the openness/closedness with respect to sulfur was calculated based on the comparison between isotope composition of sulfur bound to organic matter, sulfate from gypsum, and sulfate from CAS.

Information	Abbreviations
Carbon and oxygen isotope composition of carbonates	$\delta^{13}C_{carbonate}$, $\delta^{18}O_{carbonate}$
Gypsum content and isotope composition	ESS, $\delta^{18}O_{ESS}$, $\delta^{34}S_{ESS}$
CAS content and isotope composition	CAS, $\delta^{18}O_{CAS}$, $\delta^{34}S_{CAS}$
Content and isotope composition of organic matter	Corg, $\delta^{13}C_{Corg}$, $\delta^{34}S_{Corg}$
Amount of refractory material (e.g. silicates)	Refract

2. Study Area and Geologic Framework

The Paradox Basin in southwestern Colorado is home to massive caprock formations composed of carbonate minerals (Giles et al., 2012), which are similar in nature to caprock deposits found along the Gulf Coast (Pierce and Rich, 1962). The evaporites in the Pradox Basin belong to the Paradox Formation, which is Pennsylvanian in age. The Paradox Formation is composed of evaporites such as salt, anhydrite, gypsum, but also contains carbonates and black shales. The Paradox Formation is overlain by Pennsylvanian marine carbonates belonging to the Honaker Trail Formation. This is important because carbonates in the study area, which are located on top of gypsum caprock and are overlain by fluvial siliciclastic sediments of the Triassic Chinle Formation have previously been identified as part of the Honaker Trail Formation. These carbonates, which are the target of study target of this thesis, have been subsequently remapped and identified as carbonate caprock, which formed simultaneously or slightly earlier to the deposition of the Chinle Formation (Giles et. al, 2012). The outcrops examined in this study are located on a salt shoulder (McFarland, 2016).

Gypsum Valley is a depression located where strata – mostly gypsum – related to the salt diapir are exposed. The principal structures found within the Paradox Basin are a series of five collapsed anticlines, which contain cores of salt and intermixed gypsum and clastic sediments. The major geologic features occur mainly in a northwest trending belt between eastward-dipping monoclines on the west side of the valley and westward-dipping monoclines on the east side of the valley (Shoemaker, 1958) mirrored by the direction of the valley axis.

Figure 4 is a basic representation of the general study area. Figure 5 is a USGS geologic map for Gypsum Valley. Figure 6 is the same map with the area of interest redrafted and Figure 7 is a

closer view of the redrafted portion of the map with the study area magnified and a stratigraphic profile. Figure 8 shows a panoramic photograph of the study area, where the delineation between gypsum, carbonate caprock and overlying siliciclastics are evident.

The stratigraphy of the study area, Mary Jane Draw, is representative of the overall stratigraphy found within the Paradox Basin. The studied carbonate caprocks are assumed to be of the same or older age as the Triassic Chinle Formation because this formation shows onlap onto the carbonate caprocks.

3. METHODS

This study employed a variety of methods, which included:

- Field observations, including mapping of contacts, transects, detailed outcrop descriptions and petrographic descriptions in the field, and sample collection.
- Petrographic thin section analysis.
- Geochemical analyses including the analysis of the carbon and oxygen isotope composition of carbonates, the determination of the content and sulfur and oxygen isotope composition of easily soluble sulfate (ESS) and carbonate associated sulfate (CAS), the analysis of the sulfur and oxygen isotope composition of gypsum, and the determination of the sulfur and carbon content and isotope composition of the acid-insoluble fraction of carbonate caprock.
- The calculation of a basic mathematical model, which aids in the interpretation of the relative openness or closedness of the caprock formational system.

3.1 FIELD WORK

Mary Jane Draw is a narrow northeast trending incision into a massive sandstone cliff (Wingate Formation to Navajo Formation) with an intermittent creek, and the adjacent areas expanding several km to the East and West, which were chosen for this study due to the outstanding quality of the outcrops. The excellent outcrop conditions in the study area are mainly a result of the steep flanks of valleys, which lead to deep incisions created by intermittent creeks, and gravity-driven removal of debris.

Field observations included a detailed description of different carbonate caprock varieties and their spatial distribution. Approximately 90 oriented hand specimens were collected from Mary Jane Draw and the surrounding area in order to provide a suitable overview of the succession of gypsum

and carbonate caprocks. Additionally, profiles along incisions were recorded. Mapping of the contact between gypsum caprock and carbonate caprock, as well as, mapping of the contact between carbonate caprock and overlying strata (Triassic Chinle Formation) and measurements of strike and dip of the beds, and structural features such as folds and faults (if present) were also recorded. The coordinates of locations were recorded with a GPS device.

3.2 PETROGRAPHIC ANALYSIS

Hand specimens were slabbed, from which billets were cut. The billets were sent out for thin section preparation, which included an alizarin red in an acid solution stain for carbonate identification and a ferrous stain for iron identification. Microscopic analyses focused on grain size and relative abundance or percentage of grains, carbonates types – dolomite or calcium carbonate – detritus, i.e. siliciclastics, authigenic silicates, cement types, and diagenetic features, such as indicators for mineral dissolution. Skeletal grains were not observed due to the presumed subsurface nature of carbonate caprock formation in the Paradox Basin. Grain abundance plates were utilized to aid in the creation of quantification tables based upon these observations.

3.3 GEOCHEMICAL ANALYSES

3.3.1 Powdering of Samples for Subsequent Geochemical Analyses

Samples were prepared for geochemical analyses by the crushing and powdering of the rock samples with a hand mortar. Sieving samples with a 150 micron USA Standard Test Sieve ensured consistent grain size.

3.3.2 Carbon and Oxygen Isotope Analysis of Carbonates

Aliquots (~1g) of the powdered samples were taken from the samples for carbon and oxygen isotope analysis. Briefly, the analytical procedure is a two-step procedure, where the carbonate sample is digested in phosphoric acid and the produced carbon dioxide (CO_2) is subsequently analyzed for its isotope composition on an Isotope Ratio Mass Spectrometer (IRMS). The analyses were carried out at a light stable isotope facility at the Department of Geology, ETH Zurich, Switzerland. The carbon and oxygen isotope composition of carbonates was reported according to the common standard delta notation:

$$\delta^{13}C_{sample}=(R^{13}C_{sample}/R^{13}C_{VPDB}-1)*1000‰ \text{ and} \quad \text{Eq. 6}$$

$$\delta^{18}O_{sample}=(R^{18}O_{sample}/R^{18}O_{VPDB}-1)*1000‰, \quad \text{Eq. 7}$$

with $R^{13}C_{sample}$ corresponding to the isotope ratio $^{13}C/^{12}C$ of a sample, $R^{13}C_{VPDB}$ corresponding to the isotope ratio $^{13}C/^{12}C$ of Vienna Pee Dee Belemnite (VPDB, an international standard); and $R^{18}O_{sample}$ corresponding to the isotope ratio $^{18}O/^{16}O$ of a sample and $R^{18}O_{VSPDB}$ corresponding to the isotope ratio $^{18}O/^{16}O$ of VPDB.

3.3.3 Sequential Extraction

Sequential extraction for the determination of the content and sulfur and oxygen isotope composition of easily soluble sulfate and carbonate associated sulfate, and the determination of the sulfur and carbon content and isotope composition of the acid-insoluble fraction of carbonate caprock.

Overview: the sequential leaching procedure aims to recover sulfur from different sulfur pools in a rock sample. Figure 9 is a schematic illustration of the method. The procedure first extracts easily soluble sulfate (ESS; such as sulfate from gypsum) with the help of a sodium chloride

solution, then proceeds to extract carbonate associated sulfate (CAS), and finally obtains refractory material from the dissolution procedure, which may include silicates, barite ($BaSO_4$), pyrite (FeS_2), and organic matter – the latter three of these phases contain sulfur.

Method in detail: First, samples were exposed to a leaching step with sodium chloride (10% NaCl, ~2 M, for ~24 hours). This leaching step dissolved easily soluble sulfate (ESS) minerals, such as gypsum. The dissolved sulfate was retrieved from the leachate after acidification with 1 ml of concentrated hydrochloric acid (HCl, ~12 M HCl) by the addition barium chloride solution ($BaCl_2$, 1M $BaCl_2$ solution), which induced precipitation as barium sulfate ($BaSO_4$). The remaining residue was then washed with deionized water.

In a second leaching step, the residue was exposed to concentrated HCL (~12 M), which dissolved all carbonates and thereby released carbonate associated sulfate (CAS) into solution. The CAS is recovered by the addition of a barium chloride solution ($BaCl_2$, 1M). The remaining residue was washed with deionized water and kept frozen.

At each step of the sequential extraction procedure, the weight of the remaining sample and the weights of ESS and CAS (collected as $BaSO_4$) were recorded. This allowed the determination of the ESS, CAS, and organic matter content of the samples.

The sulfur isotope composition of ESS and CAS was determined by combustion of the $BaSO_4$, which yields sulfur dioxide gas (SO_2) and subsequent isotope analysis of the SO_2 with an IRMS. The oxygen isotope composition of ESS and CAS was determined by carbothermic reduction of the $BaSO_4$, a process that yields carbon monoxide gas (CO) and subsequent isotope analysis of the CO with an IRMS was conducted. These analyses were carried out at a light stable isotope facility at the Department of Geology, ETH Zurich, Switzerland. The oxygen and sulfur isotope

composition of ESS and CAS ($BaSO_4$) was reported according to the common standard delta notation:

$$\delta^{18}O_{sample}=(R^{18}O_{sample}/R^{18}O_{VSMOW}-1)*1000‰ \text{ and} \quad \text{Eq. 8}$$

$$\delta^{34}S_{sample}=(R^{34}S_{sample}/R^{34}S_{VCDT}-1)*1000‰, \quad \text{Eq. 9}$$

with $R^{18}O_{sample}$ corresponding to the isotope ratio $^{18}O/^{16}O$ of a sample and $R^{18}O_{VSMOW}$ corresponding to the isotope ratio $^{18}O/^{16}O$ of Vienna Standard Mean Ocean Water (VSMOW, an international standard), $R^{34}S_{sample}$ corresponding to the isotope ratio $^{34}S/^{32}S$ of a sample, and $R^{13}C_{VPDB}$ corresponding to the isotope ratio $^{34}S/^{32}S$ of Vienna Canon Diablo Troilite (VCDT, an international standard).

Finally, an aliquot of the sample residue was combusted in an Elemental Analyzer (Pyrocube, Elementar), a process that produces CO_2 and SO_2 from combustible compounds. The amount and isotope composition of produced CO_2 and SO_2 was then analyzed with a GeoVisION IRMS (Elementar) at the Light Stable Isotope Laboratory at the Department of Geosciences, University of Texas at El Paso. In the framework of this study, combustible refractory compounds mostly corresponded to carbon and sulfur associated with organic matter (Corg). The carbon and sulfur isotope composition was reported according to the common standard delta notation:

$$\delta^{13}C_{sample}=(R^{13}C_{sample}/R^{13}C_{VPDB}-1)*1000‰ \text{ and} \quad \text{Eq. 10}$$

$$\delta^{34}S_{sample}=(R^{34}S_{sample}/R^{34}S_{VCDT}-1)*1000‰. \quad \text{Eq. 11}$$

Because some of the sample residues displayed anomalously high contents of sulfur, the presence of barite was suspected. To test this, sample residues were treated with a strong chelator, which dissolves barite. The supernatant was then separated from the insoluble residue, and barium sulfate re-precipitation was achieved by the addition of acid barium chloride solution, which renders the chelator inactive, and provides barium ions for the precipitation of barium sulfate. The sulfur isotope composition of the chelator-extracted sulfate was then determined by combustion with an Elemental Analyzer (Pyrocube, Elementar), coupled to a GeoVisION IRMS (Elementar) at the Light Stable Isotope Laboratory at the Department of Geosciences, University of Texas at El Paso. The sulfur isotope composition was reported according to the common standard delta notation:

$$\delta^{34}S_{sample}=(R^{34}S_{sample}/R^{34}S_{VCDT}-1)*1000‰.$$

3.4 BOX MODEL

Figure 10 depicts a graphical representation of a mathematical box model, which was developed in order to gain a quantitative understanding of the relative openness or closed-ness of the system. The model investigated the manner in which changing ratios between the sulfate reduction (flux within carbonate caprock formation system) and fluxes into and out of the carbonate caprock formation system affected the sulfur isotope signature of CAS ($\delta^{34}S_{CAS}$) and sulfur associated with organic matter ($\delta^{34}S_{Corg}$). This part of the project was carried out under the close supervision and guidance of the project supervisor, Dr. Benjamin Brunner at the University of Texas at El Paso.

The model was developed as a process consisting of three processes: gypsum dissolution, microbial sulfate reduction to sulfide, and transport of sulfate and sulfide out the investigated system:

- The dissolution of gypsum is considered a unidirectional process, i.e. there is no re-precipitation of gypsum during carbonate caprock formation. This process is described by two parameters, the flux from gypsum-sulfate into solution (f_{gy}) and the sulfur isotope composition of sulfate derived from gypsum ($\delta^{34}S_{gy}$).
- Microbial sulfate reduction is considered a unidirectional process as well; however, the relative amount of how much of the sulfate that is provided by gypsum dissolution is reduced to sulfide can vary from 0 to 100%. The parameter x describes this relationship, with x=0 corresponding to no sulfate reduction, and x=1 corresponding to 100% sulfate reduction. Microbial sulfate reduction is assumed to preferentially prefer isotopically light sulfur, which can be described by the isotope enrichment factor ($\varepsilon^{34}S_{SR}$). The microbes use dissolved sulfate (which can be incorporated into formed carbonate as CAS), which has a sulfur isotope composition ($\delta^{34}S_{sulfate}$) that may differ from the sulfur isotope composition of sulfate derived from gypsum dissolution, i.e. $\delta^{34}S_{gy}$. The sulfur isotope composition of produced sulfide ($\delta^{34}S_{sulfide}$) is offset from $\delta^{34}S_{sulfate}$ by $\varepsilon^{34}S_{SR}$, i.e., $\delta^{34}S_{sulfide} = \delta^{34}S_{sulfate} + \varepsilon^{34}S_{SR}$.
- It is assumed that the carbonate caprock forming system operates at steady state, which means that the sum of the transport of sulfate ($f_{sulfate}$) and sulfide ($f_{sulfide}$) out the investigated system is equal to sulfate entering the system, i.e., $f_{sulfate} + f_{sulfide} = f_{gy}$.

From this follows that

$$x = f_{sulfide} / (f_{sulfate} + f_{sulfide}) = f_{sulfide} / f_{gy}, \quad \text{Eq. 13}$$

whereas the isotope composition of the sulfate in solution can be calculated from an isotope mass balance that considers the isotope composition of sulfate that is added and removed:

$$d/dt\ ([sulfate]^* \delta^{34}S_{sulfate}) = +f_{gy}*\delta^{34}S_{gy} - f_{sulfate}* \delta^{34}S_{sulfate} - f_{sulfide} *(\delta^{34}S_{sulfate} + \varepsilon^{34}S_{SR}). \quad \text{Eq. 14}$$

Since the system is considered to be at steady state, the left side of the equation (the derivative after the time) becomes zero, from which follows after division by f_{gy}:

$$0= \delta^{34}S_{gy} - f_{sulfate} / f_{gy} * \delta^{34}S_{sulfate} - f_{sulfide} / f_{gy} *(\delta^{34}S_{sulfate} + \varepsilon^{34}S_{SR}), \quad \text{Eq. 15}$$

which is identical to

$$0= \delta^{34}S_{gy} – (f_{gy} - f_{sulfide}) / f_{gy} * \delta^{34}S_{sulfate} - f_{sulfide} / f_{gy} *(\delta^{34}S_{sulfate} + \varepsilon^{34}S_{SR}), \quad \text{Eq. 16}$$

and to

$$0= \delta^{34}S_{gy} – (1 - x) * \delta^{34}S_{sulfate} - x *(\delta^{34}S_{sulfate} + \varepsilon^{34}S_{SR}). \quad \text{Eq. 17}$$

This equation turns out to be very convenient, as the fluxes, which are typically unknown in a geological context, have been replaced by the parameter x. The latter can be determined if three out of the four parameters, $\delta^{34}S_{gy}$, $\delta^{34}S_{sulfate}$, $\delta^{34}S_{sulfide}$, or $\varepsilon^{34}S_{SR}$ can be determined. In the case of the Gyspum Valley carbonate caprock, $\delta^{34}S_{gy}$ is assumed to be equal to the average sulfur isotope composition of gypsum caprock, $\delta^{34}S_{sulfate}$ is assumed to be equal to the average sulfur isotope composition of carbonate associated sulfate of carbonate caprock ($\delta^{34}S_{CAS}$), and $\delta^{34}S_{sulfide}$ is assumed to be equal to the lightest sulfur isotope composition of sulfur in the refractory sulfur pool ($\delta^{34}S_{Corg}$, organically bound sulfur). The isotope enrichment factor is then calculated as:

$$\varepsilon^{34}S_{SR} = \delta^{34}S_{sulfide} - \delta^{34}S_{sulfate},$$

and x is obtained by re-arranging the isotope mass balance, according to:

$$x *(\delta^{34}S_{sulfate} + \varepsilon^{34}S_{SR}) - x * \delta^{34}S_{sulfate} = \delta^{34}S_{gy} - \delta^{34}S_{sulfate}, \quad \text{Eq. 18}$$

and

$$x *(\delta^{34}S_{sulfate} + (\delta^{34}S_{sulfide} - \delta^{34}S_{sulfate})) - x * \delta^{34}S_{sulfate} = \delta^{34}S_{gy} - \delta^{34}S_{sulfate}, \quad \text{Eq. 19}$$

resulting in:

$$x *(\delta^{34}S_{sulfide} - \delta^{34}S_{sulfate}) = \delta^{34}S_{gy} - \delta^{34}S_{sulfate}, \quad \text{Eq. 20}$$

and

$$x = (\delta^{34}S_{gy} - \delta^{34}S_{sulfate})/(\delta^{34}S_{sulfide} - \delta^{34}S_{sulfate}) = (\delta^{34}S_{gy} - \delta^{34}S_{sulfate})/ \varepsilon^{34}S_{SR}. \quad \text{Eq. 21}$$

In the application for Gypsum Valley carbonate caprock, this equation corresponds to

$$x = (\delta^{34}S_{gy} - \delta^{34}S_{CAS})/(\delta^{34}S_{Corg} - \delta^{34}S_{CAS}). \quad \text{Eq. 22}$$

This means that if the isotope composition of gypsum and CAS are identical (x is near 0), only little sulfate is reduced to sulfide relative to the export of sulfate out of the system – which we refer to as an open system. If the isotope offset between CAS and gypsum (i.e. CAS is isotopically much heavier than gypsum) is almost as large as the isotope offset between sulfur bound to organic matter and CAS (i.e. the isotope composition of organically bound sulfur approaches the isotope composition of gypsum), x becomes close to 1, indicating that almost no sulfate leaves the system, which is referred to as a closed system.

3.5 Data Collection and Availability of Samples

All data, including percentage weights, isotope data and procedures were recorded in an Excel spreadsheet and associated MS Word documents. The files were shared with the project

supervisor. Thin sections and remaining rock samples remain in the care of Dr. Benjamin Brunner at the University of Texas at El Paso.

Appendix A details the sample preparation protocol and includes:

- Sample Selection
- Sample Crushing
- Gypsum Dissolution
- Sequential Extraction of NaCl Leachable & HCl Leachable Sulfate
- HCl Procedure
- Secondary Sulfate Precipitation
- Preparation for Mass Spectrometer Run
- Additional Procedures and Notes
- Methods Conclusions

4. RESULTS

4.1 PETROGRAPHY

4.1.1 Field/Hand Samples

The caprock in the area of Mary Jane Draw exhibits a wide range of lithologies and structural elements. These lithologies include gypsum, limestone, and dolomite. The gypsum caprock forms a series of mounds, which indicate that they are resistant to weathering, or that local uplift of the gypsum balances erosion. The weathering color and fresh surface color of gypsum is dominated by white, which makes the gypsum caprock easily identifiable, which is apparent on satellite photos (Figure 11). The carbonate caprock, which comprises calcitic and dolomitic limestone, shows a much higher variability in colors. East and west of the Mary Jane Draw, tan and red colors dominate, whereas within the Mary Jane Draw, green colors are predominant (Figure 12). The majority of the samples are petroliferous, i.e. the smell of petroleum is readily apparent when a sample is struck with a hammer and the fresh surface is exposed. The greenish calcitic carbonate caprocks smell most strongly, but sometimes also dark red colored rocks were petroliferous.

Throughout the study area, the gypsum bedding varied from the mm scale to the meter scale, without obvious consistency in thickness. The color of the gypsum is typically whitish green. The entirety of the gypsum thickness outcropping found in the Mary Jane Draw is approximately 10m, however, it is obvious that the gypsum continues into the subsurface. In outcrop, the carbonate caprock typically forms distinct benches. These carbonate benches vary in thickness throughout the study area, and thickness can range from several cm to the meter scale. One of the thickest benches (approximately a meter) found in the study area was nicknamed the ‘Conchita Member’

(Figure 13). The Conchita Member can be followed over more than 100 m distance, although it is interrupted in several locations.

Three transects were used to gain an overview of the different lithologies in the study area at Mary Jane Draw, from West to East (Figure 14). The total thickness of carbonate caprock in transect II is 20m, transect I, 22m (the contact to the gypsum not outcropping, inferred from projections), and transect III, 19m. There is an enormous fabric richness observed in the different lithologies found at Mary Jane Draw, which exceeds what has been reported at another caprock location in the Paradox Basin, the Castle Valley (Shock, 2012). The observed fabrics include massive layered, brecciated, and porphyritic lithologies (Figures 15-18). Occasionally observed is changing fabrics within a bed, for example: from massive to laminated to brecciated. Within these fabrics, several different subgroups have been identified, such as laminated, micro-laminated, and zebra. This fabric inventory was further formalized to become a fabric classification scheme (see discussion and conclusions). Also apparent is deformation, which includes convolute, folding, boudinage and shear bands. Figures 19-23 are a few of the notable examples of this deformation. The main gypsum fabric found in the study area is banded, with several different sub-fabrics, which range from zebra to convolute, with a range of colors including white, gray and greenish, with bands of red, brownish, and reddish to black. The following section contains a detailed study of a specific outcrop, which includes descriptions of selected thin sections. This detailed outcrop study demonstrates that observations can indeed be grouped and that it is possible to identify and distinguish patterns that apply to multiple samples, by assigning rock fabrics to each of the varying lithologies.

4.1.2 Multi-Outcrop

An outcrop found on Transect I (Figure 14) is an excellent example of the extensive carbonate caprock variability – both with respect to fabric as well as bench thickness – found in the study area. Figure 24 is a field drawing of this outcrop and Figure 25 is a photo of this outcrop. Samples from this outcrop included samples numbers GVP-015 – GVP 022. These samples include the following:

Sample GVP-015, Section I, (Figure 26), was from the bottom of the bench and was found to measure approximately 25 cm thick. This sample is a solid, black, petroliferous carbonate with deformed zebra fabric in the middle of the bench and marl at the top of the bench. The main fabric was classified as Layered, with a Zebra sub-fabric, which is characterized by alternating silicified and calcitic Zebra bands.

Sample GVP-016-II, Section II, (Figure 27), is a sample that was collected from a bench that is approximately 61 cm thick and thins down to approximately 20 cm in thickness. The sample collected from this bench had varying levels of petroliferous odor – more where the bench was thick as compared to where it was thin. The sample consisted of a dark carbonate, very similar to sample GVP-015, but exhibited a zebra-type banding at the top. The sample also displays opaline silica that likely replaced gypsum. The main fabric was classified as Layered, with a Zebra sub-fabric which is characterized by alternating silicified and calcitic Zebra bands.

Sample GVP-017, Section III, is a sample from a bench that displayed varying thickness: 41 cm on the left side, 20 cm in the middle and 43 cm on the right side, displaying boudinage. The sample is a dark carbonate with laminated seams of light colored carbonate, and gypsum present along the borders. The main fabric was classified as Layered.

Sample GVP-018, Section IV, (Figure 28), is a sample from a bench that tapered in thickness from 36 cm down to about 5 cm. The sample is a dark carbonate with large (7 cm) clasts and cracks phreatic infills of calcite. The main fabric of this sample was classified as Brecciated with a Mosaic sub-fabric.

Sample GVP-019, Section VI, is a sample from a bench that tapered in thickness from 35 cm down to about 7 cm. The sample is a light reddish colored, platy carbonate with rounded clasts and with the exception of 1-2 cm clasts, and it is not petroliferous. Also apparent is phreatic infilling in the cracks. The main fabric was classified as Layered with a Micro-Laminae sub-fabric.

Sample GVP-020, Section V, (Figure 29), is a sample that came from a bench that was prominent on the left side (approximately 48 cm) with calcite crystals apparent on the right side. This sample is a dark, laminated, petroliferous carbonate with zebra gypsum on the left side. The fabric was classified as Massive.

Sample GVP-021, Section VII is a sample that came from a bench that was 43 cm at the thickest point. The sample has a beige weathered surface with a red sandy coating and displays thick zebra stripes that are irregularly laminated with calcite crystals. The fabric was identified as Layered with a Zebra sub-fabric.

Sample GVP-022, Section VIII, is a dark petroliferous carbonate sample that was classified as having a Massive fabric.

4.1.3 Thin Sections

Petrologic analyses focused on grain size and relative abundance or percentage of grains, carbonates types – dolomite or calcium carbonate – detritus, i.e. siliclastics, authigenic silicates,

cement types, and diagenetic features, such as indicators for mineral dissolution. Skeletal grains were not observed due to the presumed subsurface nature of carbonate caprock formation in the Paradox Basin. Grain abundance plates were utilized to aid in the creation of quantification tables based upon these observations. Appendix B, contains a detailed description of the hand samples used for thin section creation, as well as, a detailed description of each thin section.

Based upon the observed fabrics and the large variety of carbonate caprocks in the study area, representative samples from each of the fabric and sub-fabric (where applicable) types are as follows:

Sample GVP-047, (Figure30), is an example of a sample initially thought to be banded gypsum with thick white layers with nodules. Later petrographic analysis, however, proved the sample to be mainly comprised of microcrystalline dolomite, with chert nodules and a small amount of secondary dolomite, and a few small quartz crystals. The sample was classified as Massive.

Sample GVP-045, (Figure 31), is a gypsum sample with black and white 5 mm layers. Petrographic analysis indicated the presence of microcrystalline dolomite as well as gypsum. Interesting in the thin section of this sample, is that gypsum can be seen "actively" replacing microcrystalline dolomite. The main fabric of this sample was classified as Brecciated and the sub-fabric was classified as Mosaic.

Sample GVP-071, (Figure 32), is a dolomitic carbonate sample. Petrographic analysis indicated that the dolomite was recrystallized Fe-rich dolomite. The weathered surface is reddish/tan/orange, while the fresh surface is dark gray with some calcite. The main fabric was classified as Brecciated and the sub-fabric was classified as Disorganized.

Sample GVP-081, (Figure 33), is also a petroliferous dolomitic carbonate sample. The weathered surface is karst-like and tan/greenish with laminae visible on the outside and slightly visible inside as well, with a dark purple evident. The fresh surface is dark gray. The main fabric type was classified as Layered and the sub-fabric was classified as Micro-Laminae.

Sample GVP-059A & B, (Figure 34), is a gypsic sample that displayed alternating black and white layers on a mm scale. The bench from which this sample was taken was fairly compact. Petrographic analysis confirmed the gypsum field identification along with a very small amount of microcrystalline dolomite and quartz. The main fabric of this sample was classified as Layered and the sub-fabric was identified as Micro-Laminae.

Sample GVP-013B, (Figure 35), is another example of a sample that was initially thought to be zebra gypsum, but later analysis proved the sample to be composed of recrystallized calcite and Fe-rich baroque dolomite (recrystallized). The main fabric of this sample was classified as Layered with a Zebra sub-fabric.

The main fabric of samples GVP-015 and GVP-016-II was classified as Layered with a Zebra sub-fabric (as described in 4.1.3, above).

Sample GVP-061, (Figure 36), is a mostly heterogeneous gypsum sample with some white and black layers with dark colored clasts. Petrographic analysis indicated that the sample was composed mostly of gypsum with recrystallized dolomite. The fabric of this sample was classified as Porphyritic.

Additional information regarding these specific samples are available on Tables 1, and 2, and in Appendix 2.

4.2 PROFILES

Three profiles, bisecting the contact between the caprock and sandstone and the contact between the caprock and gypsum, were measured in the study area. The westernmost transect is № II, the middle transect is № I, and the easternmost transect is № III, which are illustrated on Figures 12 and 37.

The main profile, Transect № III, comprises both gypsum and carbonate caprock (for detailed profile description, schematic sketch and photograph, of these outcrops please see Figures 37, 38 and 39. The base of the profile is dominated by gypsum caprock, with white weathering colors, and benches that are 10 to 40 cm thick. The gypsum benches are mostly massive and homogeneous. Further up section, the massive benches start to alternate with benches that show black banding, as well as, porphyritic lithologies. The top of the gypsum caprock is typically associated with a change in topography to a shallower slope, and a gap in outcrop. Only rock pieces can be found in this zone, which is approximately 50 cm thick. The pieces are typically smaller than 4 cm and display banding. Beginning at the base of transect № III and moving up section, the first gypsum section was approximately 3 m thick and was followed 2 m gap. This section was marked mainly by white gypsum with brownish inclusions in the weathered surface. Fabrics encountered in this section included a Banded main fabric and a convolute sub-fabric. The second section of gypsum was approximately 7 meters thick and was comprised of approximately six benches. This section also included white gypsum as well as black and white layered gypsum and some samples with carbonate inclusions. The fabrics encountered in this area included Banded and Porphyritic and sub-fabrics included both Clotted and Convolute.

The first carbonate bench that was found was a single fine-grained, petroliferous bench approximately 20 cm in thickness. The weathered surface was tannish with breccia at the bottom

and the fresh surface was dark gray, almost black. The fabric of this carbonate bench was classified as Massive Homogeneous. This bench was followed by a 50 cm gap. The second carbonate bench encountered was approximately 40 cm thick and displayed alternating gray and dark gray convolute bands on a millimeter scale. The main fabric of this sample was classified as Banded with a Convolute sub-fabric. This sample was followed by a ~1m gap of float and rubble. The next series of carbonate benches that were encountered was comprised of approximately 9 benches that ranged in thickness from .3 meters to 1.2 meters. These benches included samples, which were petroliferous, with dark gray fresh surfaces, and included samples with convolute laminae. Fabrics identified in this section included Massive Homogeneous, Brecciated, and Banded main fabrics with Polymict and Convolute sub-fabrics. This series of benches was followed a gap of float and rubble that was approximately 1 m.

Moving up-section, another series of two carbonate benches was encountered, which ranged from 20 cm to 40 cm in thickness. These benches displayed medium dark gray and dark purple/gray/orange weathered surfaces. Fresh surfaces were light gray with purple banding and dark gray. Both samples displayed large or secondary crystals. The fabrics in this area were classified as Brecciated main fabrics with Mosaic /Crackle and Polymict sub-fabrics. These benches were followed by another gap of float and rubble that measured approximately 2 meters. A single 25 cm carbonate bench was then encountered that displayed a gray, tan and purple, laminated weathered surface with a gray fresh surface that had a purple banding. The main fabric was identified as Banded and the sub-fabric was identified as Clotted. This section was followed by a ½ meter gap of float and rubble. The next series of carbonate benches that was encountered was approximately 5 meters thick and included six benches that ranged in thickness from 20 cm to 75 cm. This section included many different colors found on both the weathered and fresh

surfaces. Fine laminations, phreatic infilling with calcite, banding, brecciated fabrics, and both fine and coarser grained fresh surfaces were also encountered. The main fabrics for this section were classified as Massive Homogeneous and Brecciated with Mosaic/Crackle, Polymict and Convolute sub-fabrics. A gap of ~50 cm followed this package of caprock before the next series of carbonate benches was encountered. This series of two benches displayed medium and dark gray and purple, orange weathered tops with light gray with purple bands and dark gray fresh surfaces. Also apparent was coarse (recrystallized grains). The fabrics for both of these samples were classified as Brecciated with Mosaic/Crackle sub-fabrics. Following these carbonate benches, another gap of float and rubble was encountered that continued for approximately 2.1 meters. Following this gap, the final carbonate bench before the sandstone was encountered. This bench was approximately 65 cm thick and was marked by silicification. Weathered surfaces were reddish/purple/gray, laminated and brecciated. The fresh surfaces were dark gray and purple. An interesting sample was collected from this bench that appeared to be a carbonate/sandstone example that looked as if it was welded together, (Figure 40).

The general trend of transect № III, indicated that the base of this profile was dominated by gypsum, followed by carbonate caprocks. Moving up section, but prior to the sandstone, an increase of siclification is apparent. The profile is marked by several gaps of float and rubble, but this general trend is apparent throughout the study area.

4.3 Upper & Lower Contact of Carbonate Caprock, Implications for Thickness

Carbonate caprock thickness data was obtained based upon the sandstone/carbonate caprock contact and the carbonate caprock/gypsum caprock contact. The results obtained from the central part of the study area will be discussed initially, because it is the largest, and therefore most likely

to be the most representative investigated sector. This discussion is followed by the eastern and western portions of the study area.

Figure 41 is a topographic map, displaying the sandstone/caprock contact and the caprock/gypsum contact (black lines). Additionally, elevation projections for these interfaces are represented by colored lines, which represent the strike of the geologic units. Colored dots represent intersects where the contact lines cross certain elevations, which provided reference points for the aforementioned elevation projections. Dip lines were drawn perpendicular to the elevation projections in select locations. These projections were used to determine the dip and thickness of the carbonate caprock unit at various locations within the studied area.

Figure 42 is a representation of the profiles for both the sandstone/caprock contact and the caprock/gypsum contact at the selected points, which correspond to the locations of the dip lines in Figure 41.

Beginning with the most representative area of the sandstone caprock contact, dip line numbers 1-3, it is apparent that the strike (SE to NW) is consistent. Closest to the axis of the salt wall, the carbonate caprock unit dips 'into the mountain' at an average of approximately 30° and with increasing distance from the salt wall axis (and increased depth of the carbonate caprock unit), the dip shallows out to an average of approximately 20°. Important to note is that each dip line changes its slope from steep to shallow with increased distance from the salt wall axes, and that the dip profiles are different between different profiles. The dip variance for this section ranges from 42.55° to 4.78°. These dip angles aid in creating a picture of the geologic unit as it dips at varying rates and indicates that the plane of the caprock unit undulates along the length of this section as it dips from steep to shallow into the mountain. Further indications, include the fact that the strike

is consistent, while the dips of the units are less consistent, but still within reason. The main conclusion to be drawn from this data is that the caprock unit is dipping into the mountain or walls of the valley, initially at a fairly steep angle of approximately 30° and as the unit dips deeper, the unit shallows out to relatively low angle of approximately 5°.

The easternmost part of the study area proved difficult to classify. This area is structurally compromised by a combination of faults and folds and did not allow for the utilization of the above described colored line and dot method. As such, no data regarding thickness, elevation projections, strike, or dip lines were obtained in this particular area.

Moving to the Western side of Mary Jane Draw, a different story is presented. The strike of the caprock unit (E/W) differs from that of the Western side. Not only does the strike differ, but based on the reconstruction, the carbonate caprock unit, dips from 42.55° to 31.53° *towards* the valley, rather than into the mountain (Dip Line № 5, on Figure 41, as seen on the Western side of Mary Jane Draw). Moving further West and thereby likely towards the axis of the salt wall and more closely to the neck position with respect to the Salt Shoulder, the carbonate caprock unit displays the expected dip (26.65°) into the mountain. It would be interesting to study the dip of the carbonate caprock unit further in the westward direction; however, the upper and lower contacts are no longer exposed in proximity to the Dolores River.

In summary, the following carbonate caprock unit thicknesses were found (represented on Figure 41 by a dark brown line), drawn perpendicular to the sandstone caprock contact line and the caprock gypsum contact line, intersecting both contact lines. These are marked ‘A,’ ‘B,’ and ‘C.’ These locations were chosen due to their relative close proximity between both contact lines to eliminate as much variation as possible.

- ‘A’ unit thickness is 64.99’ (19.81 meters)
- ‘B’ unit thickness is 74.03’ (22.56 meters) based upon the average dip and 52.06’ (15.87 meters) for the smallest dip
- ‘C’ unit thickness is 55.90’ (17.04 meters) based upon the average dip and 29.88’ (9.11 meters) for the smallest dip

Throughout the study area, several areas of collapse were observed, which resulted in unexpected dips, particularly for the gypsum – carbonate caprock contact that were contrary to what was expected. The explanation for this phenomenon is threefold:

1) The interaction of a rising diapir coupled with the dissolution of salts due to meteoric water infiltration,
2) combined with the weak constitution of the underlying gypsum units, likely caused the area represented by dip line № 5 to collapse. This could also be considered a reasonable explanation for the change in strike direction of the Western side of Mary Jane Draw when compared to the Eastern side. Additionally,
3) faulting in Mary Jane Draw likely impacted the structural rigidity of the geologic units resulting in strike direction change, as well as, collapse.

Additionally, important to note is that the collapses seen on the sandstone/caprock contact on the West side of Mary Jane Draw, as well as the collapses seen along the length of the caprock/gypsum contact, were likely caused by the interaction of a rising diapir coupled with the dissolution of salts due to meteoric water infiltration, weak rigidity of the gypsum unit and faulting.

4.4 GEOCHEMICAL ANALYSES

4.4.1 $\delta^{13}C$ and $\delta^{18}O$ of Carbonate

The isotope composition of $\delta^{13}C$ and $\delta^{18}O$ found in carbonates is represented on Figure 43. Results indicate the following:

- The range for oxygen isotopes was -18‰ to -3‰
- The range for carbon isotopes was 15‰ to -6‰
- The isotope composition for micritic dolomite falls into a very narrow range
- The isotope composition for recrystallized calcite fell into a fairly broad range

4.4.2 Content and Isotope Composition of Carbon and Sulfur of Carbonate-Free Sample Residue

The isotope composition and C:N ratio and the sulfur found in organic matter is represented on Figure 44. Findings are as follows:

- The S:C ratio range was from 0.05 to 1.4
- The sulfur isotope composition was -23‰ to +5‰
- There was no clear pattern for different rock types

4.4.3 Content and Isotope Composition of ESS and CAS

The carbonate associated sulfate content of carbonate caprock found in the study area is represented on Figure 45. Results indicate that the average, median, minimum and maximum ppm sulfate values for calcitic caprock were: 759; 733; 345; and 1345, respectively. The results also indicate that the average, median, minimum and maximum ppm sulfate values for dolomitic caprock were: 61; 18; 7; and 256, respectively.

The content and isotope composition of easily soluble sulfate was utilized to assess the potential of ESS to cause artifacts in the CAS isotope composition. There is a low change for artifacts if the content of ESS is small compared to the CAS content, and if the isotope composition of ESS and CAS are close to each other. The opposite is the case if the quantity of ESS is high relative to CAS (danger of contamination), and if the isotope composition of CAS and ESS strongly differ (already a small contamination could cause a big shift in the isotope composition of CAS). This 'quality control' did not reveal any critical issues.

4.4.4 Sulfur and Oxygen Isotope Composition of Gypsum

The sulfur and oxygen isotope composition of CAS and gypsum are represented on Figure 46. Results indicate the following:

- The range for the sulfur isotope composition in gypsum was 13‰ to 16‰
- The range for the oxygen isotope composition in gypsum was 12‰ to 15‰
- The CAS range for $\delta^{18}O$ in calcite was 16‰ to 20‰
- The CAS range for $\delta^{34}S$ in calcite was 16‰ to 18‰
- The CAS range for $\delta^{18}O$ in dolomite was 16‰ to 18‰

It must be noted that the isotope composition of CAS from dolomite is prone to artifacts, because these rocks contain very little CAS, which makes to sample more vulnerable to contamination, and also increases the potential errors during isotope analysis.

5. DISCUSSION

5.1 CAPROCK LITHOLOGIES

The carbonate caprock classification based on the U.S. Gulf Coast diapir province is distinguished by a lower banded (zebraic) and an upper variegated section. It is possible that the variety of carbonate caprocks fabrics found within Gypsum Valley could be assigned to the variegated section, as the term 'variegated' implies that there may be a multitude of fabrics included in that category. However, two insights are evident. First, the fact that carbonates replaced gypsum or anhydrite needs to be acknowledged, which means that they may inherit a pre-existing fabric. This implies that it is logical that fabric nomenclatures for carbonate and gypsum caprocks should, where applicable, be identical. Second, the simple division in an upper and lower section for the Gypsum Valley carbonate caprock is problematic (see discussion below); whereas, classification into fabric groups has the potential to reveal an internal 'caprock stratigraphy'. For these reasons, it is apparent that a standardized caprock fabric nomenclature would be highly beneficial to future researchers and collaborators in different regions throughout the world. The identification of similar fabrics within different lithologies (gypsum, calcite, dolomite, silicified) led to the insight that for this new classification scheme, the fabric – and not the mineralogy or rock chemistry – should be the starting point for distinguishing between different caprock types. This does not at all imply that the latter can be ignored, rather it calls for increased caution: For example, a sample that was thought to be 'zebra gypsum', turned out to be almost entirely calcite.

Based on these insights, a new classification scheme has been extensively discussed and developed by a group of students and faculty at the University of Texas at El Paso, and it continues to evolve

(Table 1; Poe et al., 2008b). Four main fabrics were observed in Mary Jane Draw, which consisted of the following:

- Massive
- Banded
- Brecciated
- Porphyritic

Within these main fabrics, several sub-categories were identified. The Massive and Porphyritic fabrics do not contain sub-categories; however, the Layered main fabric includes sub categories of Micro-Laminae and Zebra. The Brecciated fabric type includes sub categories of Mosiac, and Disorganized.

During the writing of this thesis, the classification scheme continued to undergo development, and the utilized classification is current as of December, 2017 (Table 1). The fabric classification scheme is meant to include accessory minerals, which are found. In the case of this study area, such grains include: quartz, chalcedony, chert, residual pyrite – iron sulfide.

5.2 Is There an Internal Stratigraphic Order of the Carbonate Caprock Assemblage?

The US Gulf Coast caprock assemblage is typically described as an upward sequence starting with anhydrite on top of the salt, followed by gypsum, which in turn is overlain by carbonate caprock that consists of two units, a banded calcite and a variegated calcite unit (Posey and Kyle, 1988b). The question that arises is whether or not the caprock at Gypsum Valley also exhibits an internal stratigraphic order.

Based on the three established transects (Westernmost transect is № II, the middle transect is № I, and the Easternmost transect is № III; Figure 11, 14), and on observations in the field, a general pattern was evident. In ascending order, the generalized petrographic stratigraphy includes:

1. Gypsum
2. Recrystallized or secondary dolomite
3. Primary calcite
4. Secondary dolomite
5. Primary or microcrystalline dolomite

Typically, there is a gap (0.5 m to 2 m) in between the gypsum and the carbonate caprock. The lowermost bench is separated from the gypsum caprock by a gap that only exposes rock fragments. One of the key outcrop features are individual carbonate caprock benches that can sometimes be followed over 100's of meters, which range in thickness from 10cm to more than a meter (Figure 13, e.g. Conchita member). These benches crop out close to the top of the gypsum caprock and continue often all the way to the overlying sandstones of the Chinle Formation. The transition from the benches into the sandstones can be continuous, but sometimes comprises chaotic rock – and often strongly altered – packages that may have been caused by mass wasting and/or karst collapse. As the carbonate caprock benches approach the Chinle sandstone, a trend to stronger silificiation is observed. The sicilification is not pervasive; rather, there is an increased, but sporatic occurrence of silicified specimens, particularly in areas comprising the mass wasting deposits. Figure 37 comprises the complete № III transect and illustrates the internal stratigraphic order found in the study area. Using the caprock classification scheme (Table 1) the gypsum and carbonate caprocks can be bundled into groups, and in combination with the observed trend in silicifiaction, one can attempt to correlate these groups (Figure 14). To achiveve this for the

carbonate caprock section, massive fabrics were first correlated, following the presumption that the massive fabrics, which often coincide with benches that, in outcrop, can be followed over long distances. Based on this framework, it was possible to also correlate bundles of predominantly brecciated fabrics adjacient to the 'massive' groups. Finally, and much more tentatively, this allowed the inferrence of a laminated central bundle. For the gypsum caprock, a similar approach could be envisioned, which would indicate that massive gypsum is followed by layered gypsum that may have a porphyritic sub-category (Figure 14). Thus, a preliminary fabric based stratigraphy can be established:

1. Massive Gypsum
2. Layered (porphyritic) Gypsum
3. Massive Carbonate
4. Brecciated Carbonate
5. Layered Carbonate
6. Brecciated Carbonate
7. Massive Carbonate
8. Massive, altered 'mass waste' Carbonate

This indicates that while fabric type varied greatly from bench to bench, certain correlations can, be inferred.

Taking this a step further, the question becomes: if the benches, the dominant caprock feature found in Gypsum Valley, are considered equivalent to the banded calcite cap found within the U.S. Gulf Coast salt diapir province. The zebra-textured zone with band thicknesses of less than 1.2 cm is reminiscent of zebra-calcite caprock found at Bridge Canyon, where it is found right above

the gypsum caprock. However, a vast majority of the benches found elsewhere do not show this texture. Thus, at Gypsum Valley, the equivalent to the banded calcite top from the U.S. Gulf Coast salt diapirs could correspond to the lowermost zebra-calcite caprock only, which is a unit between gypsum caprock and the bench-dominated caprock that is in most cases, covered by detritus. Correspondingly, the variegated calcite cap from the Gulf Coast salt diapirs could correspond to the occurrences of mass-waste and karst deposits, as well as the chaotic intervals that replace the bench-type appearance. Much of the uncertainty with respect to the question regarding the bench-dominated caprock from Gypsum Valley, and whether or not it can truly be put into the same stratigraphic position as the banded calcite cap from the U.S. Gulf Coast diapirs, is due to the lack of a means to properly compare the lithologies from different regions. The current information with respect to the carbonate caprocks found in the U.S. Gulf Coast diapir region, is based upon outcrops in quarries, which display massive, steep cliffs. The outcrops in Gypsum Valley are found on a, comparatively, much gentler slope, which favors the appearance of single, competent benches. The important take-home message from this discussion is that it is possible that even a geologist intimately familiar with the stratigraphy of carbonate caprock from the U.S. Gulf Coast may not immediately recognize carbonate caprock at the Gypsum Valley salt wall.

5.3 Slope Variations of the Carbonate Caprock-Sandstone Contact and Carbonate-Gypsum Caprock Contact – Relationship to Salt Shoulder and Removal of Gypsum

Unit thicknesses are based on intersects of contacts with topography, (Figure 41), by a dark brown line drawn perpendicular to the sandstone-caprock contact line and he caprock-gypsum contact line, intersecting both contact lines. These are marked 'A,' 'B,' and 'C.'

Based upon these observations it becomes apparent that the caprock thickness throughout the study area thins slightly from West to East. The slope of the contact between carbonate caprock and overlying sandstones becomes shallower with increasing distance from the axis of the salt wall. This pattern is expected, because the Mary Jane study area likely comprises the neck and adjacent shoulder of the salt shoulder observed at Bridge Canyon.

5.4 Dolomite vs. Limestone – Which was 'More Primary'?

Dolomite is an abundant carbonate caprock lithology in Gypsum Valley – likely equal in abundance to calcitic caprock (limestone). This is in stark contrast to the carbonate caprocks associated with the U.S. Gulf Coast salt diapirs, where dolomite is often a rare accessory mineral. First, dolomite, or its precursor proto-dolomite, (for a review see Petrash et al., 2017) which is a mineral that formed early, i.e. 'primary' in the conversion of sulfate caprock (gypsum and/or anhydrite) into carbonate caprock; or, is it a mineral that replaced calcite, i.e. is it 'secondary' dolomite? Second, if the origin of dolomite is 'primary', what does that imply with regard to the system in which the carbonate caprock formed? The first question is important because, canonically, dolomite is presumed to be of secondary origin, coinciding with the assumption that the dolomitization process caused an increase in porosity, which would have implications for the

permeability and porosity of carbonate caprock. Secondary dolomite was undeniably found in several samples taken from Mary Jane Draw; however, the vast majority of the dolomite that was found was microcrystalline in origin, and the micritic dolomite grain sizes were generally smaller than those observed for the calcitic caprocks. Additionally, the porosity of the dolomite samples is far below the classical ≤ 12% dolomite porosity, usually attributed to secondary dolomite. The carbon isotope composition of the dolomite is similar to that of the calcitic caprocks, indicating that either lithology could have been formed from the oxidation of hydrocarbons. Also, the comparison of the oxygen isotope composition of dolomite to calcitic samples indicates that the oxygen isotope composition of fluids from which the minerals formed may have been similar – again not providing evidence that calcite was replaced by late-stage dolomite. Consequently, it was not possible to definitively conclude that the microcrystalline dolomite is primary, but there is a strong possibility that this is indeed the case.

Investigation into the carbonate caprocks that were found in Gypsum Valley, indicated that dolomite directly replaced gypsum, without a calcitic precursor, and that oxidation of hydrocarbons fueled this process. This implies that microbial dolomite formation is not an isolated process tied to rather exotic environments, but can also constitute massive sedimentary deposits. It also indicates that the presumption that dolomite in caprocks is of secondary origin, and as such, typically porous, is not correct, calling for a differentiated view on dolomites as potential reservoir rocks.

To date, the general wisdom is that hydrocarbon oxidation coupled to the reduction of sulfate supplied from gypsum and anhydrite is responsible for the formation of carbonate caprocks. However, the dolomitic carbonate caprocks from Gypsum Valley contain very little sulfate, which is only negligibly enriched in heavy sulfur (^{34}S) and oxygen (^{18}O) isotopes relative to sulfate from

gypsum. This fundamentally contradicts the expectation that these rocks formed in a sulfate-rich environment wherein sulfate-reducing organisms thrived. The overwhelming majority of dolomite found in the study area is microcrystalline in origin. Regarding ^{13}C isotopes, neither calcite nor dolomite fall into the same range, with one exception – organic-rich calcite (Figure 43). This indicates that the addition of the carbonate mixture did not occur at a late stage - very little carbon was added to the system. Conversely, ^{18}O isotope data seems to support the idea that dolomite occurred late stage and was not affected by diagenetic fluid.

Figures 45 and 46 illustrate the CAS and ppm sulfate values of $\delta^{18}O$ vs. $\delta^{34}S$ and indicate the amount of sulfate trapped in the system. In this range, calcite is a bit heavier for sulfur isotopes. The dolomitic CAS is lighter than the calcitic, which is interpreted to signify that the isotope composition of the extracted CAS was affected by sulfur oxidation and therefore cannot be considered to be a primary indicator. Indications are that dolomites found in Gypsum Valley contain very little CAS, which suggests that there was an absence of sulfate during formation - likely during the recrystallization of dolomite. Sulfate was lost as magnesium and calcium reordering took place. Thus, the absence of sulfate in the Gypsum Valley dolomite samples cannot be taken as evidence that it was formed late stage – the sulfate was removed from the system during the reordering of calcium and magnesium. Although definitive proof that dolomite is primary is lacking, based upon these findings, there is a strong indication that the dolomite was formed during an early stage of Gypsum Valley caprock genesis.

5.5 Microbial Sulfate Reduction as Key Player in Carbonate Caprock Formation at Gypsum Valley – A Summary

In order to determine if sulfate reducing microorganisms were responsible for carbonate caprock (limestone and/or dolomite) formation, the sulfur geochemistry of the Mary Jane Draw samples was analyzed. Sulfate reducing organisms typically cause a large sulfur isotope fractionation between remaining sulfate, which becomes isotopically heavier, and produced sulfide, which, relative to the sulfate source, is isotopically light. Isotope ratio mass spectrometer results provided evidence that isotopically light sulfur was indeed present in samples procured from the study area, namely in the form of sulfur associated with organic matter. Based on this observation, it can be concluded that sulfate reducing microbes were likely present in the system in which the carbonate formed. However, it must also be noted, that classical geochemical indicators for the activity of sulfate reducing microorganisms were absent.

5.5.1 Pyrite

Pyrite is considered the hallmark of sulfate reduction. It forms when sulfide – presumably produced by sulfate reduction – gets in contact with reduced (ferrous) or oxidized (ferric) iron, for example according to the reaction

$$2H_2S + 2FeOOH \Rightarrow FeS_2 + Fe^{2+} + 2H_2O + 2OH^-, \quad \text{Eq. 23}$$

where FeOOH refers to iron oxy-hydroxide. Therefore, finding pyrite could be considered a 'smoking gun' for the activity of sulfate reducing microorganisms. Interestingly, pyrite was not found in the field, in hand specimens, nor in any of our thin sections. As such, sulfur isotopes could not be measured.

The absence of pyrite can be explained in four different ways:

i) no sulfide was formed (i.e. absence of sulfate reducing microbes),

ii) iron was not present in the system; thus, no pyrite could be formed,

iii) pyrite was formed, but subsequently removed by oxidation,

iv) sulfide was produced, but quickly removed.

Sulfate reducers are typically active in systems where hydrocarbons, sulfate and water are available, as was the case in Gypsum Valley during the time of carbonate caprock formation. Thus, explanation i) is not a likely scenario for the study area. Moreover, samples from the study area indicate elevated sulfur content in organic matter, which is typically the result of sulfurization of organic matter by sulfide produced by SRB. Explanation ii) is appealing, because it can be argued that the gypsum caprock is poor in iron; however, it must be considered that the Paradox Formation contains multiple intervals of organic rich clays, which would imply that iron was available to at least some degree. Moreover, the rich color palette of carbonate caprocks in the investigated area, ranging from dark green to red, indicates the presence of metals. This would imply that iron was present during the original formation of the carbonate caprocks, unless the metals were added at a subsequent stage, overprinting an iron-poor lithology. The wide variety in colors indicates that fluids altered the redox state of metals in the carbonate caprocks, which highlights that possibity that pyrite was removed by oxidizing fluids, (explanation iii). No obvious signs of such a pervasive oxidation were observed (e.g. pyrite-shaped voids in carbonate), but it is possible that acid formation during pyrite oxidation destroyed such patterns by dissolving the carbonate, according to

$4FeS_2 + 15O_2 + 16CaCO_3 + 10H_2O \Rightarrow FeOOH + 8SO_4^{2-} + 16HCO_3^- + 16Ca^{2+}$. Eq. 24

Finally, there is also the possibility that sulfide was removed very quickly, (explanation iv), which did not permit for the formation of pyrite. In a system, open to advective fluid flow, sulfide could be transported away quickly. Alternatively, formed sulfide might be sequestered into a different phase, such as organically bound sulfur (sulfurization of organic matter).

5.5.2 Carbon and Oxygen Isotope Composition of Carbonate (Dolomite and Limestone), and Carbon Isotope Composition of Acid-Insoluble Organic Matter as Indicators for Organically-Derived Carbonate

Isotopically light carbon isotope signatures of carbonates are typical for systems in which a considerable portion of carbonate is originally derived from the oxidation of isotopically light organic matter: oil, or methane (Drake, et. al., 2015). In order to test this, the isotope composition of carbonates (limestone and dolomite), and of the organic matter residue after the dissolution of the carbonate with hydrochloric acid, was determined. The oxygen isotope composition of the carbonates, which was determined simultaneously to the carbon isotope composition of the carbonate, is a function of the oxygen isotope composition of the water in which the carbonate was formed and/or diagenetically overprinted, the mineralogy of the carbonate (i.e. dolomite vs. calcite), and the ambient temperature during formation/overprinting of the carbonate rocks.

The results of these tests indicated that the $\delta^{13}C$ and $\delta^{18}O$ of carbonate range for oxygen isotopes was -18‰ to -3‰, and the range for carbon isotopes was 15‰ to -6‰. Additionally, the isotope composition for micritic dolomite fell into a very narrow range, while the isotope composition for recrystallized calcite (limestone) fell into a fairly broad range (Figure 43).

The generally light isotope composition of the carbonates in the caprocks from the Mary Jane site give a clear indication that carbonate from the oxidation of organic matter was a contributor, and based upon on the carbon isotope composition of residual carbonate, the contribution (x) of the organically-derived portion of the carbonate based can be estimated by utilizing the following isotope mass balance:

$$\delta^{13}C_{carbonate} = (1\text{-}x) * \delta^{13}C_{inorganic\_carbonate}\ (0\ ‰) + x * \delta^{13}C_{organic\_carbon}\ (\text{-}xx\ ‰), \quad \text{Eq. 25}$$

This mass balance, yields the contribution of organic carbon of approximately 35%. The oxygen isotope data does not show a consistent pattern relative to the carbon isotope composition or the carbonate caprock, indicating that oxidation of organic carbon took place under varying hydrological conditions, or that the carbonates were later diagenetically overprinted.

In summary, the carbon isotope data of the carbonates are compatible with the hypothesis that the carbonate caprock formed as a result of the oxidation of organic matter (in conjunction with the co-precipitation of significant amounts of inorganic carbon), however, it does not provide proof that this process is tied to sulfate reduction. Interesting is to consider the impact of different oxidants on the potential for the formation of carbonates. Below, three different types of organic matter are considered, methane, acetic acid, and sugar, and how the oxidation reactions with sulfate and oxygen impact carbonate formation.

Oxidation with sulfate:

$$CH_4 + SO_4^{2-} => CO_3^{2-} + H_2S + H_2O \quad \text{Eq. 26}$$

$$CH_3COOH + SO_4^{2-} => 2HCO_3^{-} + H_2S \quad \text{Eq. 27}$$

$C_6H_{12}O_6 + 3SO_4^{2-} => 6HCO_3^- + 3H_2S$ Eq. 28

Oxidation with atmospheric oxygen:

$CH_4 + 2O_2 => CO_2 + 2H_2O$ Eq. 29

$CH_3COOH + 2O_2 => 2CO_2 + 2H_2O$ Eq. 30

$C_6H_{12}O_6 + 6O_2 => 6CO_2 + 6H_2O$ Eq. 31

Overall observations are that reactions with sulfate have a higher potential for carbonate formation (bicarbonate or carbonate is formed), while reactions with molecular oxygen tend to have a lower potential to form carbonates (carbon dioxide/carbonic acid is formed). This can be taken as an argument that sulfate reduction may have been an important factor in the formation of carbonate caprocks.

5.5.3 The Content and Isotope Composition of Carbonate Associated Sulfate as Indicator of the Role of Microbial Sulfate Reduction in the Formation of Carbonate Caprock

If the sulfur and oxygen isotope composition of CAS was significantly heavier than the isotope values for gypsum, the presumed sulfate-source, a conclusion could be drawn that during the precipitation of carbonate minerals, whereby the CAS becomes trapped, sulfate reducing microorganisms actively removed isotopically light sulfate. CAS for calcitic caprock (limestone) indicated a spread of 733 ppm to 1345 ppm, while the gypsum spread was as follows:

- Sulfur isotope composition in gypsum was 13‰ to 16‰
- Oxygen isotope composition in gypsum was 12‰ to 15‰
- CAS range for $\delta^{18}O$ in calcite was 16‰ to 20‰

- CAS range for $\delta^{34}S$ in calcite was 16‰ to 18‰
- CAS range for $\delta^{18}O$ in dolomite was 16‰ to 18‰

Figure 46 is a plot which represents the compilation of sulfur and oxygen data or CAS, indicating that microbial sulfate reduction likely caused enrichment of ^{34}S, ^{18}O and CAS. The sulfur and oxygen composition of gypsum ($\delta^{34}S$ and $^{18}O \approx 15‰$). Sulfur and oxygen isotopes fall into a narrow range, despite large variations in CAS content.

From these findings, it becomes evident that CAS did not become strongly enriched in ^{18}O or ^{34}S relative to the sulfate source, believed to by gypsum. It is possible that it was slightly enriched in ^{18}O and ^{34}S, a pattern that has been observed for microbialites, which are formed in marine environments, and where the formation process has been linked to the activity of sulfate reducing organisms (Heindel et al. 2012; Gischler et al. 2017). The latter form in open environments where sulfate is constantly supplied and removed by currents, a situation that efficiently suppresses strong enrichment in ^{34}S or ^{18}O, because isotopically light sulfate is re-supplied.

Noteworthy, is that the carbonate caprocks in Gypsum valley contain very little sulfate (345 to 1,345 ppm range for calcitic caprock and 7 to 256 ppm for dolomitic caprock), while the average sulfate range found in the Damon Mound region is 8,337 ppm (Labrado et al., 2018). This may point to a strong re-crystallization of the carbonates, which is observed in thin section, and is expected for dolomite because this is a well-ordered mineral. It may also point to rather low sulfate concentrations during the precipitation of the carbonates, which raises the question as to whether or not the carbonates were in close contact to gypsum while they formed. One possibility is that the carbonates formed some distance from the gypsum, which would allow for the dilution of sulfate derived from gypsum. It could also be speculated that the carbonates formed in freshwater,

which dissolves less sulfate than salt water (~2.4g/l in freshwater, ~6.8g/l in seawater,). Pure fresh water is virtually absent in the natural environment, because the interaction with other minerals and gases affect the pH. For example, atmospheric CO_2 dissolves and freshwater, forming carbonic acid which, increases the acidity, which would enhance the ability to dissolve sulfate minerals.

In summary, the isotope composition of CAS does not provide unambiguous evidence for the activity of sulfate-reducing bacteria during carbonate caprock formation. If sulfate reducing bacteria were involved in the formation of carbonate caprock in Gypsum Valley, the system would have been open with respect to sulfate loss, causing the isotope composition of dissolved sulfate in the system – and thereby the sulfate trapped as CAS – to display values closed to those from gypsum.

5.5.4 Sulfurized Organic Matter – The Hidden Fingerprint of Sulfate Reduction at Gypsum Valley

Organically bound sulfur is an indicator for the early diagenetic incorporation of sulfide (H_2S) into organic matter (OM), a process frequently observed in organic-rich marine sediments (Riedinger et al., 2017; Wehrmann et al., 2017; Francois, 1987; Kohnen et al., 1989; Vairavamurthy and Mopper, 1987; Mossmann et al. 1991; Ferdelman et al., 1991). After digestion with hydrochloric acid to liberate CAS, the sulfur content and isotope composition of the organic matter left in the residue was analyzed. For a number of samples, the sulfur-carbon (S/C) ratio of the sample exceeded a ratio 0.1, and the sulfur isotope composition scattered around -20‰, which is clear indication for the addition of sulfur from sulfide to organic matter (Bein et al., 1990; Böttcher et al., 2006). However, there was also a number of samples that displayed S/C ratios exceeding 1,

with sulfur isotope compositions between -4‰ and +12‰ (Figure 44). Such an enrichment of organic matter in sulfur does not appear reasonable. Therefore, it was speculated that the samples may have contained barite ($BaSO_4$), an insoluble sulfate mineral. To test this, a strong chelator, DTPA, was used to dissolve and re-precipitate barite (Bao, 2006). The DTPA extraction method did not reveal the presence of barite, and the cause for the high sulfur contents remains unresolved.

In summary, isotopically light sulfur bound to organic matter was found in multiple samples, which is evidence for the presence of sulfide at some time during the sedimentary and burial history of organic carbon. While the presence of sulfide strongly indicates past activity of sulfate reducing organisms, it is not entirely certain if this happened during the formation of carbonate caprocks, or at some other stage. For example, the sulfur-rich organic matter may have been transported with the hydrocarbons to the site where carbonate caprock formed. Therefore, isotopically light sulfur bound to organic matter cannot be considered definitive evidence for the involvement of sulfate reducing bacteria in carbonate caprock formation.

6. CONCLUSIONS

For oil and gas exploration, carbonate caprocks associated with salt diapirs are important for several reasons: they can act as reservoirs or conduits for hydrocarbons, and their miss-identification as carbonate lithologies belonging to the stratigraphy of the sedimentary sequences adjacent to the diapir, which can jeopardize the accurate interpretation of seismic profiles. Much of today's understanding of caprocks – in particular of their geochemistry – is heavily influenced by observations from salt diapirs found along the US Gulf Coast salt diapir province, which comprises the famous Spindletop oil field. Another salt diapir province in the United States, the Paradox Basin, hosts several salt diapirs that are associated with carbonate caprocks. This study explored carbonate caprock from one of these diapirs, the Gypsum Valley salt wall. The aim was to assess the differences and commonalities in carbonate caprock lithology and geochemistry between the commonly accepted concepts and the Gypsum Valley setting.

Compared to the thickness of the carbonate caprock, smaller than 23m at the Mary Jane locality in Gypsum Valley, it appears that the carbonate caprocks form the US Gulf Coast, tend to be thicker. For those localities, it was observed that "some limestone bodies are more than 100 feet thick" (~30m, Fenneman, 1906), and the thickness for well-documented examples, such as Damon Mound, TX (maximum ~77m; Prikryl et al., 1988) or for Sulfur Dome, LA (~140m; Kelley, 1925) is well beyond of what is observed at the Gypsum Valley salt wall. With regards to the internal stratigraphy, the carbonate caprock units of the US Gulf Coast diapirs is commonly divided into an upper variegated calcite cap and a lower banded calcite cap, the latter sometimes being referred to as "zebra-textured zone" (Posey and Kyle, 1988b). The band thickness appears to vary between different domes, for example from 1-10cm at Tatum Dome, MI (Saunders et al., 1988) to less than 1.2cm at Richton Dome, MI (Werner et al., 1988). Little information is available regarding these

banded units – particularly if these banded units are bundled in benches; however, a photograph of an outcrop at Damon Mound (Machel, 2001), displays benches likely up to 20cm thick, which can be clearly discerned in a zone that might correspond to the banded calcite cap; although, it must be noted that the banded calcite is considered to be rare (Prikryl et al., 1988).

In Gypsum Valley, one of the key outcrop features are individual carbonate caprock benches. With the help of a new caprock fabric classification scheme (Table 1), these benches can be bundled into groups, which may then be correlated from one transect to groups identified in other transects (Figure 14). An attempt at developing such a correlation resulted in the finding of a generalized, tentative carbonate caprock succession for the Mary Jane study area that is dominated by massive fabrics at the contact to the gypsum, followed, in the direction to the overlying Chinle Formation, by brecciated, layered, brecciated and finally again massive fabrics. It is interesting to note that there is a variation in the abundance of fabrics that typically all fall into the 'Layered' category, with the zebraic lithology as prime example. Zebra-caprock can be found at Bridge Canyon and in transect I and II, which may represent an equivalent position with respect to the Bridge Canyon Salt Shoulder, whereas profile III is offset towards the axis of the salt wall (i.e. closer to the neck of the salt shoulder). This varied distribution in Mary Jane Draw could indicate that some areas are affected by more caprock-forming stages than others. Correlating caprock fabrics can be improved by including more profiles and better fabric categorization in the field, however, already this initial attempt demostrates that there may be an internal stratigraphy to the seemingly chaotic nature of caprocks in Gypsum Valley, and that this stratigraphy is likely different to the one from the US Gulf Coast salt diapirs, to the degree where it is possible that even a geologist familiar with the stratigraphy of carbonate caprock from the US Gulf Coast may not immediately recognize carbonate caprock at the Gypsum Valley salt wall. The new classification scheme, which is based

on fabric and not the mineralogy or rock chemistry, will continue to undergo development (Poe, et al. 2018a; Poe, et al. 2018b), and will enable researchers to effectively compare caprock observations.

Dolomite is an abundant carbonate caprock lithology in Gypsum Valley – likely equal in abundance to calcitic caprock (limestone). This is in stark contrast to the carbonate caprocks associated with the US Gulf Coast salt diapirs, where dolomite is often a rare accessory mineral. The description of Spindletop caprock included abundant dolomite; however, it has been proposed that the Spindletop dolomite was misidentified calcite (Barton and Paxson, 1925). The observation of abundant dolomite in the Gypsum Valley carbonate caprock raises two questions. First, is the dolomite, or its precursor (proto-dolomite, for a review see Petrash et al., 2017) a mineral that formed early, i.e. 'primary' in the conversion of sulfate caprock (gypsum and/or anhydrite) to carbonate caprock, or is it a mineral that replaced calcite, i.e. is it 'secondary dolomite'? Second, if the origin of dolomite is 'primary', what does this imply with regards to the system in which the carbonate caprock formed? The first question is important because, canonically, dolomite is presumed to be of secondary origin, coinciding with the assumption that the dolomitization process caused an increase in porosity, which would have implications for the permeability and porosity of carbonate caprock. Secondary dolomite was undeniably found in several samples taken from Mary Jane Draw; however, the vast majority of dolomite found is microcrystalline, and the dolomite grain sizes that are generally smaller than those observed for the calcitic caprocks. Additionally, the porosity of the dolomite samples is far below the classical $\leq$ 12% dolomite porosity usually attributed to secondary dolomite. The carbon isotope composition of the dolomite is similar to that of the calcitic caprocks, indicating that either lithology could have been formed from the oxidation of hydrocarbons. Also, the comparison of the oxygen isotope composition of

dolomite to calcitic samples indicates that the oxygen isotope composition of fluids from which the minerals formed may have been similar – again not providing evidence that calcite was replaced by late-stage dolomite. Consequently, it was not possible to conclude that the microcrystalline dolomite is primary, but there is a strong possibility that this is indeed the case.

The second question, namely the implication of primary dolomite for the system in which the carbonate caprock formed, is tightly linked with the central question of this project: What is the Role of Sulfate Reducing Microbes in the Formation of Carbonate Caprock at the Study Area Located in the Paradox Basin? The canonical understanding of carbonate caprocks is that sulfate reducing microorganisms are responsible for carbonate caprock formation, by catalyzing the replacement of sulfate minerals with carbonate through sulfate reduction, which not only removes sulfate but also enables the simultaneous oxidation of hydrocarbons into carbonate. At Gypsum Valley, none of the typical indicators for this process were found. Pyrite or native sulfur, two minerals the are expected to be observed in rocks that were formed while sulfide was produced by sulfate reducing bacteria, are absent. Carbonate associated sulfate – which should be incorporated into carbonate rocks that form in an aqueous environment in which sulfate is available for sulfate reducing bacteria – was only detected in small quantities, and it was not enriched in ^{34}S relative to gypsum as would typically be expected if these organisms were active. The only evidence for the activity of sulfate reducing bacteria was found in the form of isotopically light sulfur, associated with organic matter, which is indicative of the addition of isotopically light sulfide to organic matter.

Presuming that sulfate reducing bacteria were responsible for carbonate caprock formation at the Gypsum Valley salt diapir, the observed geochemical patterns can only be explained by a setting in which only a minor portion of sulfate that was delivered from gypsum dissolution was reduced

to sulfide, while the remaining sulfate was removed by diffusive or advective transport. Such an open system could maintain low sulfate concentrations, as well as, little or minor enrichment of sulfate in ^{34}S relative to sulfate from gypsum, (Figure 46), while sulfide is depleted in ^{34}S relative to sulfate. Sulfide that is not transported away in such a system can, in fact, react with organic matter, a process that can be more rapid than pyrite formation. Finally, the 'open-system' scenario is also compatible with the formation of primary dolomite, as it would allow for the supply with magnesium.

Taking these arguments together, the conclusion is that the formation of carbonate caprock at the Gypsum Valley salt diapir was the result of a multi-stage process that was tied to the oxidation of hydrocarbons in conjunction with microbial sulfate reduction. An open system, potentially caused by advective fluid flow, provided magnesium and silica that enabled the precipitation of primary dolomite and silicification, while removing sulfide and sulfate. Supply with fluids also triggered the dissolution of sulfate minerals, and phase transitions between anhydrite and gypsum, resulting in rock deformation. This could explain the amazing richness and diversity in caprock fabrics found in Gypsum Valley, which constitutes the 'open-system' end member of geochemical settings that are conducive to carbonate caprock formation.

7. TABLES

Table 1. Caprock Fabric Classification Scheme Utilized in this Study.

Fabric Name	Massive	Porphyritic	Layered			Brecciated	
Sub-fabric			Laminated		Banded	Mosaic	Disorganized
			Micro-Laminae	Zebra			
Description	>30 mm; single crystal size or homogenous	>30 mm; cluster of crystals in a finer grained matrix	1-3 mm scale laminae	3-10 mm thick laminae; distinct bands of light and dark crystals	>10 mm layers	Minimal dislocation of clasts	Apparent dislocation of clasts
Modifiers			Enterolithic, Broken, Sigmoidal Porphyritic			Angular or Rounded; Polymict or Monomict	

Table 2. Caprock Fabrics for Investigated Samples.

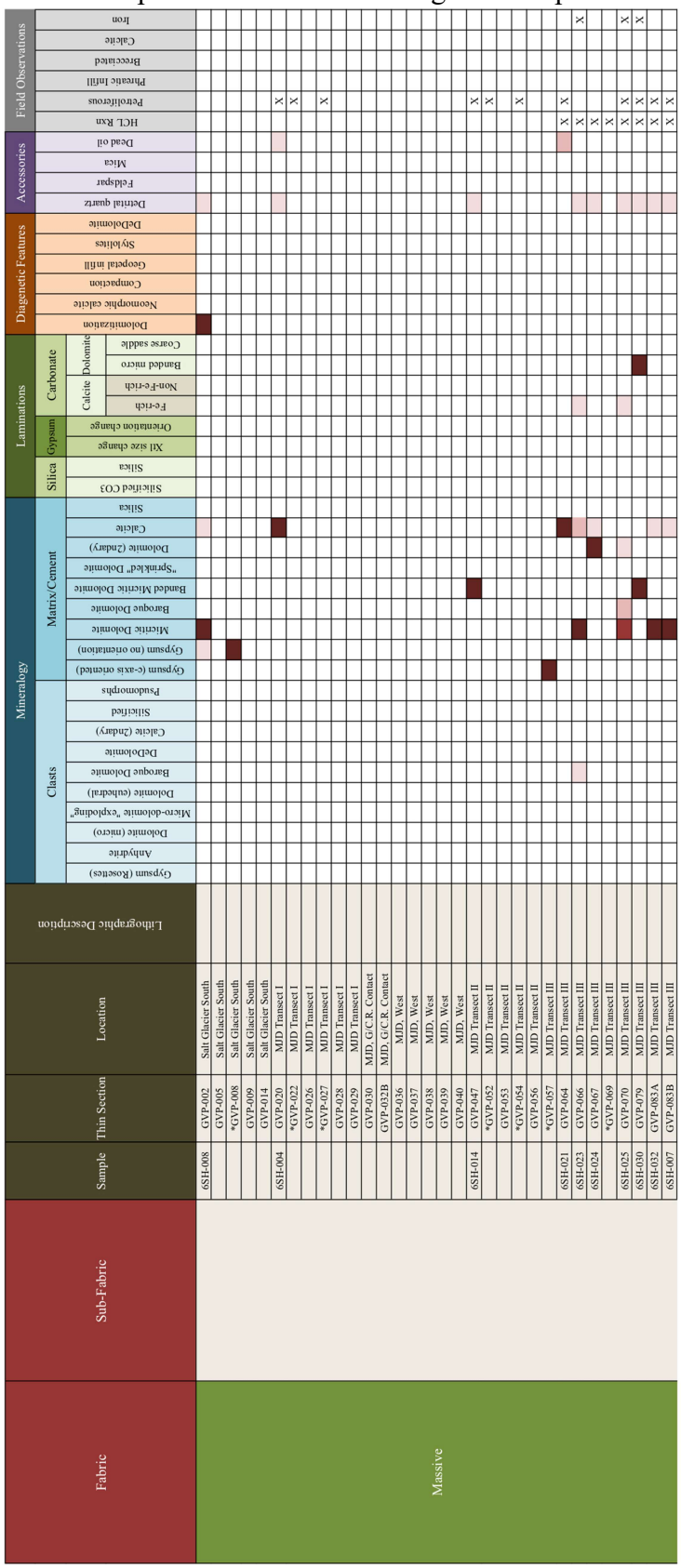

Table2 continued. Caprock Fabrics for Investigated Samples

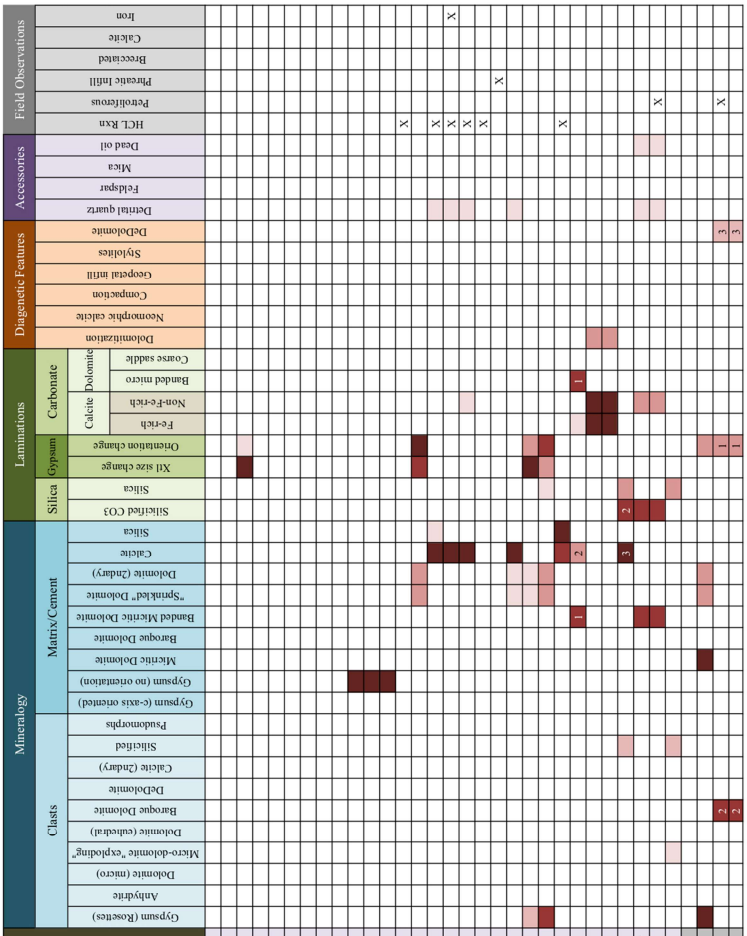

Table 2 continued. Caprock Fabrics for Investigated Samples

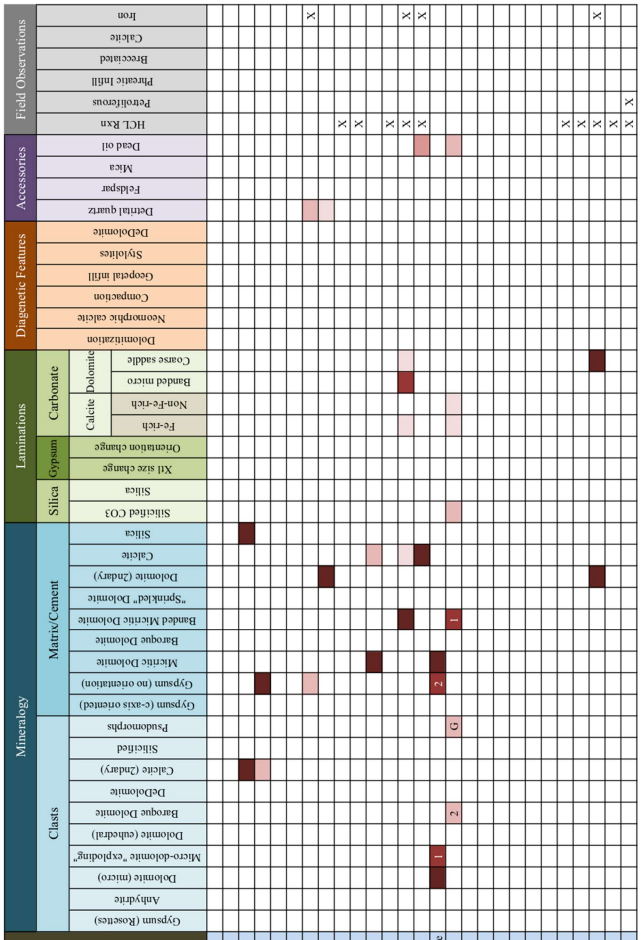

8. FIGURES

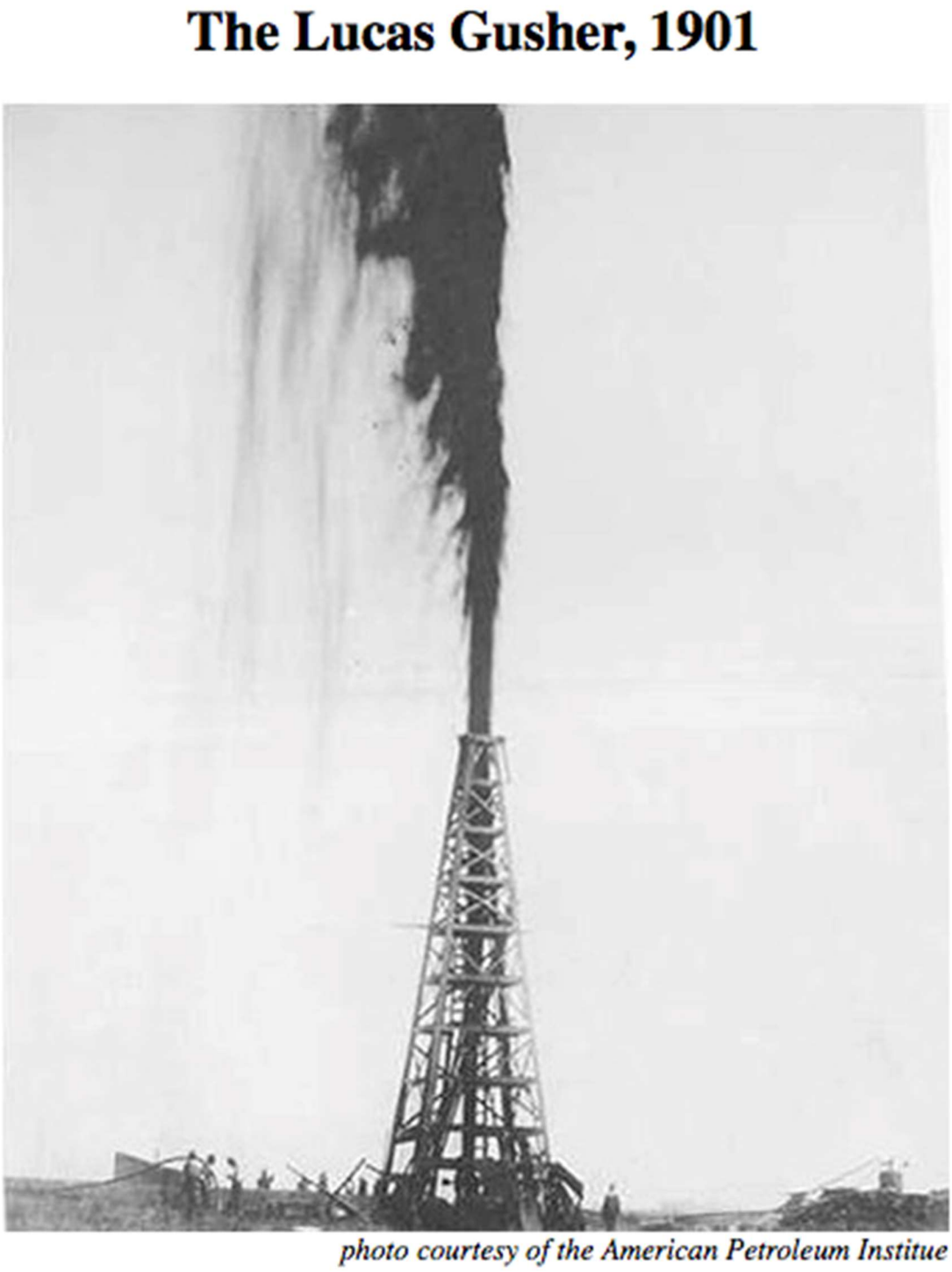

Figure 1: Lucas Gusher, 1901.

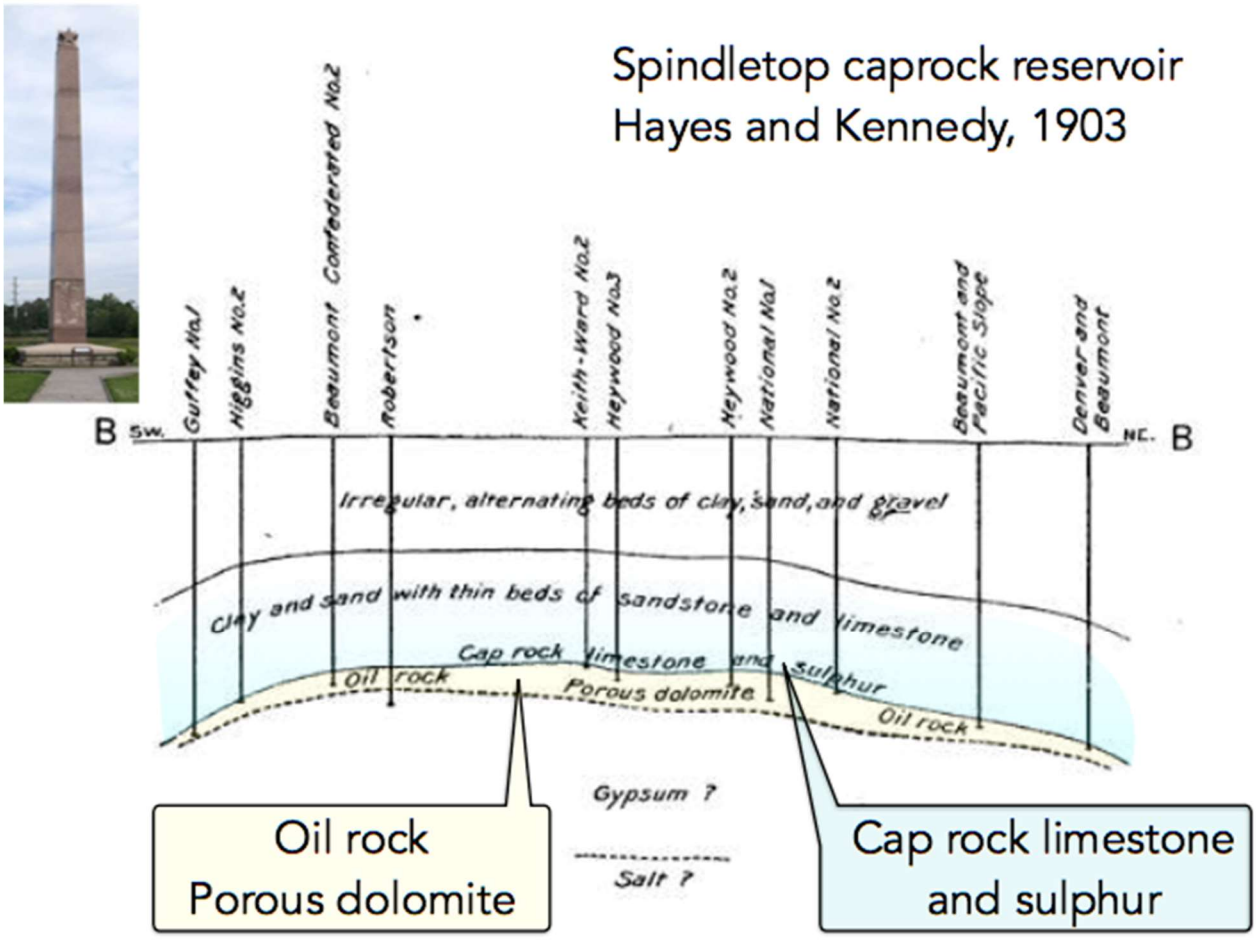

Figure 2: Spindletop, 1903.
The Spindletop carbonate caprock consists of porous dolomite and of limestone associated with native sulfur. (Hayes and Kennedy, 1903).

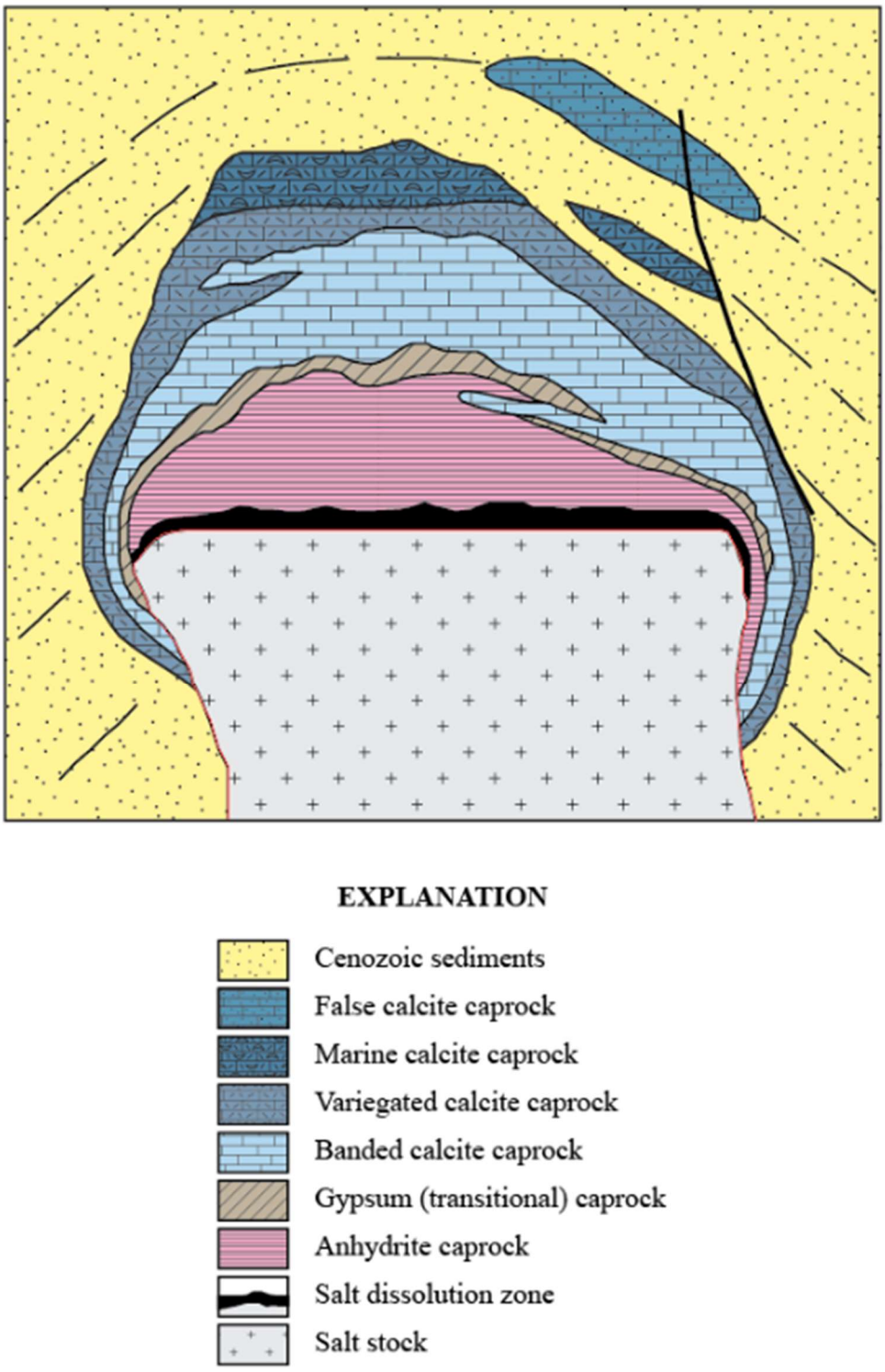

Figure 3: Sketch of a Gulf Coast salt dome with generalized caprock lithologic zonation. Modified from Enos and Kyle (2002), Redrafted by Gannaway, 2014.

Figure 4: Generalized map of the location of Paradox Basin.
Source: www.rigzone.com.

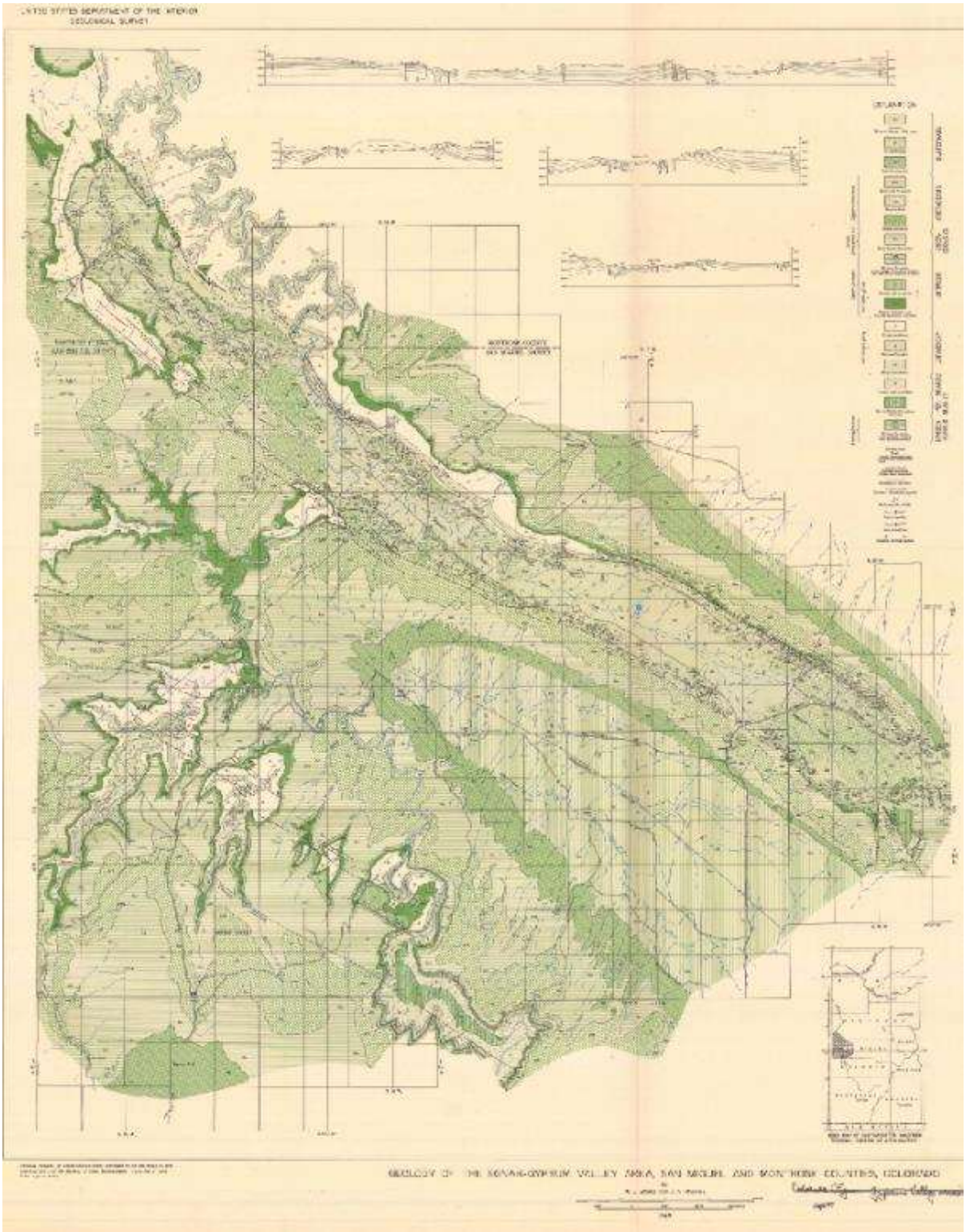

Figure 5: Geologic map of Gypsum Valley. USGS, 1948.

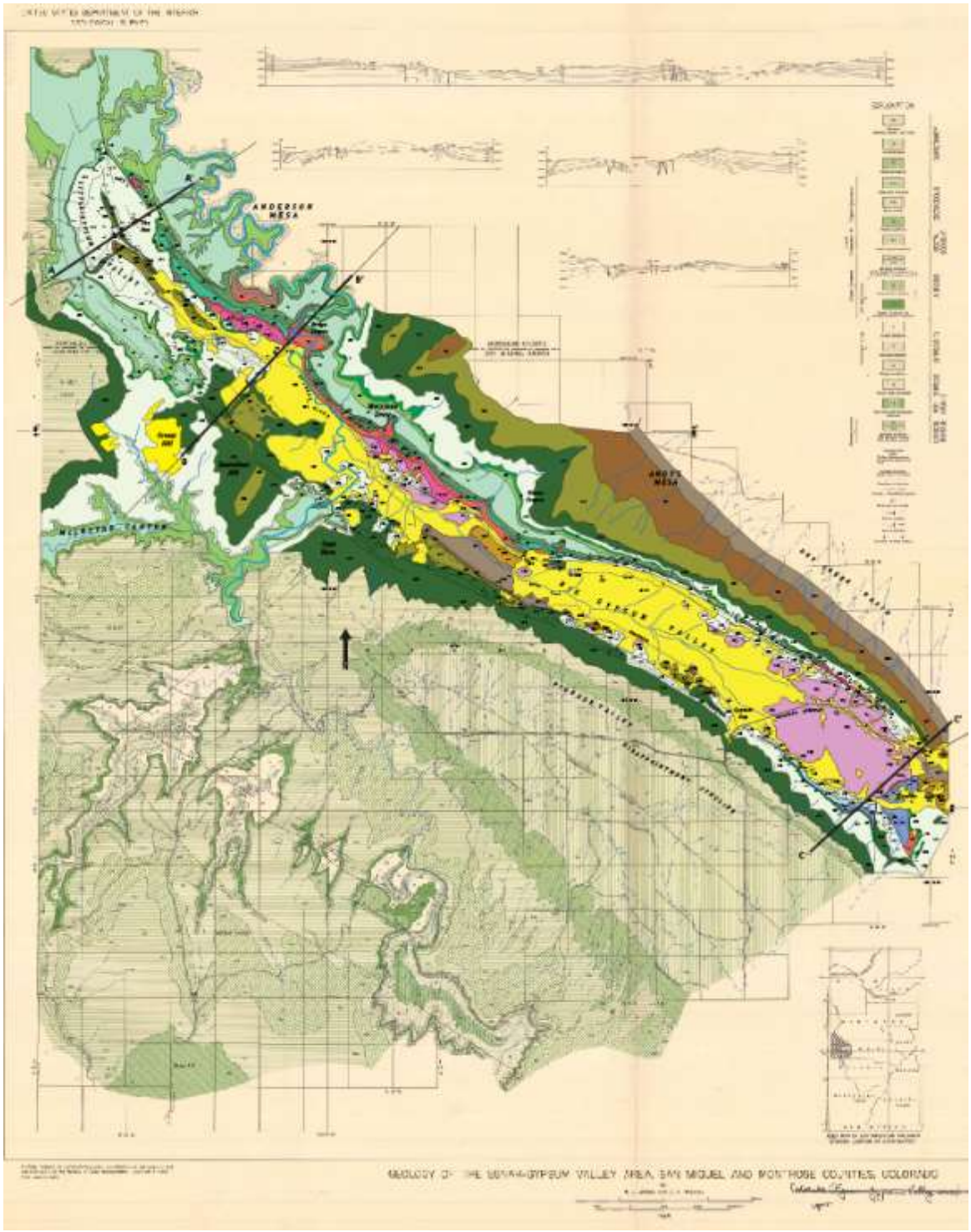

Figure 6: Geologic map of Gypsum Valley - Redrafted by Deatrick and McFarland, 2013.
This map has been redrafted in order to highlight the major geologic formations of Gypsum Valley.
For stratigraphic column, see Figure 7.

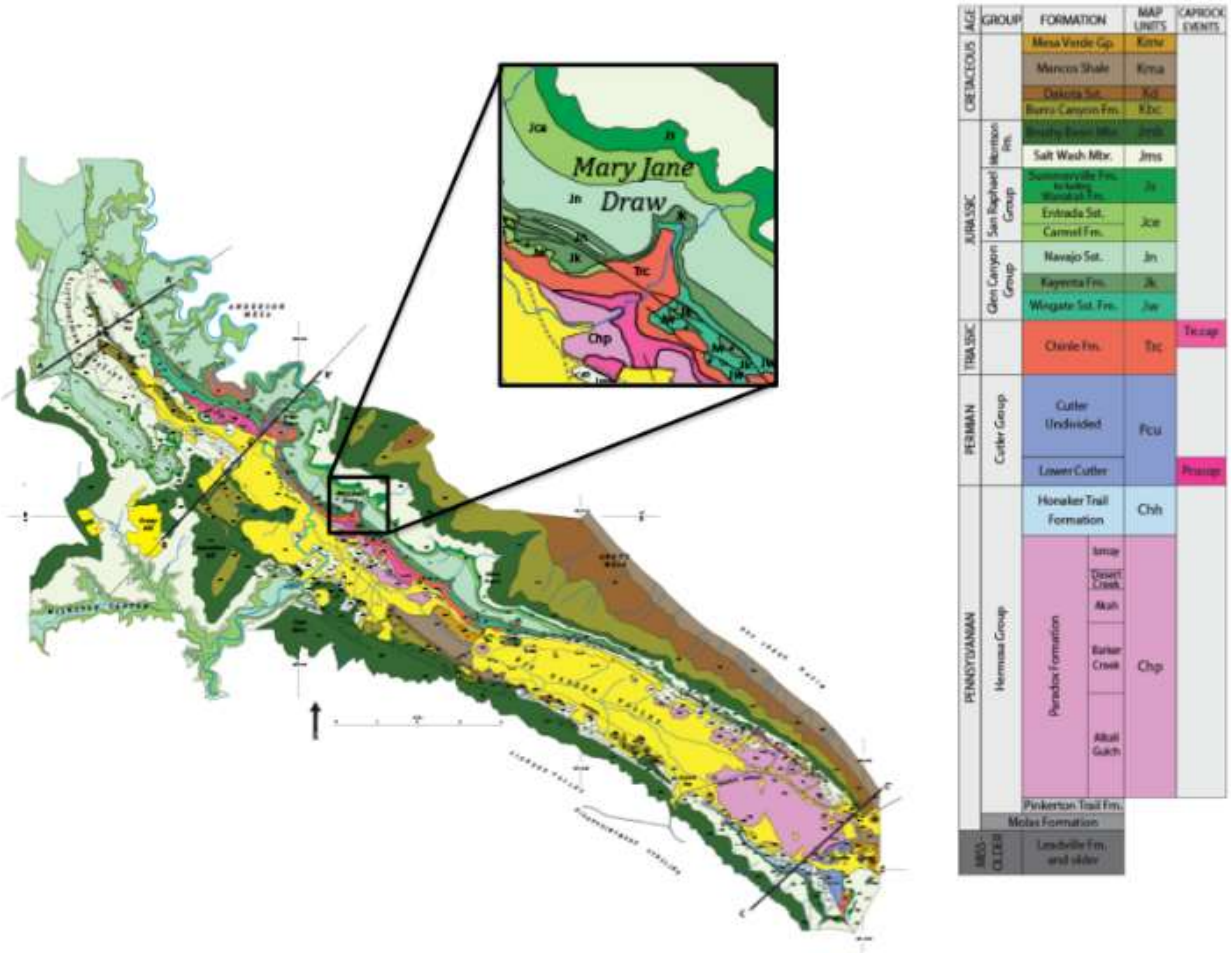

Figure 7: Enlarged map of Gypsum Valley.
This map is the Gypsum Valley portion of Paradox Basin and includes a zoom-in of the study area including a stratigraphic profile. Deatrick and McFarland, 2013. Right – Stratigraphic column. The yellow color in the map refers to Quarternary alluvium.

Figure 8: Panoramic view of a part of the study area.
The Mary Jane Draw is to the left of the photograph. Note the delineation between gypsum (light gray foothills), carbonate caprock (greenish – tanned slopes with sparse vegetation) and overlying siliclastics (at base, red, followed by yellow-red alternating beds).

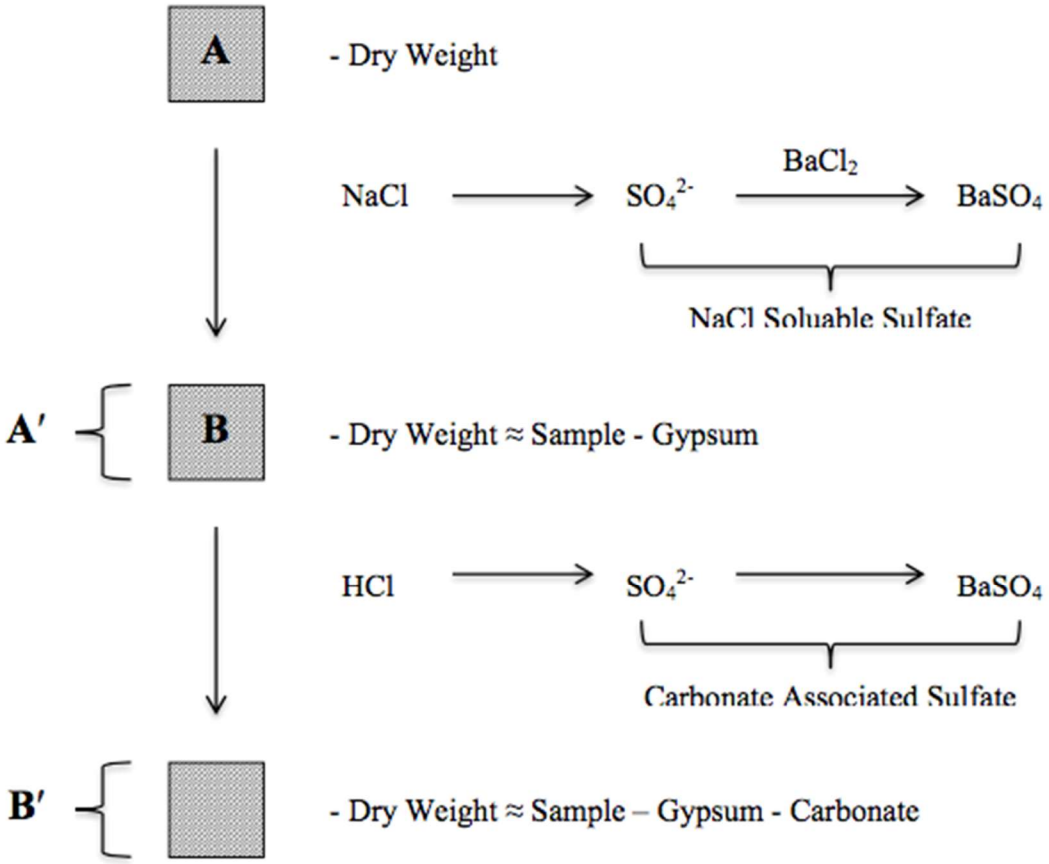

$CaCO_3^{2-}$

$CaSO_4^{2-}$ → $Ca^{2+} + SO_4^{2-}$ (traces)

Weight

A-A′ = Weight of what has been removed. Assumption: removed mineral is gypsum.

→ Calculated mols of gypsum removed.

→ $CaSO_4 \cdot 2H_2O$

= Released SO_4^{2-}

Weight of $BaSO_4$ from NaCl step = mols of precipitated SO_4^{2-}

Figure 9: Schematic representing the sequential leaching process.

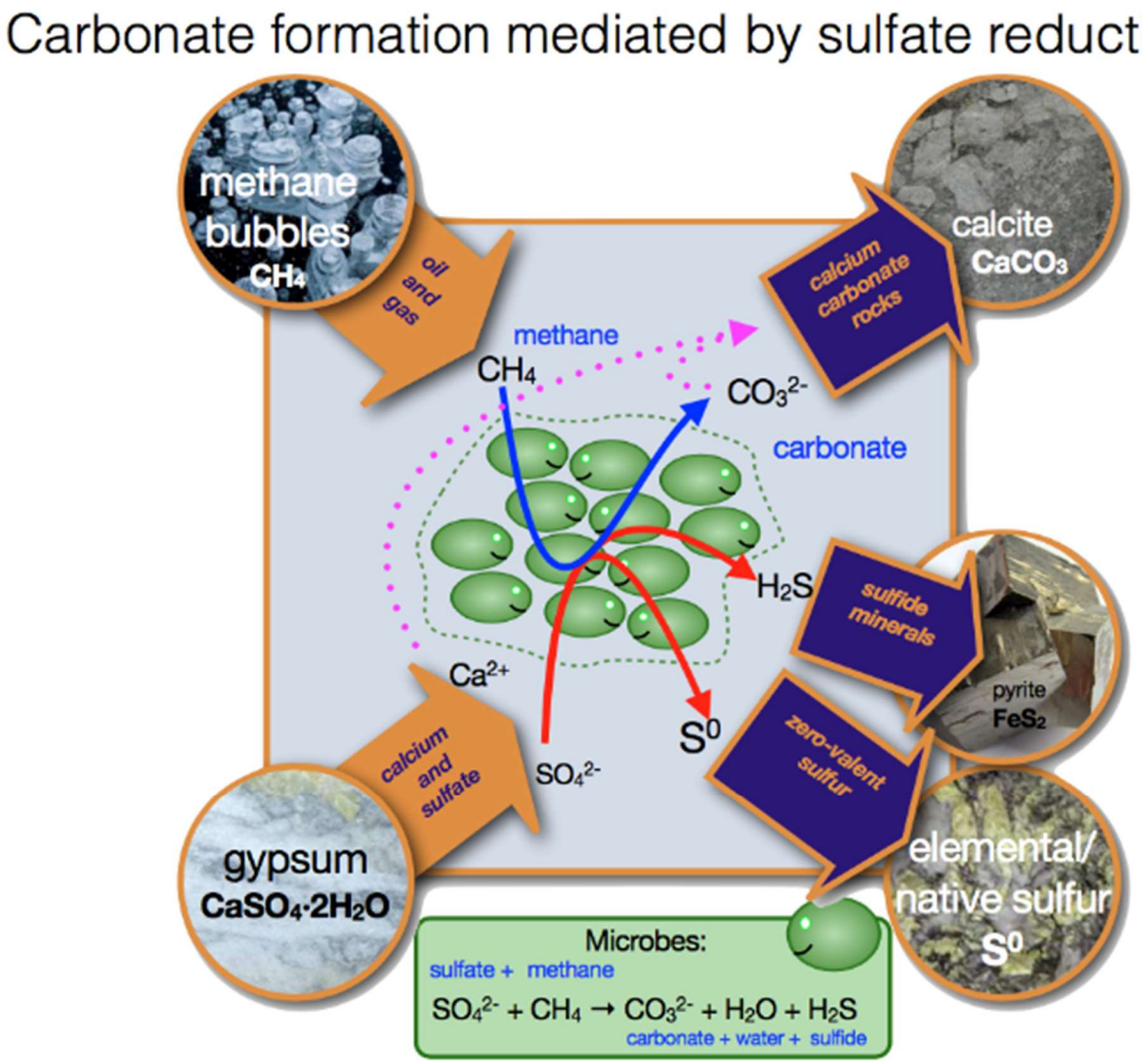

Figure 10: Schematic Box Model illustrating effects in caprock formation.
In an open system, magnesium and iron enters from oil-bearing formations. Meteoric waters could be a source for silica (H_4SiO_4), while the sulfur in gypsum ($CaSO_4{\cdot}2H_2O$) could be a sulfate source. Saline brine from sodium chloride dissolution could have an impact – if the system becomes too saline, microbes will not operate effectively. There is an isotope offset between the sulfide that was produced and the sulfate that was left over. Organic sulfur is a proxy for the isotope composition of hydrogen sulfide (H_2S) that was produced. Carbonate associated sulfate records the isotope composition of sulfate in the system, revealing if microbial sulfate reduction was active. Carbon isotope analysis reveals if additional carbon sources other than oil or methane were involved in the formation of carbonate.

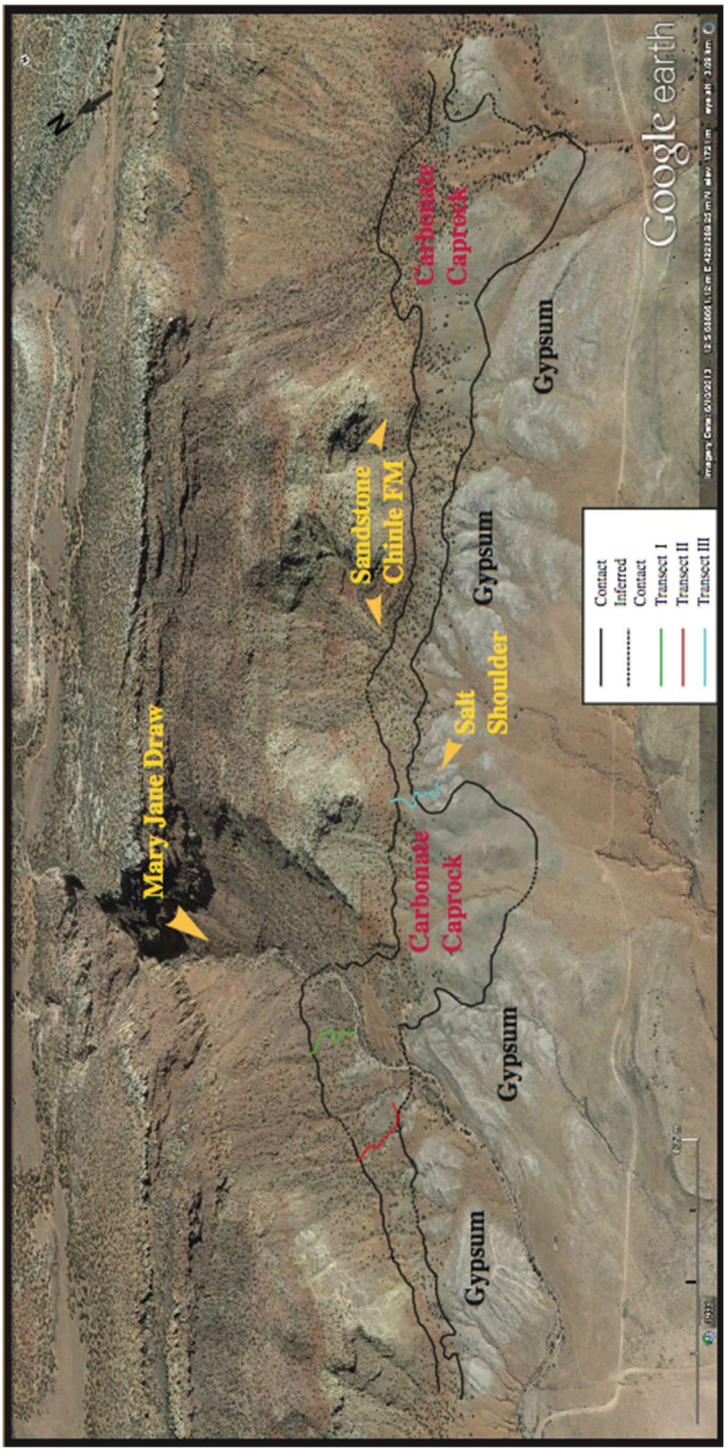

Figure 11: Google Earth image of the study area, illustrating orientation, the gypsum/caprock contact and the caprock/sandstone contact.

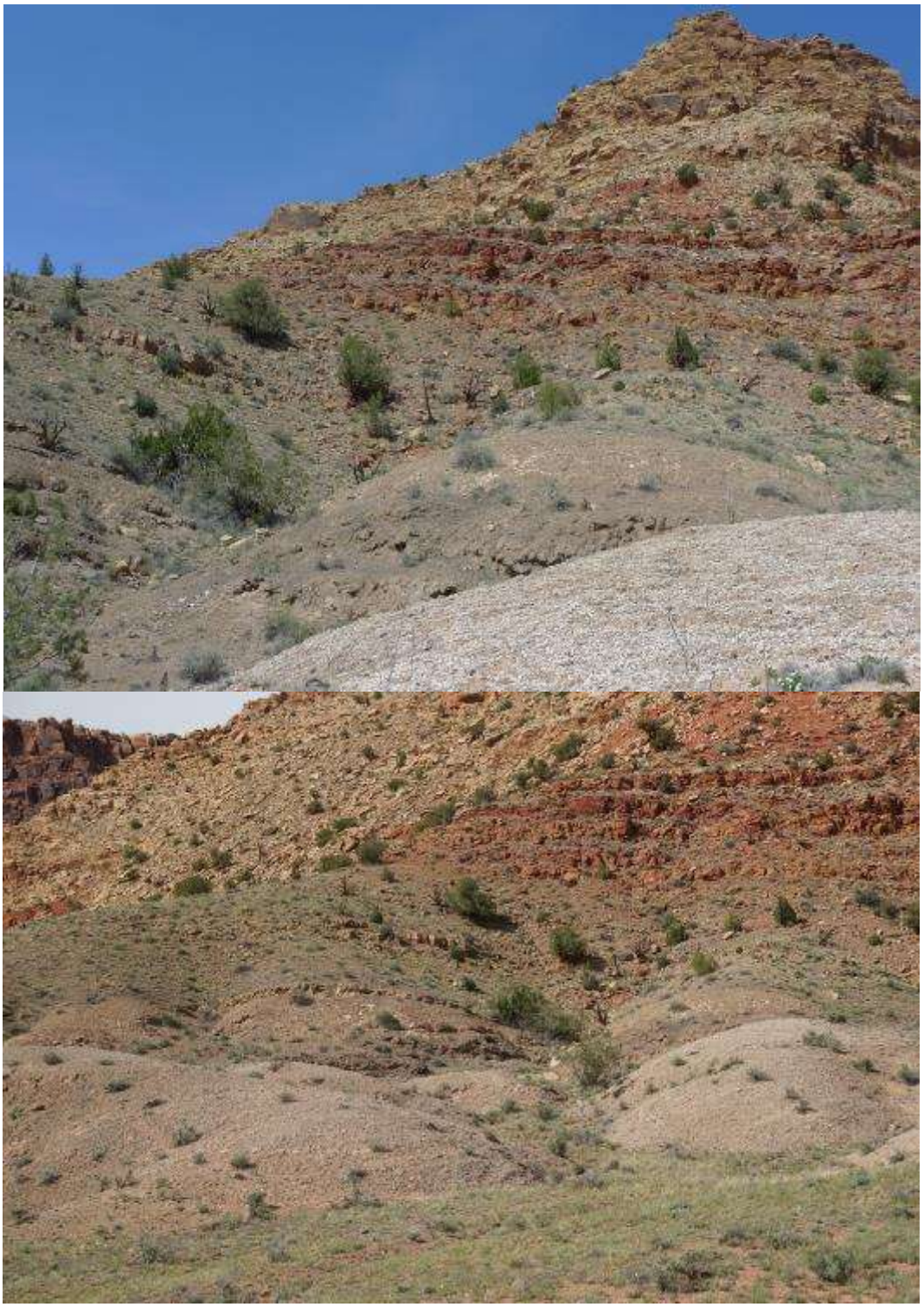

Figure 12: Photographs of the main part of the study area.
Note the delineation between gypsum (light gray foothills), carbonate caprock (greenish – tanned slopes with sparse vegetation) and overlying siliclastics (at base red, followed by yellow-red alternating beds).

Figure 13: The Conchita Member.
One of the thickest benches found in the study area was nicknamed the ‘Conchita Member’. Several benches are apparent in this photo; the ‘Conchita Member’ is the large tan-colored bench. Also apparent in the photograph is boudinage deformation.

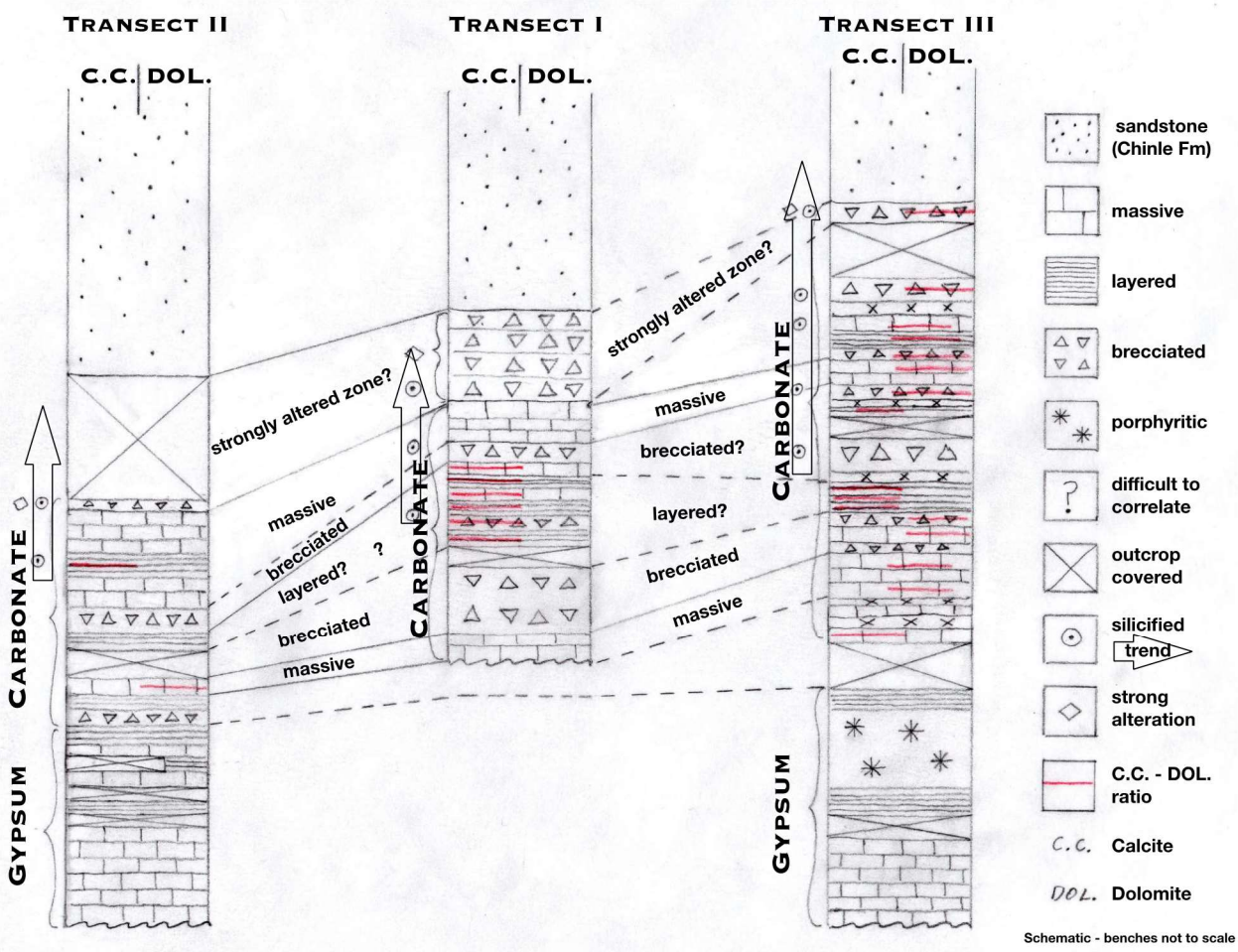

Figure 14: Schematic representation of fabrics from W to E in Mary Jane Draw.
Total thickness of carbonate caprock in transect II is 20m, transect I is 22m (not outcropping, inferred from projections), and transect III is 19m. Correlatable is an increase in silicification toward the contact with the sandstone (indicated by arrow), and bench groups that are predominantly massive. Using these correlations, one can further infer correlation of brecciated bundles, and potentially a layered central package.

Figure 15: Photograph representative of the Massive fabric utilized in the new fabric classification scheme.

Figure 16: Photograph representative of the Brecciated fabric utilized in the new fabric classification scheme.

Figure 17: Photograph representative of the Layered fabric utilized in the new fabric classification scheme.

Figure 18: Photograph representative of the Porphyritic fabric utilized in the new fabric classification scheme.

Figure 19: Deformation: this photograph is representative of a Layered main fabric, Micro-Laminae sub-fabric and Enterolithic modifier.

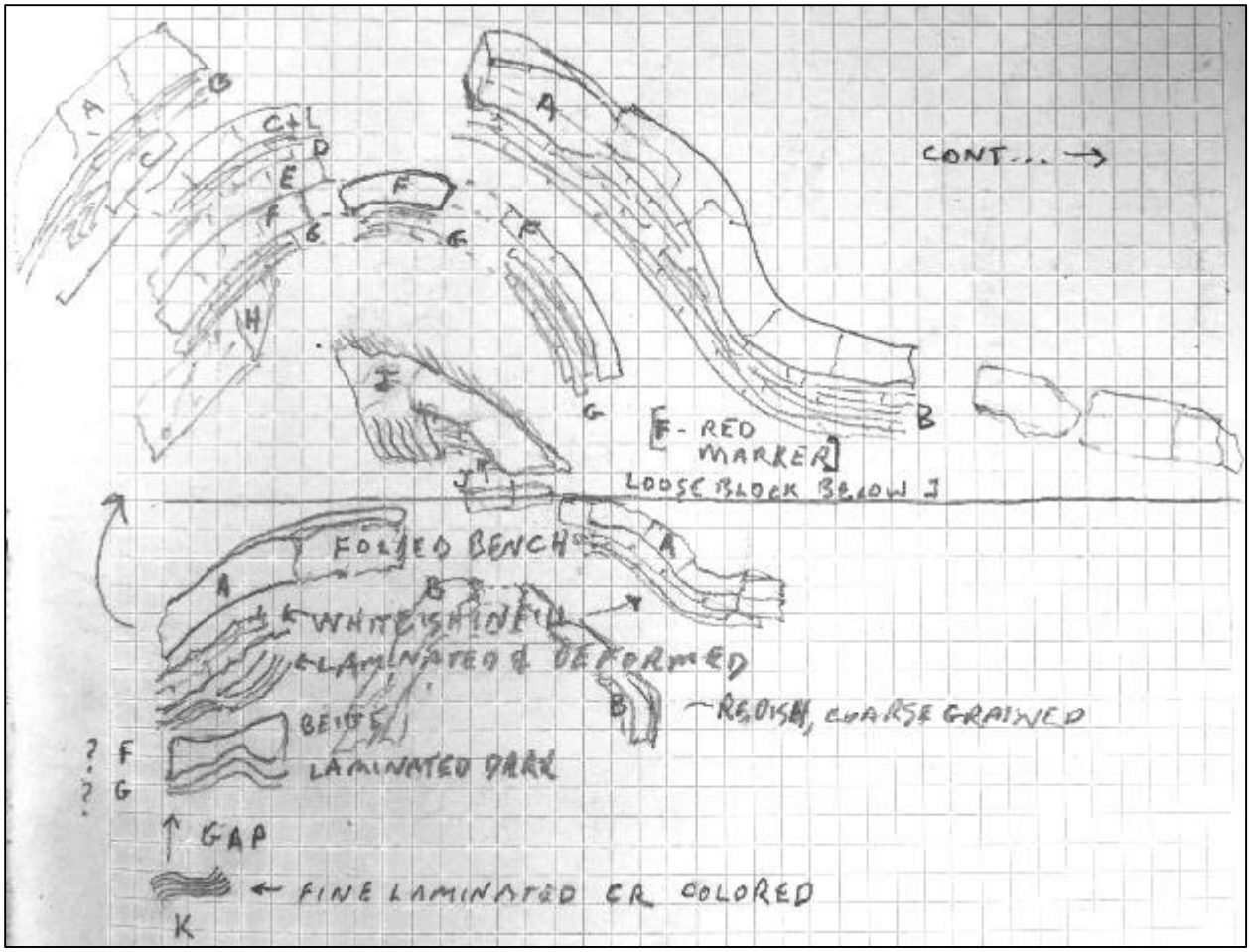

Figure 20: Deformation: this sketch is representative of folding found in the study area.

Figure 21: Deformation: this photograph is representative of folding found in the study area This (and at A as denoted in figure 20) is the right arm of a fold that collapsed at the top and then continues on the left (not pictured).

Figure 22: Deformation: this photograph is representative of folding found in the study area.

Figure 23: Deformation: this photograph is representative of the shear bands (sigmoidal) found in the study area.

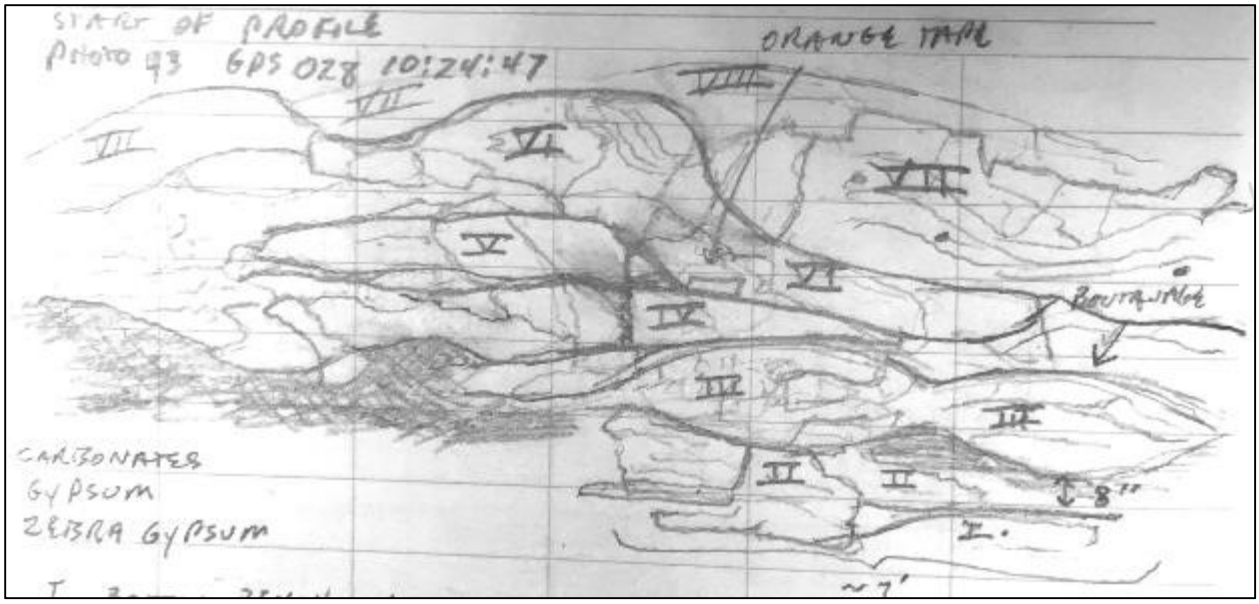

Figure 24: Field Drawing of the Multi-Outcrop.

Figure 25: Photograph of the Multi-Outcrop.
This outcrop (see also sketch, Figure 24) is an excellent example of the extensive carbonate caprock variability – both with respect to fabric as well as bench thickness – found in the study area.

Billet:

Field Observations:
Bottom bench with deformed zebra gypsum in middle. Black carbonate marl at the top. Solid ~10" thick, Petroliferous carbonate.

Thin Section:

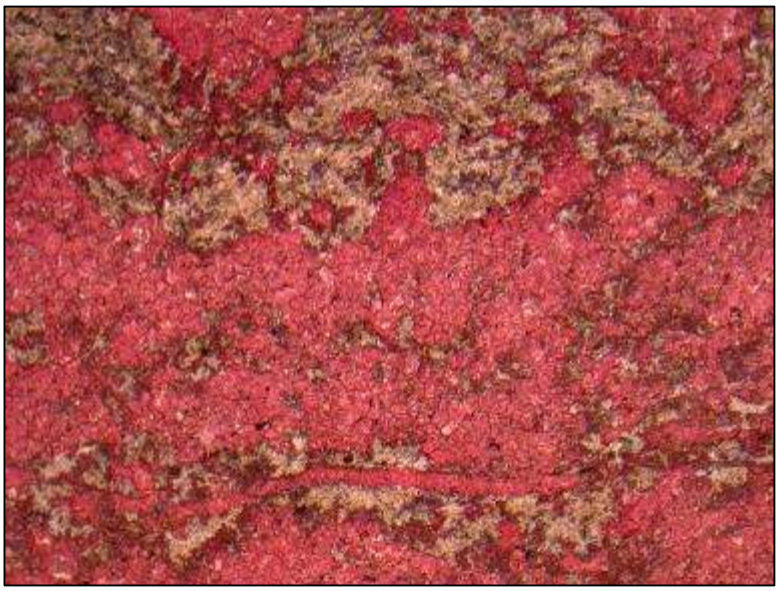

Petrographic Observations:
4X, plain light, stained.
Brown areas (opaline silica) was prob. gypsum - now silicified quartz & microcrystalline chert. May have OM. Calcite is coarse & is prob. a replacement of gypsum. Calcite may have filled the fractures & all calcite is recrystallized. Primary fabric was likely dolomite, but none was preserved. Grain size ranges from 1 hash mark to 3.5 hash marks. 82% coarse, recrystallized calcite, 15% opaline silica, 2% chert, 1% quartz.

Figure 26: KL-GVP-015/6SH-010 (8-unit profile – Profile I) *Calcite w/ Silicified Gypsum*.

Billet:

Field Observations:
~24" thick – thins to 7-8". Very petroliferous (fetid) where thin, slightly petroliferous where thick. Zebra gypsum at top of bench.

Thin Section: 4X, cross polars, stained.

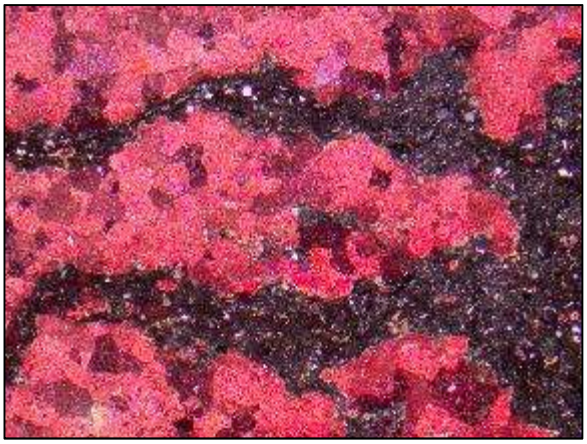

Thin Section: 4X, plain light, stained

Petrographic Observations:
4X, cross polars, stained. Probably the same as KL-GVP-015 (above). Brown areas in plain light (opaline silica) was prob. gypsum - now silicified quartz & microcrystalline chert. May have OM. Calcite is coarse & is prob. a replacement of gypsum. Calcite may have filled the fractures & all calcite is recrystallized. Primary fabric was likely dolomite, but none is preserved. Grain size ranges from 1 hash mark to 3.5 hash marks. 84% coarse, recrystallized calcite, 13% opaline silica, 2% chert, 1% quartz.

Figure 27: KL-GVP-016-II/6SH-003 (8-unit profile – Profile I) *Calcite w/ Silicified Gypsum*.

Hand Sample:

Field Observations:
Orange tape (in reference photo – not attached here). Light weathered color, rounded clasts but also platy. 1-2 cm clasts – up to 5cm. Lighter colored carbonate, not petroliferous (with exception of clasts) ~14" thick, left. ~7" thick on right. Phreatic infilling

Thin Section:

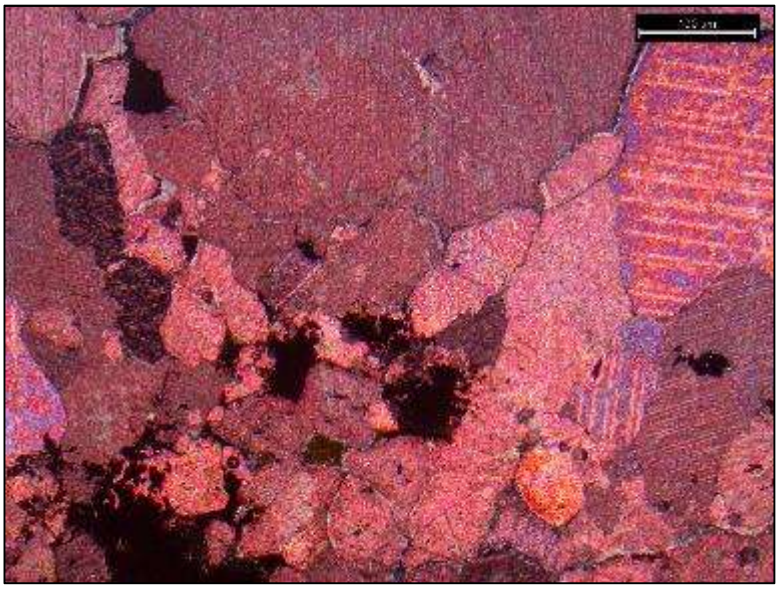

Petrographic Observations:
4X, cross polars, stained. Recrystallized calcite. Angular grains, cross hatch pattern on many grains, calcite, unit extinction, a few instances of twinning, high birefringence in some grains, rim cementation on a few grains. Grain size ranges from 1 hash mark to 2 mm. 99% recrystallized calcite, 1% iron oxide (opaque).

Figure 28: KL-GVP-018/6SH-011 (8 unit profile – Profile I) *Recrystallized Calcite*.

Billet:

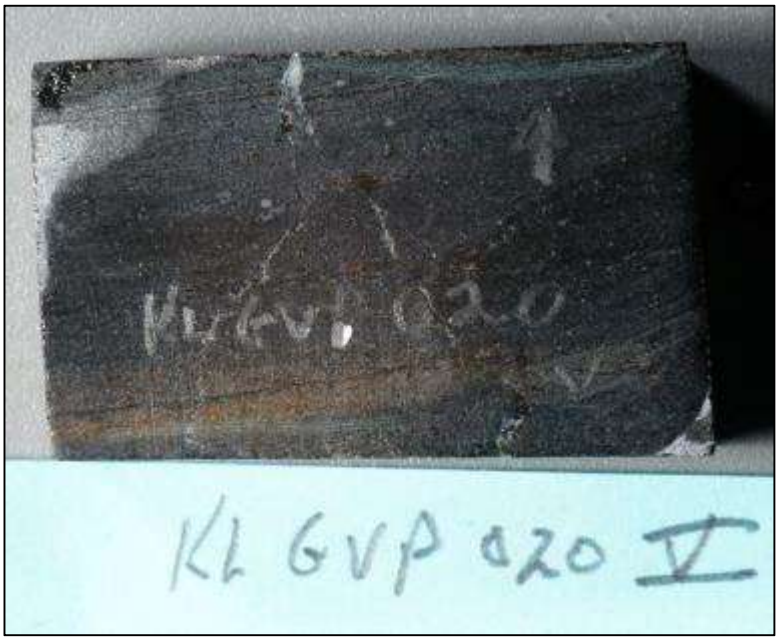

Field Observations:
Dark laminated carbonate, petroliferous, to the left side it becomes a prominent bench ~19" thick, calcite crystals on right side – diagenesis could have been much later, zebra gypsum on left side.

Thin Section:

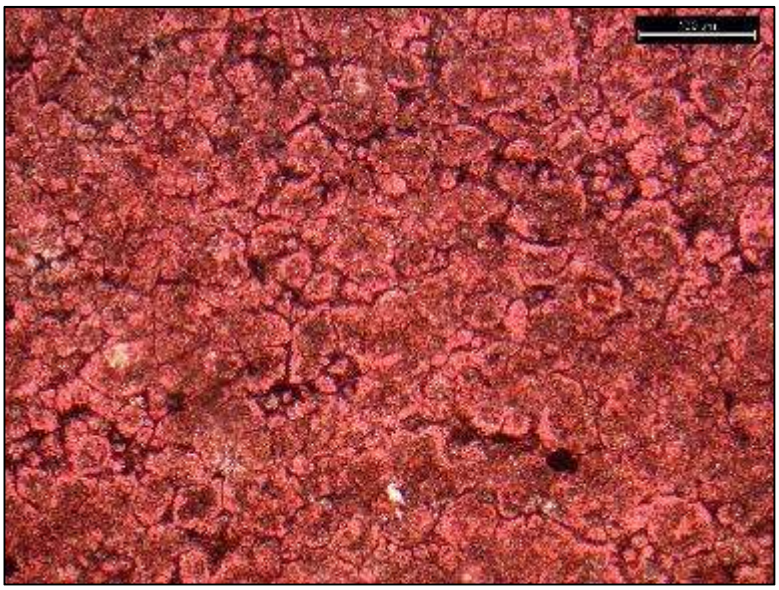

Petrographic Observations:
4X, plain light, stained. Recrystallized calcite, a few quartz grains, average grain size: 3 hash marks. Unit extinction in some grains. Laminations are more visible with the naked eye, but are slightly visible under 4X. The "matrix" which seperates the layers is black under both cross-polars and plain light and may be residual hydrocarbons. A few grains display birefringence. Grain size ranges from 1 hash mark to 5 hash marks. 95% recrystallized calcite, 4% residual hydrocarbons, 1% quartz

Figure 29: KL-GVP-020-V/6SH-004 (8 unit profile – Profile I) *Recrystallized Calcite w/ Hydrocarbons*.

Billet:

Field Observations:
Banded gypsum with some thick white layers, contains nodules, caprock below.

Thin Section:

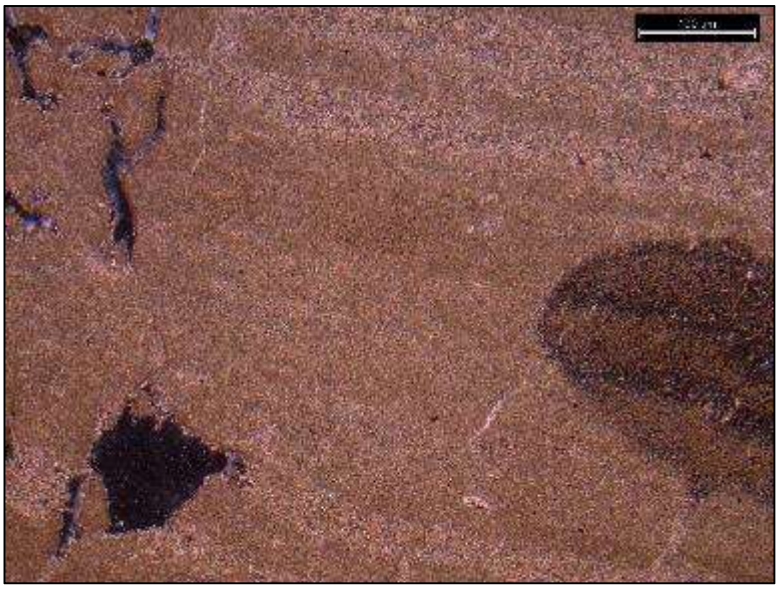

Petrographic Observations:
4X, cross polars, stained. Banded, microcrystalline dolomite (primary) with chert nodule. Chert nodule displays the same fabric as the dolomite. Some secondary dolomite in fractures, a few small quartz crystals. Some fractures filled with quartz cement – undulose extinction. 93.5% microcrystalline dolomite, 3% chert, 3% recrystallized dolomite, .5% quartz.

Figure 30: KL-GVP-047/6SH-014 (Mary Jane Draw Profile – Profile II) *Microcrystalline Dolomite*.

Hand Sample:

Field Observations:
Gypsum with back and white layers. ½ cm.

Thin Section:

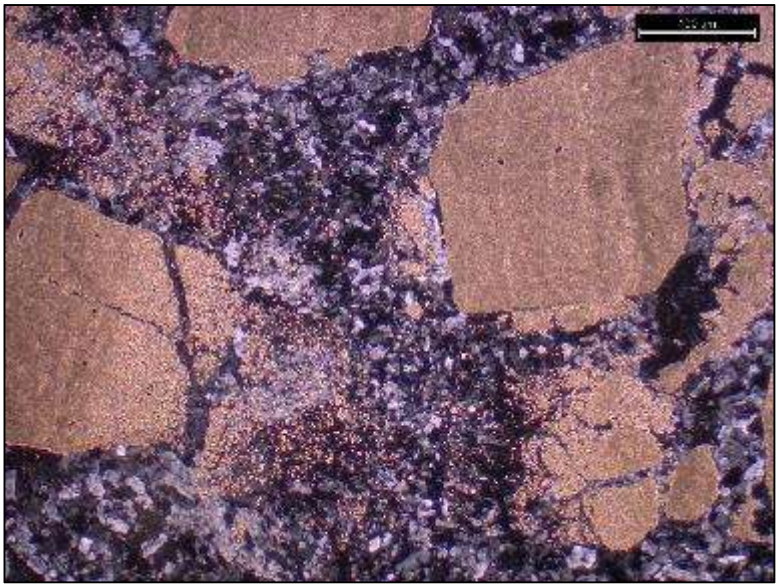

Petrographic Observations:
2.5X, cross polars, stained. Gypsum interspersed with large, tan, microcrystalline, brecciated, dolomite. Microcrystalline dolomite is likely primary. Largest block is ~5mm square. Some chalcedony. Dissolution of dolomite edges by sulfates – gypsum (corroded edges). Dolomite was there before gypsum, which is the opposite of normal conditions. 65% gypsum, 35% microcrystalline dolomite.

Figure 31: KL-GVP-045/6SH-012 (Mary Jane Draw Profile – Profile II) *Gypsum w/ Brecciated Microcrystalline Dolomite*.

Billet:

Field Observations:
Weathered surface is reddish/tan/orange, fresh surface is dark gray with some calcite – orange, red, and green. Slight reaction with HCl.

Thin Section:

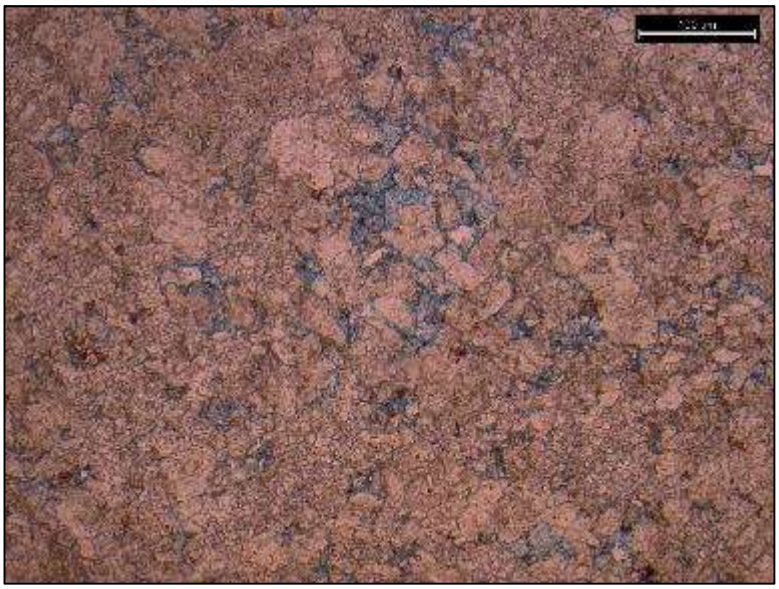

Petrographic Observations:
4X, plain light, stained. Iron-rich dolomite (blue) – occurred after standard dolomitization – majority is recrystallized (secondary) dolomite, & is coarse grained. A few completely black opaque grains – could be residual pyrite – iron sulfide. * Could also have siderite, anchorite, or Fe2 carbonate. 75% recrystallized dolomite, 23% recrystallized Fe-rich dolomite, 2% residual pyrite – iron sulfide.

Figure 32: KL-GVP-071/6SH-026 (Profile III) *Recrystallized and Iron Rich Dolomite*.

Billet:

Field Observations:
Weathered surface is karst-like and tan/greenish with laminae visible outside and slightly inside – some dark purple. Fresh surface is dark gray, petroliferous and reacts to HCl.

Thin Section:

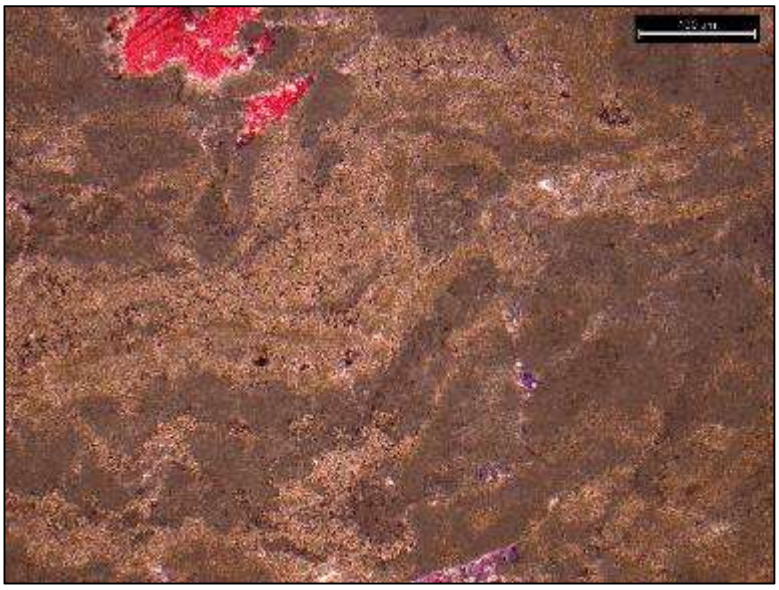

Petrographic Observations:
4X, plain light, stained Microcrystalline & rhombic, micritic, banded dolomite. Late stage, coarse crystalline, Poikilotopic calcite – unit extinction. Typically indicative of a high temperature burial environment. 89% microcrystalline dolomite, 8% calcite, 2% iron rich calcite, 1% quartz.

Figure 33: KL-GVP-081/6SH-031 (Profile III) *Banded Microcrystalline Dolomite w/ Calcite & Quartz*.

Hand Sample:

Field Observations:
Top layer with black – has alternating black and white layers on a mm scale. Fairly compact bench.

Note: Sseparated into KL-GVP-059-A/6SH-005 & KL-GVP-059-B/6SH-006

KL-GVP-059A
This Section: 4X, plain light, stained.

Thin Section: 4X, cross polars, stained.

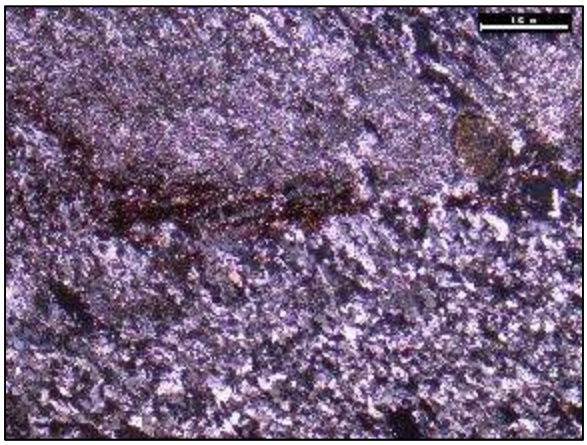

Petrographic Observations:
KL-GVP-059-A: Gypsum, chalcedony, chert. Very few grains display birefringence and some are rhombohedral. Microcrystalline dolomite. No direction indicator, but laminae are visible. Grain size ranges from .5 hash marks to 10 hash marks. 85% gypsum, 10% chalcedony, 3% microcrystalline dolomite, 2% chert.

(This Figure (34) continues on the next page)

KL-GVP-059-B

Thin Section: 4X, plain light, stained.

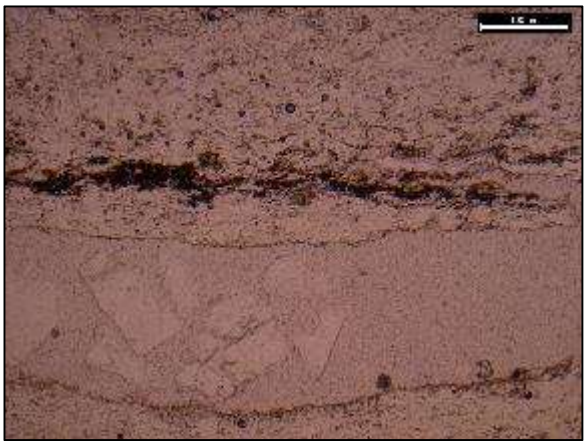

Thin Section: 4X, cross polars, stained.

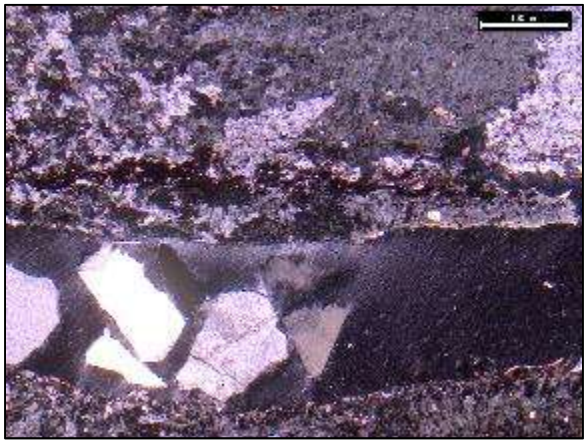

KL-GVP-059B: Gypsum, chalcedony, chert. Very few grains display birefringence and some are rhombohedral – dolomite. Laminae are visible. Some fractures are filled with quartz – undulose extinction. Grain size ranges from .5 hash marks to 15 hash marks. 85% gypsum, 10% chalcedony, 3% microcrystalline dolomite, 2% chert.

Figure 34: KL-GVP-059A/6SH-005 (Profile III) *Gypsum w/ Quartz & Microcrystalline Dolomite*.

Hand Sample:

Field Observations:
Zebra Gypsum.

Thin Section:

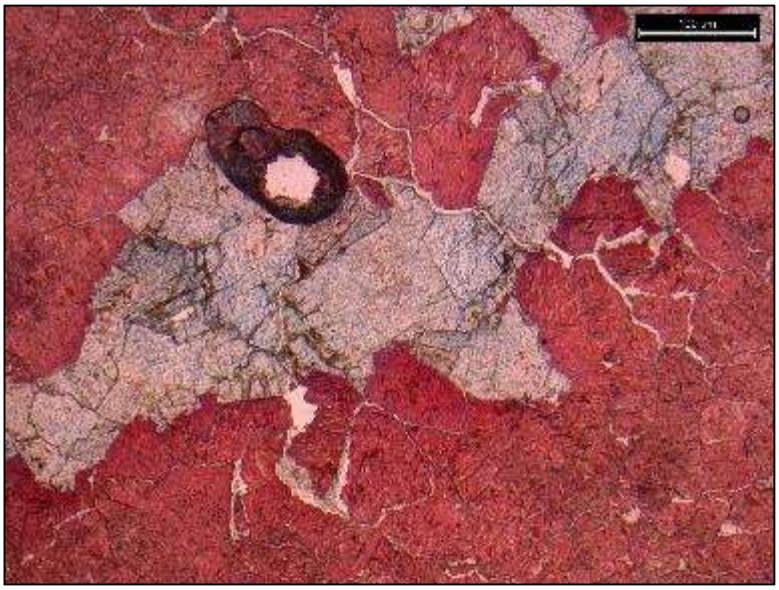

Petrographic Observations:
4X, plain light, stained.
Gypsum with calcite – red stain.
Blue staining is baroque dolomite, which is secondary in genesis.
The blue coloring is indicative of Fe. 93% recrystallized calcite, 7% Fe-rich saddle dolomite

Figure 35: KL-GVP-013B/6SH-002 (Bridge Canyon below fence line – debris flow ridge) *Iron Rich Baroque Dolomite w/ Gypsum and Calcite*.

Hand Sample:

Field Observations:
White and black layers 10-15 cm thick, mostly heterogeneous gypsum. Ranges from white to white and black layers – measles spots within the black layers. Sporatic, delayed reaction to HCl – black layers.

Thin Section:

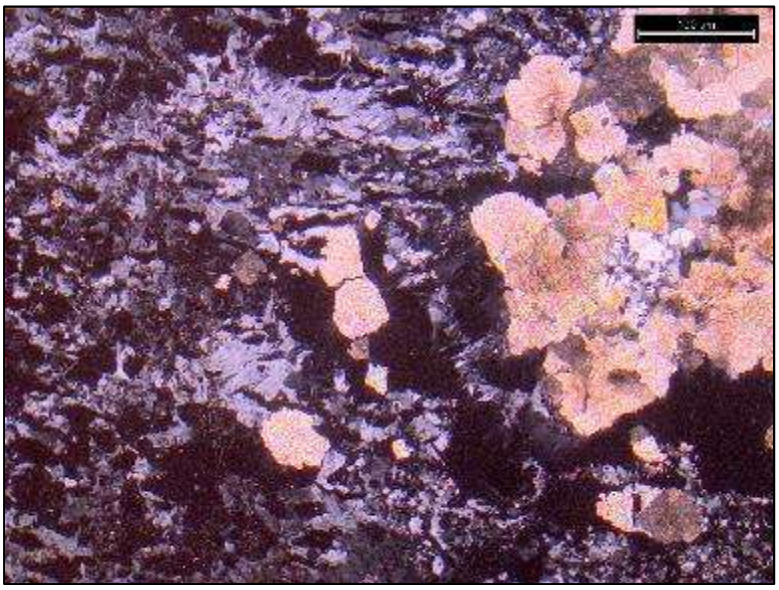

Petrographic Observations:
4X, cross polars, stained. Coarse dolomite rhombs, just starting to get corroded by the sulfate in gypsum. Dolomite halo ghosts seen in plain light – shows sweeping extinction – baroque dolomite – signature of hydrothermal fluids – may have replaced coarser dolomite due to planar edges (only slightly curved) – could be late diagenesis. Gypsum is later than the baroque dolomite. Grains range in size from 2-7 hash marks. 75% gypsum, 25% recrystallized dolomite.

Figure 36: KL-GVP-061/6SH-018 (Profile III) *Gypsum w/ Coarse Rhombohedral Dolomite*.

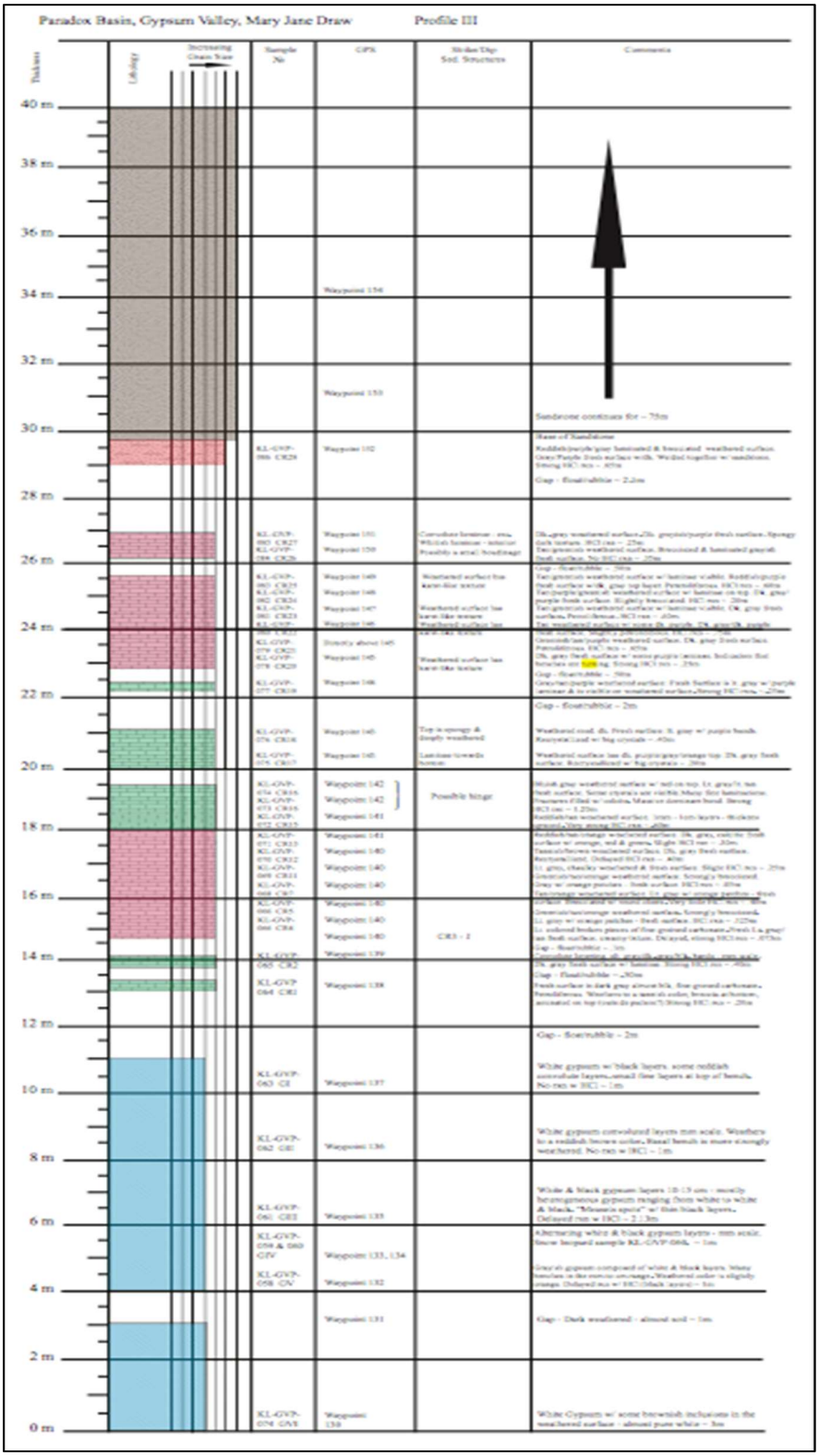

Figure 37: Transect III: Measured Section.

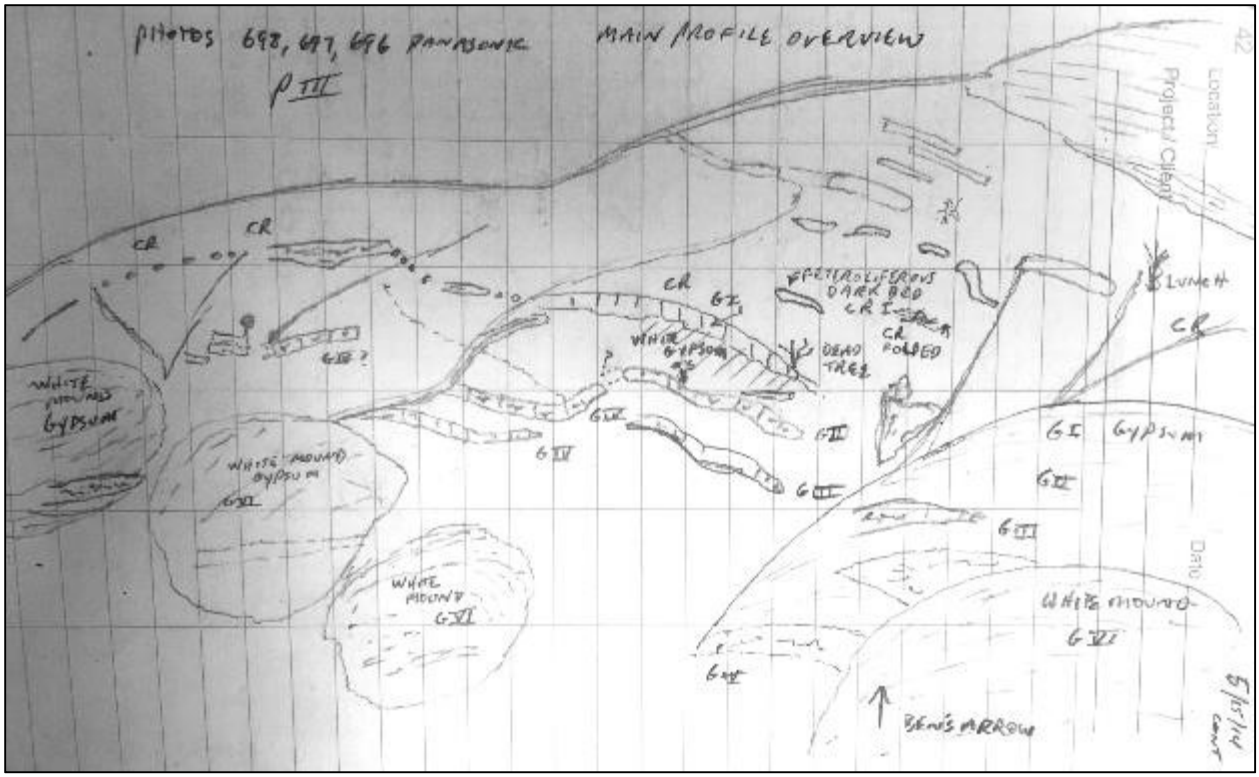

Figure 38: Field sketch of Transect III.

Figure 39: This is a photograph of Transect III, the field sketch shown in Figure 38. Apparent in this photograph is the whitish gypsum mounds in the foreground, tannish/gray/green caprock benches in the middle and reddish sandstone towards the top right.

Billet:

Field Observations:
Weathered surface is reddish/purple/gray laminated and brecciated. Fresh surface is purplish/gray. Strong HCl reaction. Welded together with sandstone.

Thin Section:

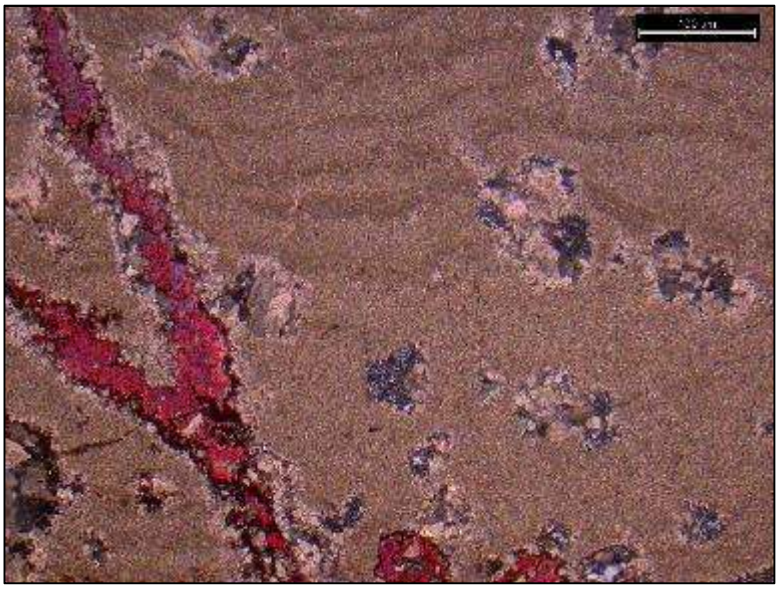

Petrographic Observations:
4X, cross polars, stained. Angular – sub angular calcite, w/ quartz grains – sand grains – undulose extinction, chert, some birefringence. Microcrystalline dolomite, Fe-rich dolomite and Fe-rich calcite. 77% microcrystalline dolomite, 10 % recrystallized, Fe-rich dolomite, 8% Fe-rich calcite, 4% chert, 1% quartz.

Figure 40: KL-GVP-086/6SH-034 (Profile III) *Microcrystalline Dolomite w/ Calcite*.

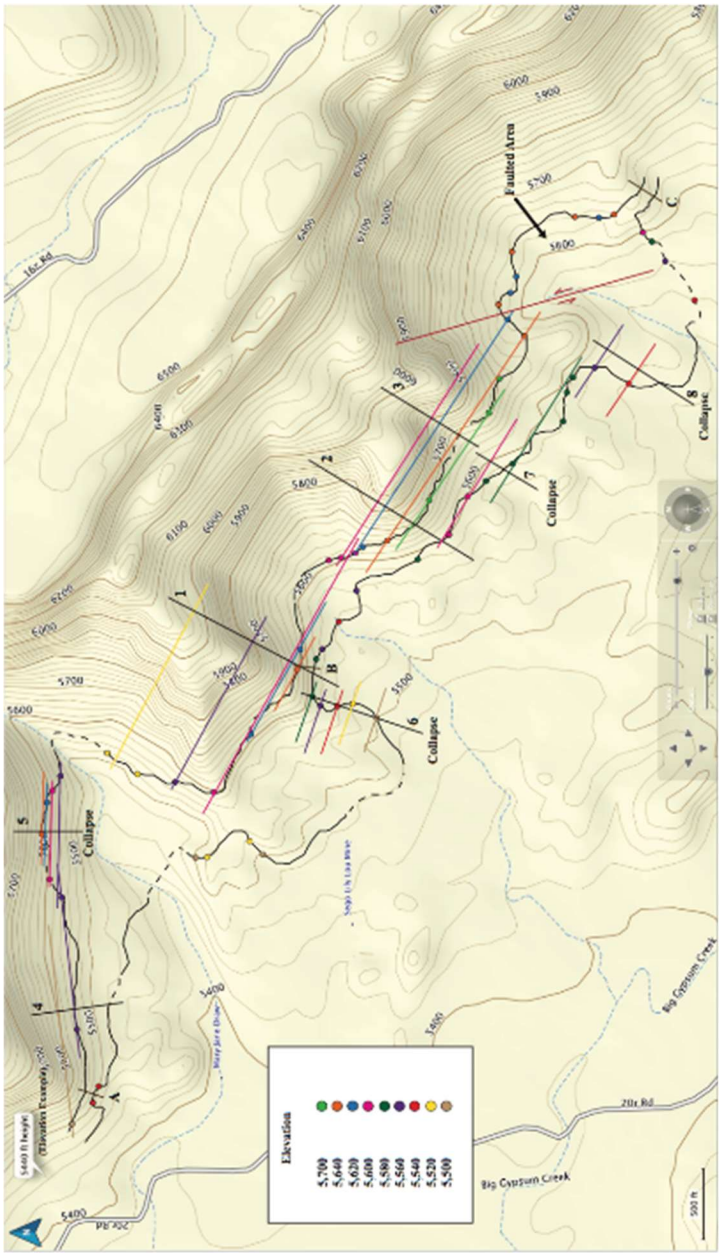

Figure 41: Topographic map, displaying the sandstone/caprock contact and the caprock/gypsum contact (black lines).

Additionally, elevation projections for these interfaces are represented by colored lines, which represent the strike of the geologic units. Colored dots represent intersects where the contact lines cross certain elevations, which provided reference points for the aforementioned elevation projections. Dip lines were drawn perpendicular to the elevation projections in select locations. These projections were used to determine the dip and thickness of the carbonate caprock unit at various locations within the studied area.

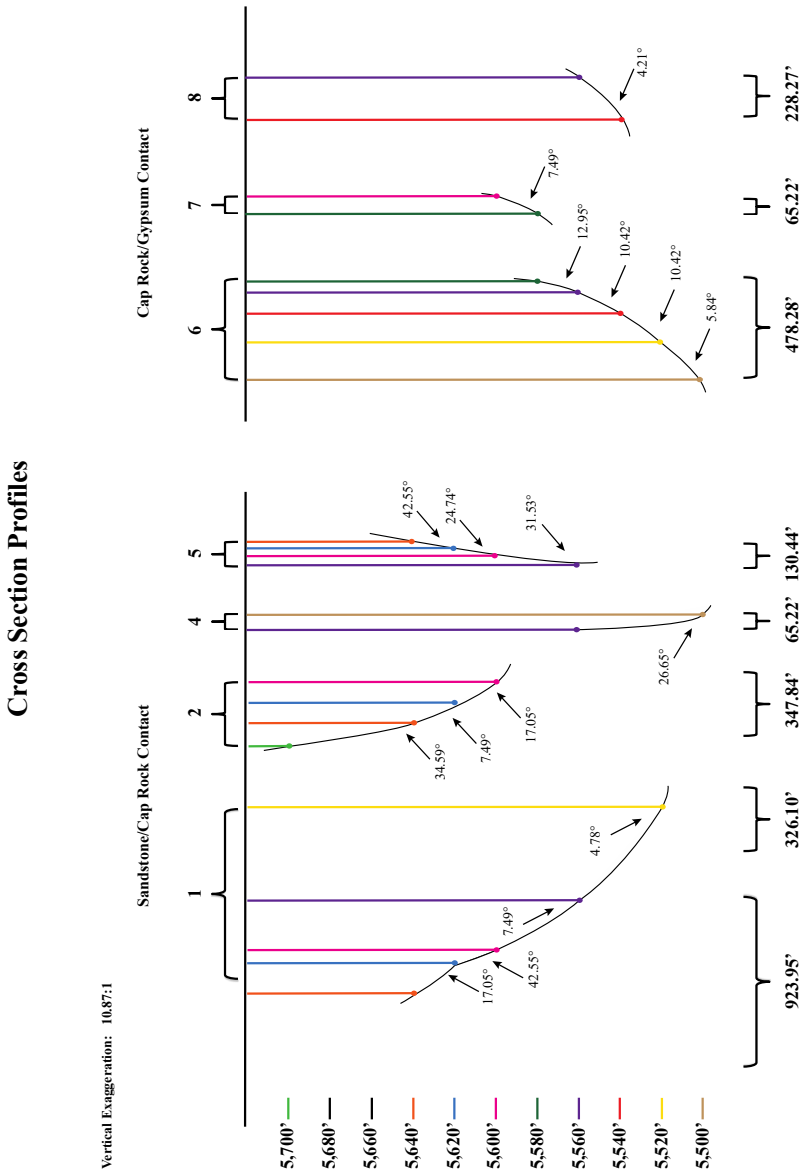

Figure 42: An illustration representing the profiles (bed dips) for both the sandstone/caprock contact and the caprock/gypsum contact at the selected points, which correspond to the locations of the dip lines shown in Figure 41.

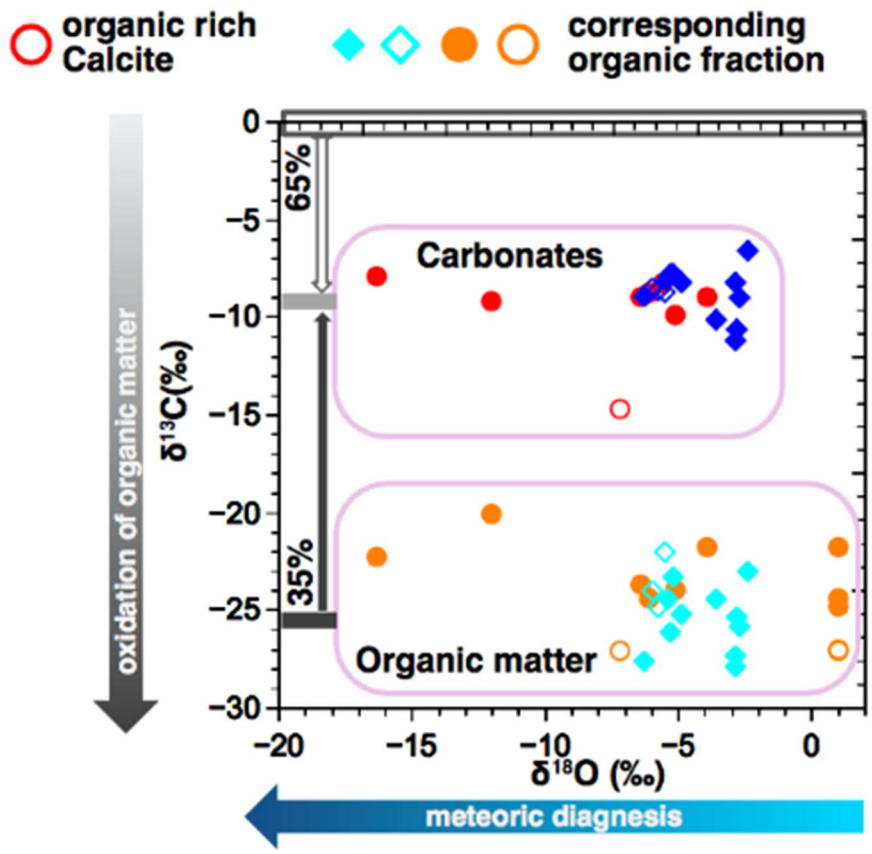

Figure 43: Carbon isotope composition of organic matter and corresponding carbonates vs. oxygen isotope composition of carbonates.
Organic matter data with no corresponding carbonate data are plotted at a $\delta^{18}O$ value of 1‰.

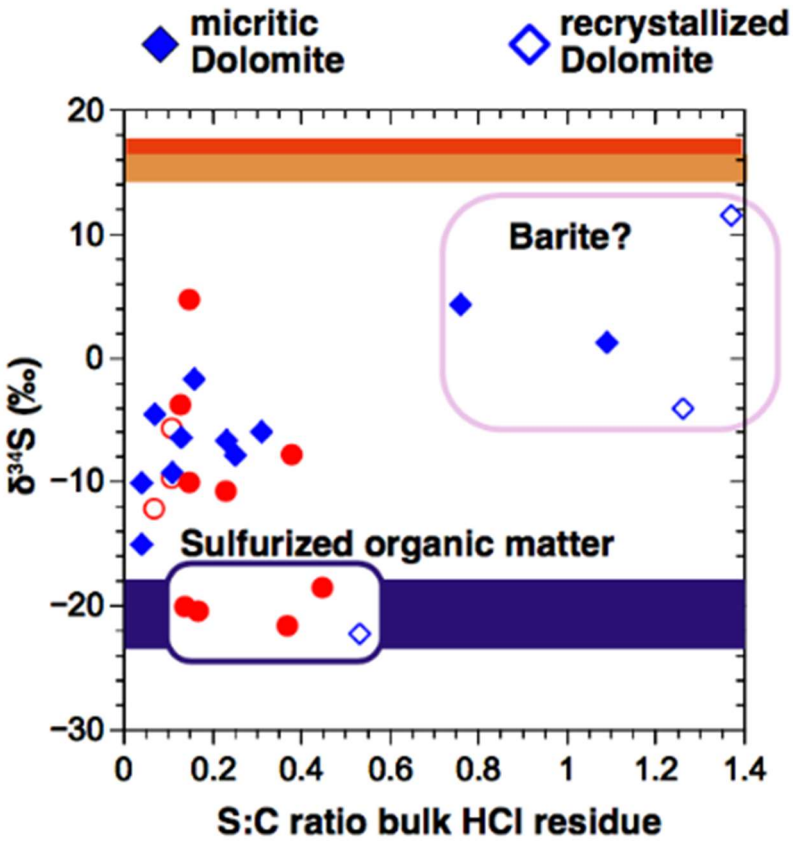

Figure 44: Sulfur isotope composition of HCl residue, and corresponding S:C ratio.

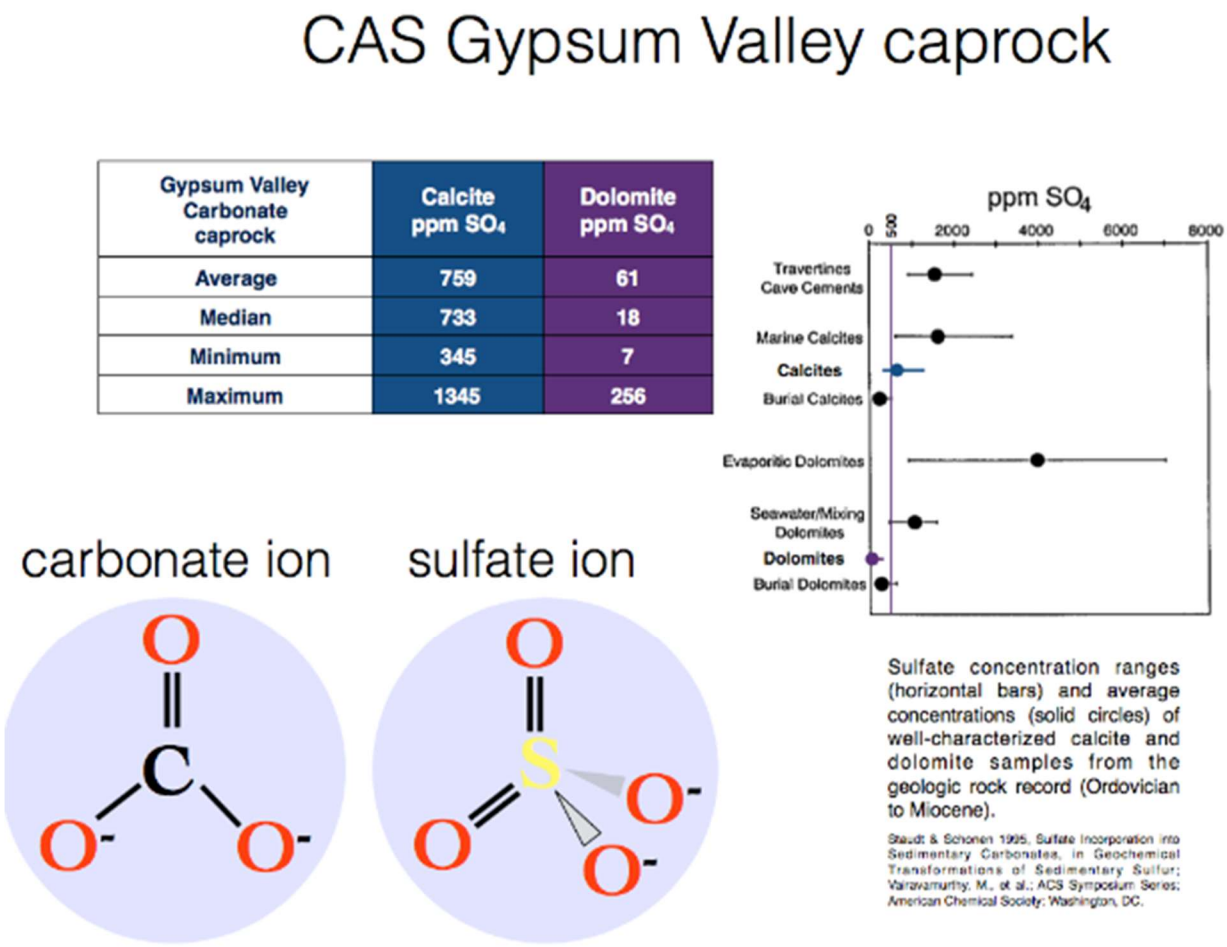

Figure 45: Carbonate associated sulfate content of carbonate caprock found in the study area.

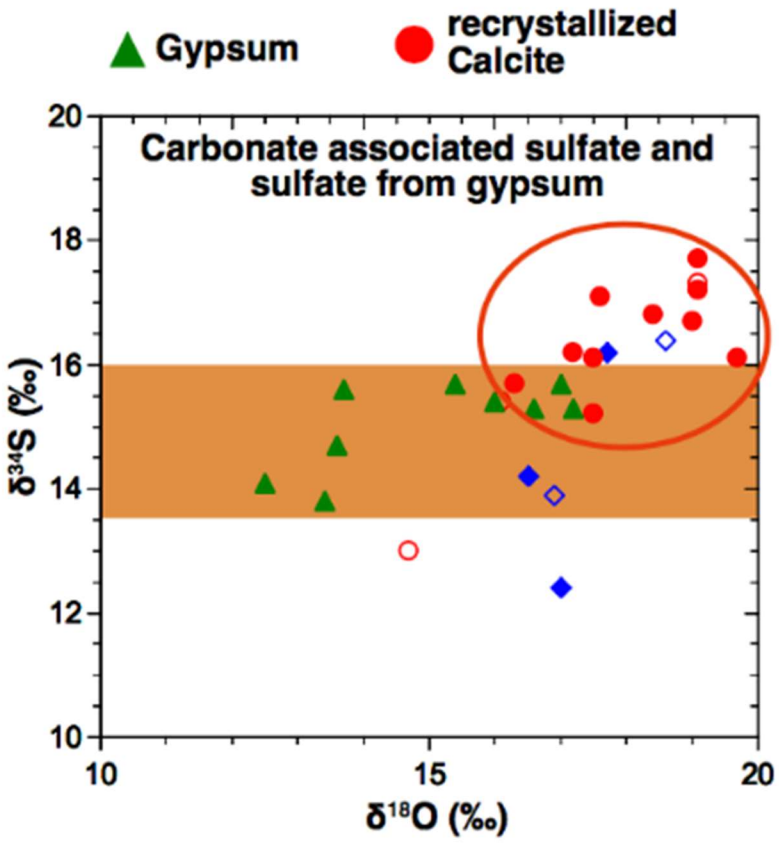

Figure 46: Sulfur and oxygen isotope composition of CAS and gypsum.

REFERENCES

Bao, H.M., 2006, Purifying barite for oxygen isotope measurement by dissolution and reprecipitation in a chelating solution: Analytical Chemistry, v. 78, p. 304–309, doi: 10.1021/ac051568z.

Barré, G., Truche, L., Bazarkina, E.F., Michels, R., and Dubessy, J., 2017, First evidence of the trisulfur radical ion S 3 − and other sulfur polymers in natural fluid inclusions: Chemical Geology, v. 462, p. 1–14, doi: 10.1016/j.chemgeo.2017.03.027.

Barton, D.C., and Paxson, R.B., 1925, The Spindletop Salt Dome and Oil Field Jefferson County, Texas: AAPG Bulletin, v. 9, p. 594–612.

Bein, A., Almogi-Labin, A., and Sass, E., 1990, Sulfur sinks and organic carbon relationships in Cretaceous organic-rich carbonates; implications for evaluation of oxygen-poor depositional environments: American Journal of Science, v. 290, p. 882–911, doi: 10.2475/ajs.290.8.882.

Bontognali, T.R.R., Vasconcelos, C., Warthmann, R.J., Bernasconi, S.M., Dupraz, C., Strohmenger, C.J., and McKenzie, J.A., 2010, Dolomite formation within microbial mats in the coastal sabkha of Abu Dhabi (United Arab Emirates): Sedimentology, v. 57, p. 824–844, doi: 10.1111/j.1365-3091.2009.01121.x.

Böttcher, M.E., Hetzel, A., Brumsack, H.-J., and Schipper, A., 2006, 9. Sulfur-Iron-Carbon Geochemistry in Sediments of the Demerara Rise, *in* Proceedings of the Ocean Drilling Program, Scientific Results, v. 207.

Burns, S.J., Mckenzie, J.A., and Vasconcelos, C., 2000, Dolomite formation and biogeochemical cycles in the Phanerozoic: Sedimentology, v. 47, p. 49–61, doi: 10.1046/j.1365-3091.2000.00004.x.

Davis, J.B., and Kirkland, D.W., 1979, Bioepigenetic sulfur deposits: Economic Geology, v. 74, p. 462–468, doi: 10.2113/gsecongeo.74.2.462.

Davis, J.B., Stanley, J.P., and Custard, H.C., 1970, Evidence Against Oxidation of Hydrogen Sulfide by Sulfate Ions to Produce Elemental Sulfur in Salt Domes: Geological Notes: AAPG Bulletin, v. 54, p. 2444–2447.

Deng, S., Dong, H., Lv, G., Jiang, H., Yu, B., and Bishop, M.E., 2010, Microbial dolomite precipitation using sulfate reducing and halophilic bacteria: Results from Qinghai Lake, Tibetan Plateau, NW China: Chemical Geology, v. 278, p. 151–159, doi: 10.1016/j.chemgeo.2010.09.008.

Dessau, G., Jensen, M.L., and Nakai, N., 1962, Geology and isotopic studies of Sicilian sulfur deposits: Economic Geology, v. 57, p. 410–438, doi: 10.2113/gsecongeo.57.3.410.

Drake, H., Åström, M.E., Heim, C., Broman, C., Åström, J., Whitehouse, M., Ivarsson, M., Siljeström, S., and Sjövall, P., 2015, Extreme 13C depletion of carbonates formed during oxidation of biogenic methane in fractured granite: Nature Communications, v. 6, doi: 10.1038/ncomms8020.

Enos, J.S., and Kyle, J.R., 2002, Diagenesis of the Carrizo Sandstone at Butler Salt Dome, East Texas Basin, U.S.A.: Evidence for Fluid-Sediment Interaction Near Halokinetic Structures: Journal of Sedimentary Research, v. 72, p. 68–81.

Feely, H.W., and Kulp, J.L., 1957, Origin of Gulf Coast Salt-Dome Sulphur Deposits: AAPG Bulletin, v. 41, p. 1802–1853.

Fenneman, N.M., 1906, Oil fields of the Texas-Louisiana Gulf Coastal Plain: Bulletin Report 282, http://pubs.er.usgs.gov/publication/b282.

Ferdelman, T.G., Church, T.M., and Luther, G.W., 1991, Sulfur enrichment of humic substances in a Delaware salt marsh sediment core: Geochimica et Cosmochimica Acta, v. 55, p. 979–988, doi: 10.1016/0016-7037(91)90156-Y.

Francois, R., 1987, A study of sulphur enrichment in the humic fraction of marine sediments during early diagenesis: Geochimica et Cosmochimica Acta, v. 51, p. 17–27, doi: 10.1016/0016-7037(87)90003-2.

Ghazban, F., and Al-Aasm, I.S., 2010, Hydrocarbon-Induced Diagenetic Dolomite and Pyrite Formation Associated with the Hormoz Island Salt Dome, Offshore Iran: Journal of Petroleum Geology, v. 33, p. 183–196.

Gieg, L.M., Jack, T.R., and Foght, J.M., 2011, Biological souring and mitigation in oil reservoirs: Applied Microbiology and Biotechnology, v. 92, p. 263, doi: 10.1007/s00253-011-3542-6.

Giles, K.A., and Rowan, M.G., 2012, Concepts in halokinetic-sequence deformation and stratigraphy: Geological Society, London, Special Publications, v. 363, p. 7–31.

Gischler, E., Heindel, K., Birgel, D., Brunner, B., Reitner, J., and Peckmann, J., 2017, Cryptic biostalactites in a submerged karst cave of the Belize Barrier Reef revisited: Pendant bioconstructions cemented by microbial micrite: Palaeogeography, Palaeoclimatology, Palaeoecology, v. 468, p. 34–51, doi: 10.1016/j.palaeo.2016.11.042.

Goldhammer, R., Oswald, E., and Dunn, P., 1991, Hierarchy of stratigraphic forcing: example from Middle Pennsylvanian shelf carbonates of the Paradox Basin: Sedimentary Modeling: Computer Simulations and Methods for Improved Parameter Definition: Kansas Geological Survey, Bulletin, v. 233, p. 361–413.

Gose, W.A., Kyle, J.R., and Ulrich, M.R., 1985, Preliminary Paleomagnetic Investigation of the Winnfield Salt Dome Cap Rock, Louisiana: v. 35, http://archives.datapages.com/data/gcags/data/035/035001/0097.htm (accessed November 2017).

Hayes, C.W., and Kennedy, W., 1903, Oil fields of the Texas-Louisiana Gulf coastal plain: US Government Printing Office, 212.

Heindel, K., Birgel, D., Brunner, B., Thiel, V., Westphal, H., Gischler, E., Ziegenbalg, S.B., Cabioch, G., Sjövall, P., and Peckmann, J., 2012, Post-glacial microbialite formation in coral reefs of the Pacific, Atlantic, and Indian Oceans: Chemical Geology, v. 304–305, p. 117–130, doi: 10.1016/j.chemgeo.2012.02.009.

Hobert, L.A., and Wetzel, A., 1989, On the relationship between silica and carbonate diagenesis in deep-sea sediments: Geologische Rundschau, v. 78, p. 765–778, doi: 10.1007/BF01829321.

Hubert, C., Voordouw, G., and Mayer, B., 2009, Elucidating microbial processes in nitrate- and sulfate-reducing systems using sulfur and oxygen isotope ratios: The example of oil reservoir souring control: Geochimica et Cosmochimica Acta, v. 73, p. 3864–3879, doi: 10.1016/j.gca.2009.03.025.

Ireland, M.T., Goulty, N.R., and Davies, R.J., 2010, Influence of pore water chemistry on silica diagenesis: evidence from the interaction of diagenetic reaction zones with polygonal fault systems: Journal of the Geological Society, v. 167, p. 273–279, doi: 10.1144/0016-76492009-049.

Jiang, L., Worden, R.H., Cai, C.F., Shen, A., and Crowley, S.F., 2017, Diagenesis of an evaporite-related carbonate reservoir in deeply buried Cambrian strata, Tarim Basin, Northwest China: AAPG Bulletin, v. 0, doi: 10.1306/0328171608517048.

Jørgensen, B.B., Isaksen, M.F., and Jannasch, H.W., 1992, Bacterial Sulfate Reduction Above 100°C in Deep-Sea Hydrothermal Vent Sediments: Science, v. 258, p. 1756–1757, doi: 10.1126/science.258.5089.1756.

Kelley, P.K., 1925, The Sulphur Salt Dome, Louisiana: AAPG Bulletin, v. 9, p. 479–496.

Kirkland, D.W., 2014, Role of hydrogen sulfide in the formation of cave and karst phenomena in the Guadalupe Mountains and western Delaware Basin, New Mexico and Texas (National Cave and Karst Research Institute, Ed.).

Kohnen, M.E.L., Damsté, J.S.S., ten Haven, H.L., and de Leeuw, J.W., 1989, Early incorporation of polysulphides in sedimentary organic matter: Nature, v. 341, p. 640–641, doi: 10.1038/341640a0.

Kyle, J.R., and Agee, W.N., 1988, Evolution of metal ratios and δ34S composition of sulfide mineralization during anhydrite cap rock formation, Hockley Dome, Texas, U.S.A.: Chemical Geology, v. 74, p. 37–55, doi: 10.1016/0009-2541(88)90145-3.

Kyle, J.R., Ulrich, M.R., and Gose, W.A., 1987, Textural and Palaeomagnetic Evidence for the Mechanism and Timing of Anhydrite Cap Rock Formation, Winnfield Salt Dome, Lousiana, *in* Lerche, I. and O'Brien, J.J. eds., Dynamical Geology of Salt and Related Structures, Academic Press, p. 497–542, doi: 10.1016/B978-0-12-444170-5.50017-8.

Labrado, A., Brunner, B., Poe, P., Giles, Katherine A., and Bernasconi, S.M., 2018, Stable isotope geochemistry of caprock from Damon Mound, TX: A closed system within a dynamic setting?

Lindtke, J., Ziegenbalg, S.B., Brunner, B., Rouchy, J.M., Pierre, C., and Peckmann, J., 2011, Authigenesis of native sulphur and dolomite in a lacustrine evaporitic setting (Hellin basin, Late Miocene, SE Spain): Geological Magazine, v. 148, p. 665–669, doi: 10.1017/S0016756811000124.

Lucia, F.J., 2004, Origin and petrophysics of dolostone pore space: Geological Society, London, Special Publications, v. 235, p. 141–155, doi: 10.1144/GSL.SP.2004.235.01.06.

Machel, H.G., 2001, Bacterial and thermochemical sulfate reduction in diagenetic settings — old and new insights: Sedimentary Geology, v. 140, p. 143–175, doi: 10.1016/S0037-0738(00)00176-7.

Machel, H.G., 1992, Low-temperature and high-temperature origins of elemental sulfur in diagenetic environments: Native Sulfur–Developments in Geology and Exploration, p. 3–22.

Mackenzie, F.T., and Garrels, R.M., 1966, Silica-Bicarbonate Balance In The Ocean And Early Diagenesis: Journal of Sedimentary Research, v. 36, http://archives.datapages.com/data/sepm/journals/v33-37/data/036/036004/1075.htm (accessed November 2014).

McFarland, J.C., 2016, Structural and stratigraphic development of a salt-diapir shoulder, Gypsum Valley, Colorado: [M.S.]: The University of Texas at El Paso, 93 p.

Meister, P., Gutjahr, M., Frank, M., Bernasconi, S.M., Vasconcelos, C., and McKenzie, J.A., 2011, Dolomite formation within the methanogenic zone induced by tectonically driven fluids in the Peru accretionary prism: Geology, v. 39, p. 563–566, doi: 10.1130/G31810.1.

Milucka, J., Ferdelman, T.G., Polerecky, L., Franzke, D., Wegener, G., Schmid, M., Lieberwirth, I., Wagner, M., Widdel, F., and Kuypers, M.M.M., 2012, Zero-valent sulphur is a key intermediate in marine methane oxidation: Nature, v. 491, p. 541–546, doi: 10.1038/nature11656.

Mossmann, J.-R., Aplin, A.C., Curtis, C.D., and Coleman, M.L., 1991, Geochemistry of inorganic and organic sulphur in organic-rich sediments from the Peru Margin: Geochimica et Cosmochimica Acta, v. 55, p. 3581–3595, doi: 10.1016/0016-7037(91)90057-C.

Peckmann, J., Paul, J., and Thiel, V., 1999, Bacterially mediated formation of diagenetic aragonite and native sulfur in Zechstein carbonates (Upper Permian, Central Germany): Sedimentary Geology, v. 126, p. 205–222, doi: 10.1016/S0037-0738(99)00041-X.

Peterson, J.A., and Hite, R.J., 1969, Pennsylvanian Evaporite-Carbonate Cycles and Their Relation to Petroleum Occurrence, Southern Rocky Mountains: AAPG Bulletin, v. 53, p. 884–908.

Petrash, D.A., Bialik, O.M., Bontognali, T.R.R., Vasconcelos, C., Roberts, J.A., McKenzie, J.A., and Konhauser, K.O., 2017, Microbially catalyzed dolomite formation: From near-surface to burial: Earth-Science Reviews, v. 171, p. 558–582, doi: 10.1016/j.earscirev.2017.06.015.

Pierce, W.G., and Rich, E.I., 1962, Summary of rock salt deposits in the United States as possible storage sites for radioactive waste materials: US Government Printing Office, v. 1148.

Poe, P., Giles, Katherine A., Brunner, B., Lerer, K., Rasbury, T., and Edmond, J., 2018a, Characterization and Geochemistry of Lateral Carbonate Caprock associated with the Gypsum Valley Salt Wall, Paradox Basion, CO: Evidence supporting the drape-fold model for lateral caprock emplacement.

Poe, P., Giles, Katherine A., Brunner, B., Kernen, R., Labrado, A., and Lerer, K., 2018b, Classification of caprock associated with salt diapirs.

Posey, H.H., and Kyle, J.R., 1988a, Preface: Chemical Geology, v. 74, p. vii, doi: 10.1016/0009-2541(88)90142-8.

Posey, H.H., and Kyle, J.R., 1988b, Fluid-rock interactions in the salt dome environment: An introduction and review: Chemical Geology, v. 74, p. 1–24, doi: 10.1016/0009-2541(88)90143-X.

Prikryl, J.D., Posey, H.H., and Kyle, J.R., 1988, A petrographic and geochemical model for the origin of calcite cap rock at Damon Mound salt dome, Texas, U.S.A.: Chemical Geology, v. 74, p. 67–97, doi: 10.1016/0009-2541(88)90147-7.

Riedinger, N.R., Brunner, B., Krastel, S., Arnold, G.L., Wehrmann, L.M., Formolo, M.J., Beck, A., Bates, S.M., Henkel, S., Kasten, S., and Lyons, T.W., 2017, Sulfur cycling in an iron oxide-dominated, dynamic marine depositional system: The Argentine continental margin: Frontiers in Earth Science, v. 5, doi: 10.3389/feart.2017.00033.

Russell, K.L., Deffeyes, K.S., Fowler, G.A., and Lloyd, R.M., 1967, Marine Dolomite of Unusual Isotopic Composition: Science, v. 155, p. 189–191, doi: 10.1126/science.155.3759.189-a.

Sánchez-Román, M., McKenzie, J.A., de Luca Rebello Wagener, A., Rivadeneyra, M.A., and Vasconcelos, C., 2009, Presence of sulfate does not inhibit low-temperature dolomite precipitation: Earth and Planetary Science Letters, v. 285, p. 131–139, doi: 10.1016/j.epsl.2009.06.003.

Sass, H., Steuber, J., Kroder, M., Kroneck, P.M.H., and Cypionka, H., 1992, Formation of thionates by freshwater and marine strains of sulfate-reducing bacteria: Archives of Microbiology, v. 158, p. 418–421, doi: 10.1007/BF00276302.

Saunders, J.A., Prikryl, J.D., and Posey, H.H., 1988, Mineralogic and isotopic constraints on the origin of strontium-rich cap rock, Tatum Dome, Mississippi, U.S.A.: Chemical Geology, v. 74, p. 137–152, doi: 10.1016/0009-2541(88)90150-7.

Shen, Y., and Buick, R., 2004, The antiquity of microbial sulfate reduction: Earth-Science Reviews, v. 64, p. 243–272, doi: 10.1016/S0012-8252(03)00054-0.

Shock, A.L., 2012, Origin and implications of Permian and Triassic diagenetic carbonate caprock adjacent to diapiric salt walls, Paradox Basin, Utah: New Mexico State University, 105 p.

Shoemaker, E.M., Case, J.E., and Elston, D.P., 1958, Salt Anticlines of the Paradox Basin: p. 39–59.

Vairavamurthy, A., and Mopper, K., 1987, Geochemical formation of organosulphur compounds (thiols) by addition of H2S to sedimentary organic matter: Nature, v. 329, p. 623–625, doi: 10.1038/329623a0.

Wallmann, K., Aloisi, G., Haeckel, M., Tishchenko, P., Pavlova, G., Greinert, J., Kutterolf, S., and Eisenhauer, A., 2008, Silicate weathering in anoxic marine sediments: Geochimica et Cosmochimica Acta, v. 72, p. 2895–2918, doi: 10.1016/j.gca.2008.03.026.

Warthmann, R., Lith, Y. van, Vasconcelos, C., McKenzie, J.A., and Karpoff, A.M., 2000, Bacterially induced dolomite precipitation in anoxic culture experiments: Geology, v. 28, p. 1091–1094, doi: 10.1130/0091-7613(2000)28<1091:BIDPIA>2.0.CO;2.

Wehrmann, L.M., Riedinger, N., Brunner, B., Kamyshny, A., Hubert, C.R.J., Herbert, L.C., Brüchert, V., Jørgensen, B.B., Ferdelman, T.G., and Formolo, M.J., 2017, Iron-controlled oxidative sulfur cycling recorded in the distribution and isotopic composition of sulfur species in glacially influenced fjord sediments of west Svalbard: Chemical Geology, doi: 10.1016/j.chemgeo.2017.06.013.

Werner, M.L., Feldman, M.D., and Knauth, L.P., 1988, Petrography and geochemistry of water-rock interactions in Richton Dome cap rock (southeastern Mississippi, U.S.A.): Chemical Geology, v. 74, p. 113–135, doi: 10.1016/0009-2541(88)90149-0.

Ziegenbalg, S.B., Brunner, B., Rouchy, J.M., Birgel, D., Pierre, C., Böttcher, M.E., Caruso, A., Immenhauser, A., and Peckmann, J., 2010, Formation of secondary carbonates and native sulphur in sulphate-rich Messinian strata, Sicily: Sedimentary Geology, v. 227, p. 37–50, doi: 10.1016/j.sedgeo.2010.03.007.

APPENDIX 1 – SAMPLE PREPARATION PROTOCOL

Note: spreadsheet column references in this Protocol refer to the Original Dataset Spreadsheet only.

1. Sample Selection:

1.1. 38 samples were chosen from the 86+ samples collected in the field from 2 trips to the Paradox Basin – Gypsum Valley – in March and in May of 2014.
1.2. The criterion for choosing these samples was to find representative samples of both gypsums and carbonates without undue repetition.
1.3. Slabs were then cut from the 38 samples in the rock lab.

2. Sample Crushing:

2.1. Once the samples were dried, they were broken up into smaller pieces using a drilling hammer or rock hammer. They were then either ground up using a mortar & pestle or pounded into a powder using a hardened steel piston and receptacle.
2.2. Samples were grouped into categories: Gypsum and Carbonate, Carbonate/Gypsum (referred to as "mixed") samples.
2.3. These crushed samples were screened using a 150 micron USA Standard Test Sieve.
2.4. Yellow, screw top tubes (2mL) were then weighed empty and recorded in column D (gypsum samples) and Z (carbonate & mixed samples) on the spreadsheet.
2.5. A yellow-top 2mL tube was filled with each of the samples for use as a back-up sample. Weights were recorded in column E (gypsum samples) and AA (carbonate & mixed samples).
2.6. Centrifuge tubes (50mL) were then weighed empty and the weights were recorded in column B (gypsum samples) and X (carbonate & mixed samples) of the Sample Weight spreadsheet.
2.7. The powdered samples were then put into the 50 mL centrifuge tubes and the sample weights ranged from approximately 6 grams to 15 grams. Filled weights were recorded in columns C (gypsum samples) and Y (carbonate & mixed samples).

3. Gypsum Dissolution (Experiment Series I):

3.1. First stage gypsum dissolution experiment (for identified gypsum samples only: 062, 011, 063, 058, 057, 060, 061, 059*, 048, 015, 020, 021).
3.2. The empty weight of a new set of 50mL centrifuge tubes was recorded in column F.
3.3. A small amount of crushed (~ 0.1g) sample was then placed into the 50mL tubes and the weights recorded in column G.
3.4. The samples were then covered with a 10% NaCl solution (~2moles NaCl/liter of DI water), which ranged from 25mL to 35mL (of solution)).
3.5. Once the NaCl solution was added to the tubes, the samples were agitated and the gypsum was dissolved for ~ 24 hours.
3.6. Samples were then filtered utilizing an older filtration unit that was slightly defective (clamp was defective). The result was that we lost ~15mL of original solution from

sample 057 and ~5mL of diluted solution from sample 020. We then switched to a new vacuum filtration unit (pore size was 0.2µm, 25 mm diameter Whatman Nucleopore filters).

3.7. Filter papers with sediments were then placed into 10 orange & 2 red screw-top 2mL tubes. No weights were recorded for this procedure.

3.8. The filtered solution was then poured back into the 50mL tubes, which had been washed with DI water.

3.9. The samples were acidified by adding 0.02mL of concentrated HCl solution to the filtered supernatant in order to prevent precipitation of barium carbonate. ~.5 mL $BaCl_2$ solution (1M $BaCl_2$ solution) was added to the filtered supernatant in order to precipitate $BaSO_4$. The samples sat overnight ~12 hrs. before additional procedures were performed.

3.10. After ~24 hrs. the samples were centrifuged (4000 RPM/5 minutes) and the supernatant was poured off into a disposal container.

3.11. These samples were then filled to 45mL w/ DI water, agitated and centrifuged (2500 RPM/3 minutes).

3.12. 4 of these samples (057, 015, 021, 020) were transferred into 2mL yellow screw top tubes.

3.13. All samples were then washed. with DI water: agitated and centrifuged (2100 rpm/3 minutes).

3.14. The supernatant was then discarded (down the drain).

3.15. Acetone was added (to cover sample), agitated and allowed to dry.

3.16. Weights for $BaSO_4$ were then recorded in columns T & U. Empty tube weight was recorded in column V (2mL tubes).

3.17. The following steps were done in order to calculate the dry weight of the sediment that was subsequently subjected to the NaCl steps.

3.18. Weights of the washed/wet sediment were recorded in column H.

3.19. Empty flip-top 2mL tube weights were recorded in column I.

3.20. A small aliquot of wet sediment was added to the 2mL tubes and the weights recorded in column J.

3.21. These samples were then allowed to dry over a period of 24-48 hrs. Weights were then recorded in column K.

3.22. * There was a discrepancy with the 059 sample. There were two samples marked 059. These samples were subsequently marked 059A & 059B. Although we cannot be 100% certain which sample is which, the prevailing theory is that 059A was the smaller sample and 059B was the larger sample. This determination was based upon the recollection that 059B caked badly and a relatively large sample was prepared since it was very soft.

4. Sequential Extraction of NaCl Leachable & HCl Leachable Sulfate (Experiment Series II):

4.1. NaCl Procedure:

4.1.1. The 50mL tubes, containing crushed and screened samples, were filled with NaCl solution (~2moles NaCl/liter of DI water) to the 50mL mark. These filled tubes were then agitated, placed on their sides and allowed to dissolve over the weekend (~60 hrs.) The samples were agitated 3 times on Friday before leaving the lab for the weekend, and twice more on Monday morning.

4.1.2. These samples were then centrifuged (2100 RPM/3 minutes) and the supernatant was transferred into a new set of 50mL tubes.
4.1.3. The supernatant was then filtered with a hand vacuum filter unit (pore size was 0.2µm, 25 mm diameter Whatman Nucleopore filters).
4.1.4. The samples were acidified by adding 0.02mL of concentrated HCl solution to the filtered supernatant in order to prevent precipitation of barium carbonate. ~.5 mL $BaCl_2$ solution (1M $BaCl_2$ solution) was added to the filtered supernatant in order to precipitate $BaSO_4$. The samples sat overnight ~12 hrs. before additional procedures were performed.
4.1.5. All samples were then washed twice with DI water: agitated and centrifuged (at 2100 RPM/2 minutes).
4.1.6. The supernatant was then discarded (down the drain).
4.1.7. Acetone was added (to cover sample), agitated and allowed to dry.
4.1.8. Weights for dry $BaSO_4$ were then recorded in column AO. Empty tube weight was recorded in column AI (red top 2mL tubes).
4.1.9. In cases where the $BaSO_4$ was too large for the 2mL tubes, medium (15mL) tubes were utilized. Empty weights were recorded in column AK & the weights for dry $BaSO_4$ were recorded in column AL.
4.1.10. Wet (NaCl) samples in the 50mL tubes were then washed twice with DI water: vortexed, centrifuged (2100 RPM/2 minutes) and the supernatant was poured off (down the drain).
4.1.11. The following steps were completed in order to be able to calculate the dry weight of the sediment that was subsequently subjected to the NaCl step.
4.1.12. Weights of the washed/wet sediment were recorded in column AD.
4.1.13. Empty flip-top 2mL tubes were recorded in column AE, a small aliquot of wet sediment was added to the 2mL tubes and recorded in column AF.
4.1.14. These samples were then allowed to dry over a period of 48 hrs. Weights were then recorded in column AG.

4.2. HCl Procedure:

4.2.1. The washed sediment from the NaCl Procedure, listed above, was transferred to glass beakers. In all cases, it was necessary to add a bit of DI water to make sure the sediment was completely transferred to the glass beaker. A concentrated HCl solution was added to dissolve the sediment (small amounts were added periodically to ensure the reaction did not bubble over) until the sample was completely dissolved. Time: maximum of 3 hrs. between the HCl being added to the samples and being centrifuged in order to minimize oxidation.
4.2.2. Once the sediment had dissolved, it was transferred back to 50mL tubes (2 tubes in some cases), which had been washed out with DI water. Again, it was necessary to add DI water to the beakers to ensure that all sediment was transferred back into the 50mL tubes (some sediment loss may have occurred). DI water was added to the tubes to fill up to the 45-50mL mark for centrifugation.
4.2.3. The mixture was then vortexed, centrifuged (2100 RPM/2 minutes) and the supernatant poured off into a new set of tubes (50mL). The sediment remaining in the original set of tubes was left intact for later washing and freezing. In cases where 2 50mL tubes were utilized, the samples were not combined.

4.2.4. The supernatant was then filtered: the hand vacuum filter unit (pore size was 0.2µm, 25 mm diameter Whatman Nucleopore filters) was not efficient on this mixture due to the smaller pore size and the smaller diameter of the filters compared to the syringe filter unit, so a hand syringe filter unit (0.45µm, 30 mm diameter PES membrane Thermo Scientific) was used on the majority of the samples, while some samples were filtered with the hand vacuum filter unit. Time factor: the syringe filter unit was much more efficient to use.

4.2.5. The 50mL tubes were then immediately washed with DI water so that the supernatant could be filtered back into the tubes (50mL).

4.2.6. ~.5 mL of $BaCl_2$ was added to the filtered supernatant (in the 50mL tubes) in order to precipitate $BaSO_4$. The mixture was left standing for ~12 hrs.

4.2.7. The solution was then centrifuged (2100 RPM/2 minutes) and the supernatant discarded in a disposal container.

4.2.8. The precipitated BaSO4 was then washed twice, where possible. If the BaSO4 samples were too small, they were only washed once and transferred to green screw top 2mL tubes. Larger $BaSO_4$ samples were transferred to 15mL tubes after washing. Washing procedure: vortexed, centrifuged (2100 RPM/2 minutes).

4.2.9. Empty, green, screw-top 2mL tube weights were recorded in column AH.

4.2.10. Empty, 15mL tubes weights were recorded in column AJ.

4.2.11. Acetone was added (to cover sample), agitated and allowed to dry. Once dry, the dry weights were recorded: 2mL tube dry weights were recorded in column AN and 15mL tube dry weights were recorded in column AM.

4.2.12. Left over HCl pulverized rock samples, in tubes, were washed twice: once with hot tap water and once with DI water. These samples were vortexed between washing and were centrifuged at 2100 RPM for 4 minutes. The solution after the first washing was disposed of as hazardous waste and the second washing was poured down the drain. The samples were then bagged and put into the freezer for future use. Samples that were in 2, 50mL tubes were not recombined at this point.

4.2.13. The following steps were completed in order to be able to calculate the dry weight of the sediment that was subsequently subjected to the HCl step.

4.2.14. Weights of the washed/wet (2200 RPM for 3 minutes; due to sediment suspension problems, sample 064 was also run at 4500 RPM for 7 minutes) sediment were recorded in column AT.

4.2.15. Empty flip-top 2mL tubes were recorded in column AU, a small aliquot of wet sediment was added to the 2mL tubes and recorded in column AV.

4.2.16. These samples were then allowed to dry over a period of 48 hrs. Weights were then recorded in column AW.

4.2.17. Hypothetical dry weights were calculated and recorded in column AX.

5. Additional Procedures/Notes:

5.1. Safety equipment utilized: lab coat, safety glasses, vinyl examination gloves and fume hood.

5.2. Notes were taken in a lab book and then transferred to digital format, where applicable.

APPENDIX 2 – PETROGRAPHIC DESCRIPTIONS

KL-GVP-002/6SH-008 (Salt Glacier South)
Microcrystalline Dolomite

Billet:

Field Observations:
Caprock, not petroliferous.

Thin Section:

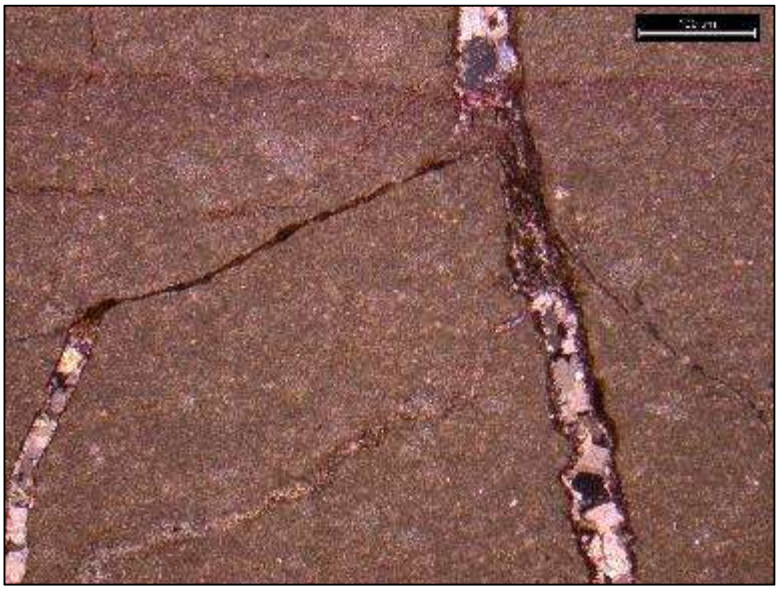

Petrographic Observations:
4X, cross polars, stained. Microcrystalline dolomite (primary). Fracture filled with quartz grains, and possibly some gypsum which has birefringence. 98.5% microcrystalline dolomite, 1% quartz, .5% gypsum

KL-GVP-011/6SH-009 (Bridge Canyon below fence line – debris flow ridge)
Gypsum

Billet:

Field Observations:
Gypsum sample.

Thin Section:

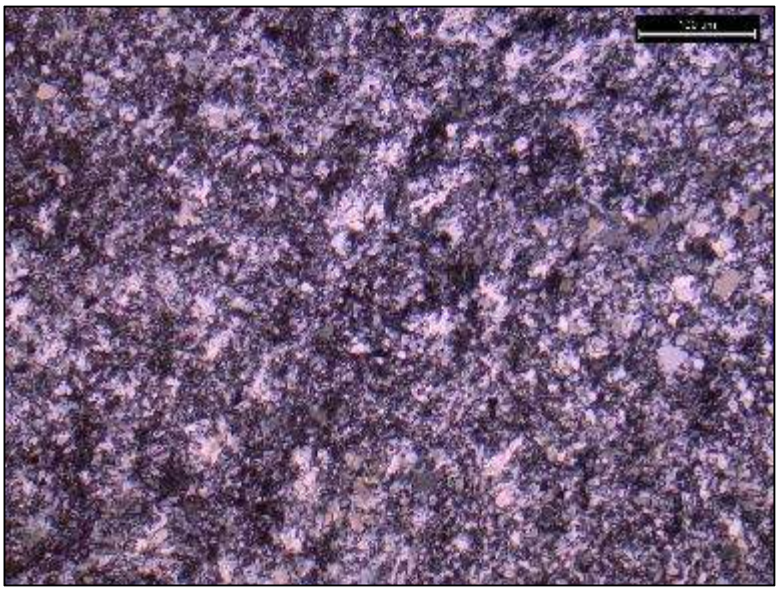

Petrographic Observations:
4X, cross polars, stained.
Gypsum, some quartz grains, fine-grained. Grain size ranges from .5 to 3 hash marks, with a few slightly larger quartz grains.
98.5% gypsum, 1% quartz, (.5% microcrystalline dolomite?)

KL-GVP-013A /6SH-001 (Bridge Canyon below fence line – debris flow ridge)
Zebra Calcite

Hand Sample:

Field Observations:
Zebra gypsum sample.

Thin Section:

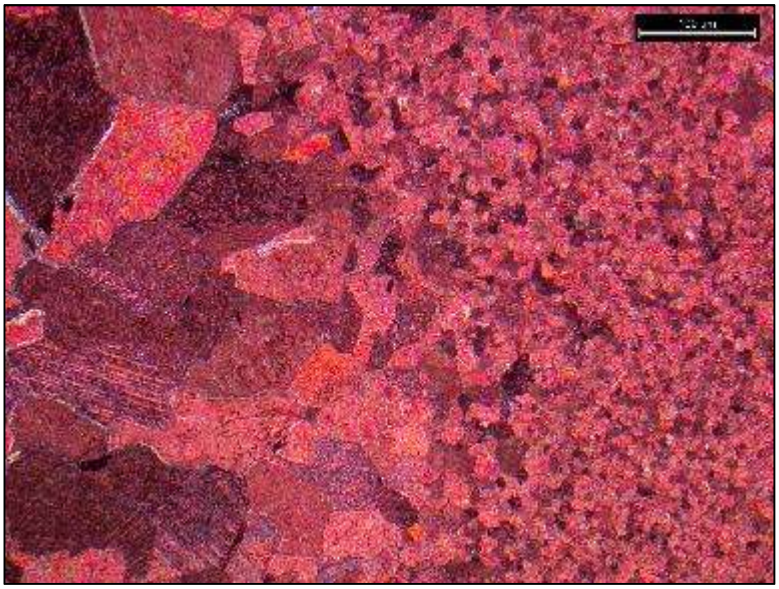

Petrographic Observations:
4X, cross polars, stained.
All recrystallized calcite. Coarse grained. Some cross-hatching, unit extinction, calcite w/ some gypsum, high birefringence in a few grains, grain size ranges from .5-60 (3mm) hash marks. Some large grains. Some rim cementation that is not calcite. Matrix is black in cross-polars and white in plain light. 99.5% recrystallized calcite, <1% Fe-rich saddle dolomite (blue)

KL-GVP-013B/6SH-002 (Bridge Canyon below fence line – debris flow ridge)
Iron Rich Baroque Dolomite w/ Gypsum and Calcite

Hand Sample:

Field Observations:
Zebra Gypsum.

Thin Section:

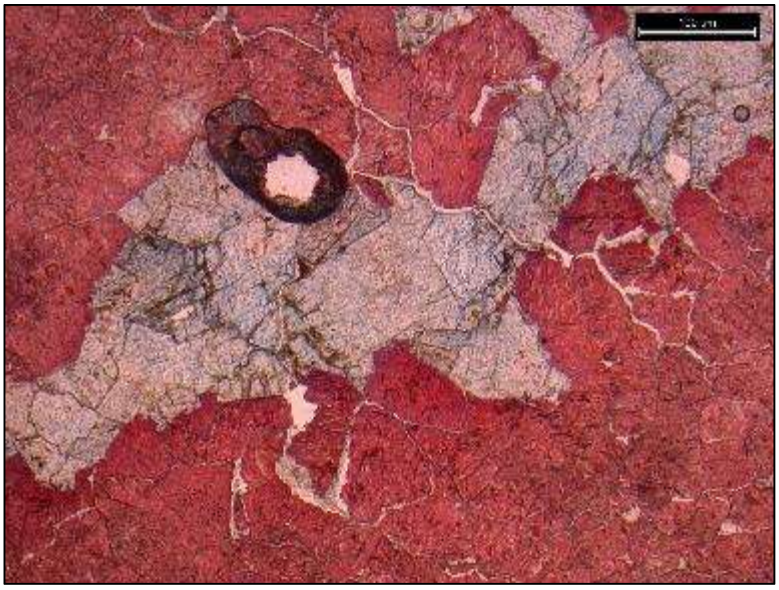

Petrographic Observations:
4X, plain light, stained.
Gypsum with calcite – red stain.
Blue staining is baroque dolomite, which is secondary in genesis.
The blue coloring is indicative of Fe. 93% recrystallized calcite, 7% Fe-rich saddle dolomite (blue).

KL-GVP-015/6SH-010 (8 unit profile – Profile I)
Calcite w/ Silicified Gypsum
Billet:

Field Observations:
Bottom bench with deformed zebra gypsum in middle. Black carbonate marl at the top. Solid ~10" thick, Petroliferous carbonate.

Thin Section:

Petrographic Observations:
4X, plain light, stained.
Brown areas (opaline silica) was prob. gypsum - now silicified quartz & microcrystalline chert. May have OM. Calcite is coarse & is prob. a replacement of gypsum. Calcite may have filled the fractures & all calcite is recrystallized. Primary fabric was likely dolomite, but none was preserved. Grain size ranges from 1 hash mark to 3.5 hash marks. 82% coarse, recrystallized calcite, 15% opaline silica, 2% chert, 1% quartz.

KL-GVP-016-II/6SH-003 (8 unit profile – Profile I)
Calcite w/ Silicified Gypsum

Billet:

Field Observations:
~24" thick – thins to 7-8". Very petroliferous (fetid) where thin, slightly petroliferous where thick. Zebra gypsum at top of bench.

Thin Section: 4X, cross polars, stained.

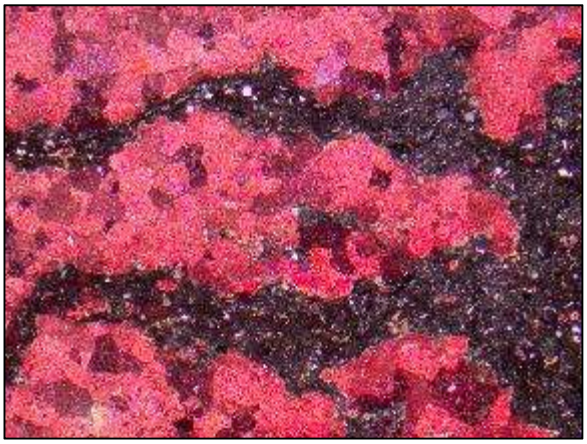

Thin Section: 4X, plain light, stained

Petrographic Observations: 4X, cross polars, stained. Probably the same as KL-GVP-015 (above). Brown areas in plain light (opaline silica) was prob. gypsum - now silicified quartz & microcrystalline chert. May have OM. Calcite is coarse & is prob. a replacement of gypsum. Calcite may have filled the fractures & all calcite is recrystallized. Primary fabric was likely dolomite, but none is preserved. Grain size ranges from 1 hash mark to 3.5 hash marks. 84% coarse, recrystallized calcite, 13% opaline silica, 2% chert, 1% quartz.

KL-GVP-018/6SH-011 (8 unit profile – Profile I)
Recrystallized Calcite

Hand Sample:

Field Observations:
Orange tape (in reference photo – not attached here). Light weathered color, rounded clasts but also platy. 1-2 cm clasts – up to 5cm. Lighter colored carbonate, not petroliferous (with exception of clasts) ~14" thick, left. ~7" thick on right. Phreatic infilling

Thin Section:

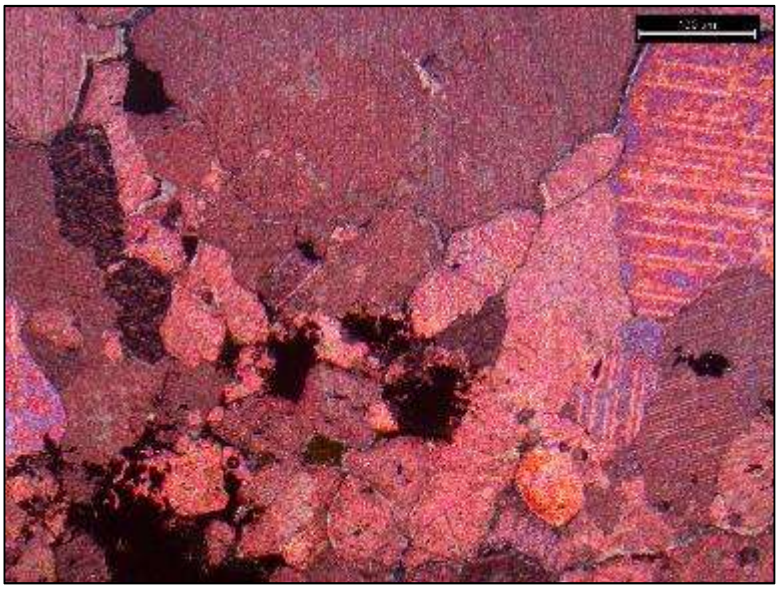

Petrographic Observations:
4X, cross polars, stained. Recrystallized calcite. Angular grains, cross hatch pattern on many grains, calcite, unit extinction, a few instances of twinning, high birefringence in some grains, rim cementation on a few grains. Grain size ranges from 1 hash mark to 2 mm. 99% recrystallized calcite, 1% iron oxide (opaque).

KL-GVP-020-V/6SH-004 (8 unit profile – Profile I)
Recrystallized Calcite w/ Hydrocarbons

Billet:

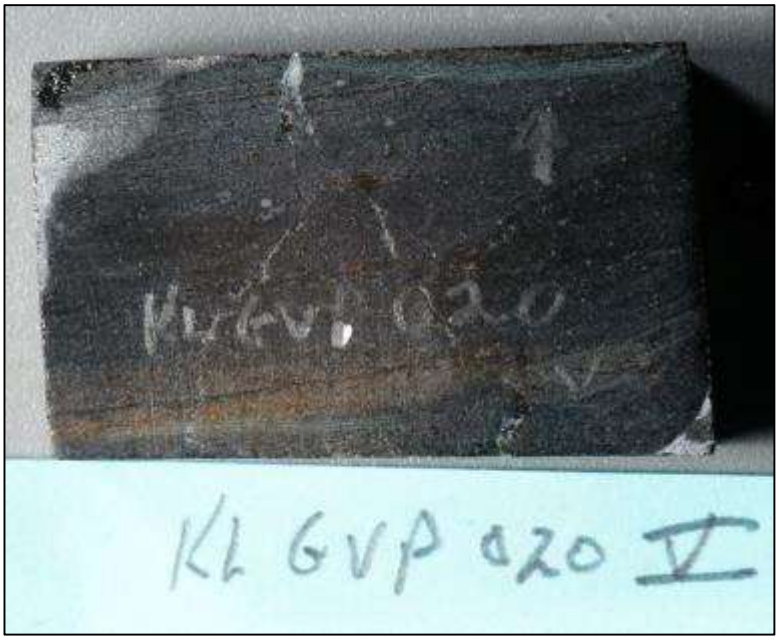

Field Observations:
Dark laminated carbonate, petroliferous, to the left side it becomes a prominent bench ~19" thick, calcite crystals on right side – diagenesis could have been much later, zebra gypsum on left side.

Thin Section:

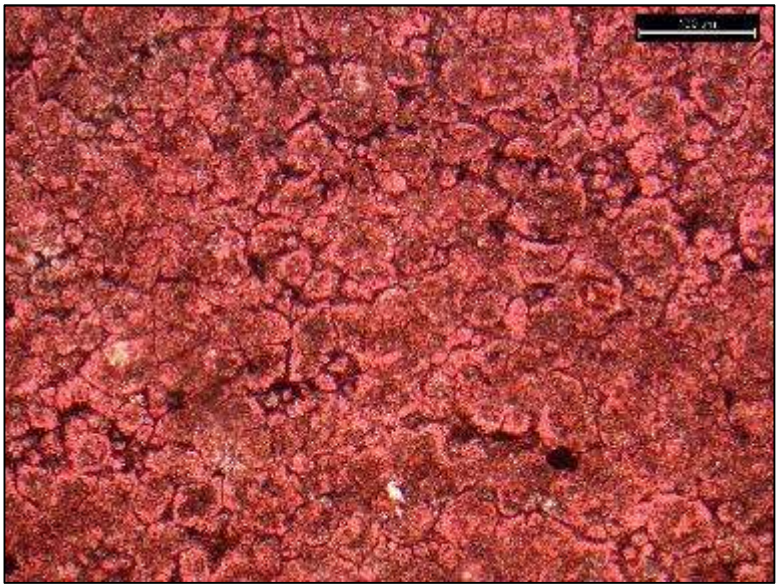

Petrographic Observations:
4X, plain light, stained. Recrystallized calcite, a few quartz grains, average grain size: 3 hash marks. Unit extinction in some grains. Laminations are more visible with the naked eye, but are slightly visible under 4X. The "matrix" which seperates the layers is black under both cross-polars and plain light and may be residual hydrocarbons. A few grains display birefringence. Grain size ranges from 1 hash mark to 5 hash marks. 95% recrystallized calcite, 4% residual hydrocarbons, 1% quartz

KL-GVP-045/6SH-012 (Mary Jane Draw Profile – Profile II)
Gypsum w/ Brecciated Microcrystalline Dolomite

Hand Sample:

Field Observations:
Gypsum with back and white layers. ½ cm.

Thin Section:

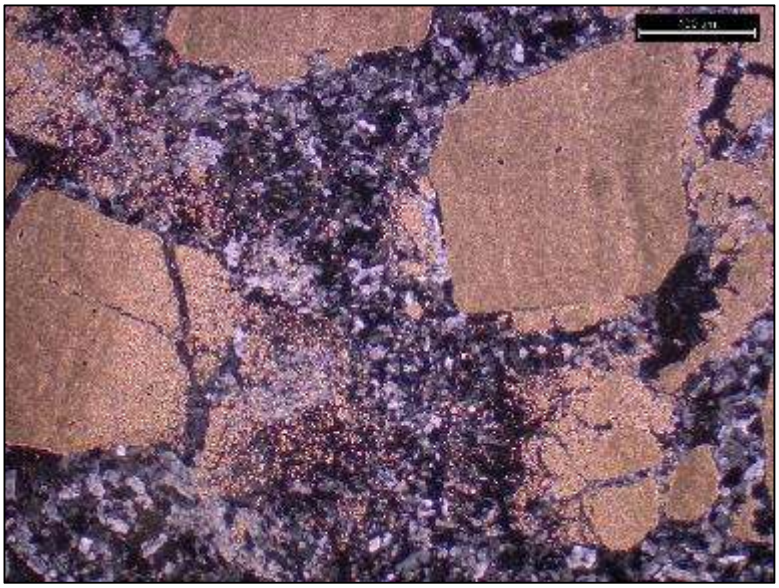

Petrographic Observations:
2.5X, cross polars, stained. Gypsum interspersed with large, tan, microcrystalline, brecciated, dolomite. Microcrystalline dolomite is likely primary. Largest block is ~5mm square. Some chalcedony. Dissolution of dolomite edges by sulfates – gypsum (corroded edges). Dolomite was there before gypsum, which is the opposite of normal conditions. 65% gypsum, 35% microcrystalline dolomite.

KL-GVP-046/6SH-013 (Mary Jane Draw Profile – Profile II)
Gypsum w/ Coarse Dolomite Crystals

Hand Sample:

Field Observations:
Deformed black layers within gypsum – weathered out

Thin Section:

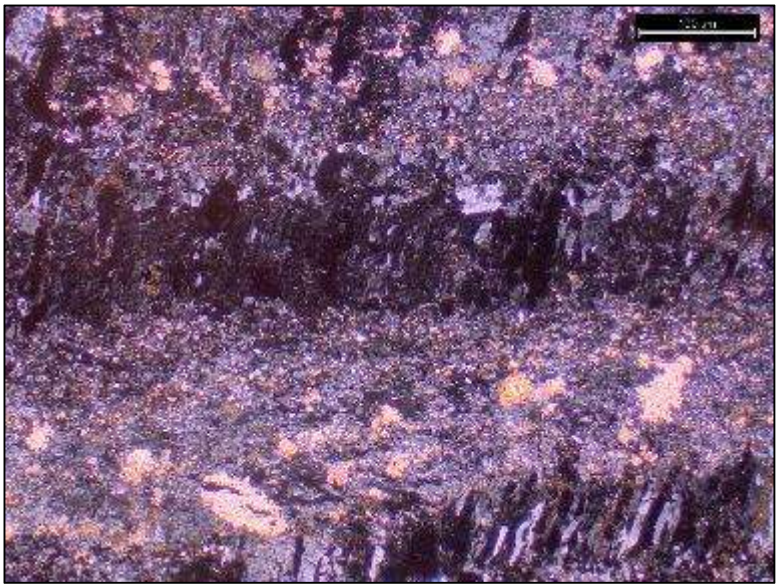

Petrographic Observations:
2.5X, cross polars, stained. Mostly gypsum with some pinkish, tan, coarse, dolomite crystals. Dissolution of dolomite edges by sulfates – gypsum (corroded edges). Dolomite was there before gypsum, which is the opposite of normal conditions. Many overprints. Groundwater moved through FM & precipitated gypsum. 90% gypsum, 10% coarse dolomite.

KL-GVP-047/6SH-014 (Mary Jane Draw Profile – Profile II)
Microcrystalline Dolomite

Billet:

Field Observations:
Banded gypsum with some thick white layers, contains nodules, caprock below.

Thin Section:

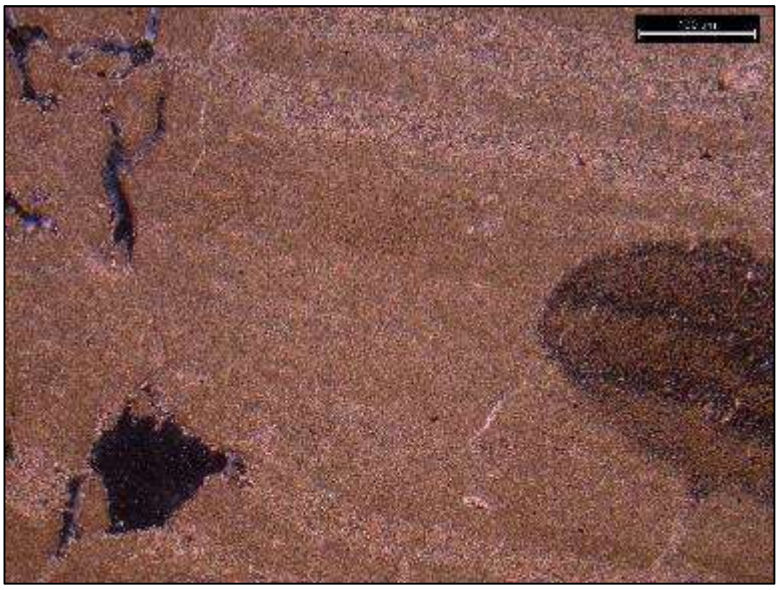

Petrographic Observations:
4X, cross polars, stained. Banded, microcrystalline dolomite (primary) with chert nodule. Chert nodule displays the same fabric as the dolomite. Some secondary dolomite in fractures, a few small quartz crystals. Some fractures filled with quartz cement – undulose extinction. 93.5% microcrystalline dolomite, 3% chert, 3% recrystallized dolomite, .5% quartz.

KL-GVP-051/6SH-015 (Mary Jane Draw Profile – Profile II)
Breccia?

Hand Sample:

Field Observations:
Iron oxide, brecciated.

Thin Section:

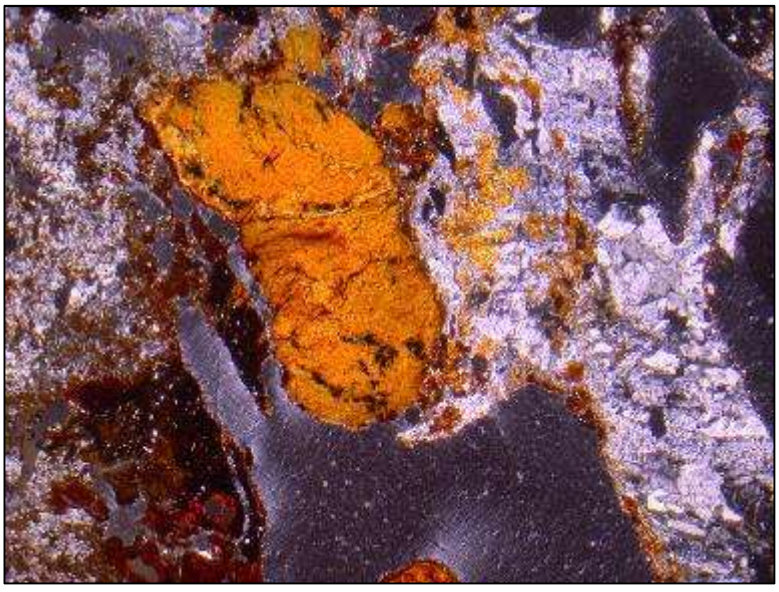

Petrographic Observations:
4X, cross polars, stained.
Looks like Fe_2O_3 but is not stained blue. Fe3 does not fit into charge balance and therefore will not stain blue. Fe2O3 Hemitite is the same Quartz, chalcedony, chert – sweeping extinction, matrix is extremely fine grained & gray – gypsum? – could be mictitic carbonate or dolomite. Unit extinction on a few grains. 25% chert, 25% quartz/chalcedony, 25% gypsum, 25% iron oxide (these percentages need to be re-evaluated!)

KL-GVP-055/6SH-016 (Mary Jane Draw Profile – Profile II)
Calcite w/ Quartz

Billet:

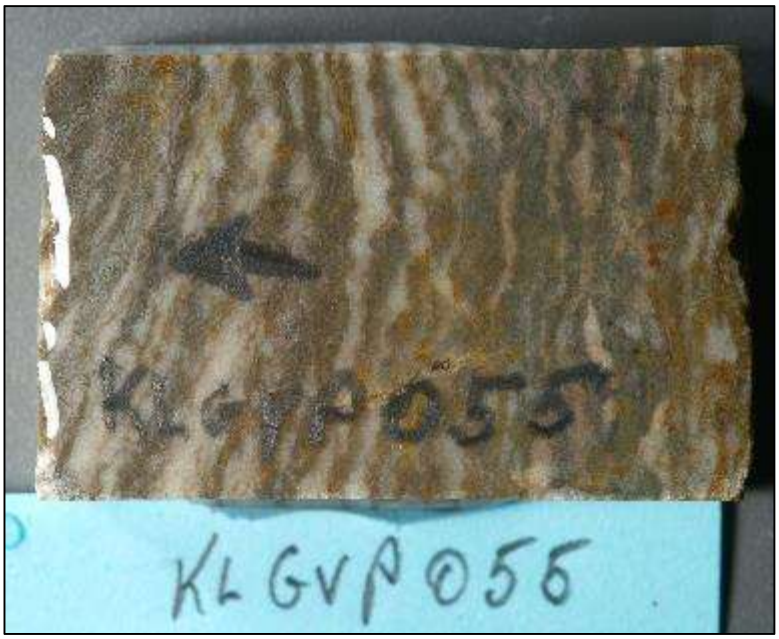

Field Observations:
Zebra, calcite. Base of unit has eroded gypsum.

Thin Section:

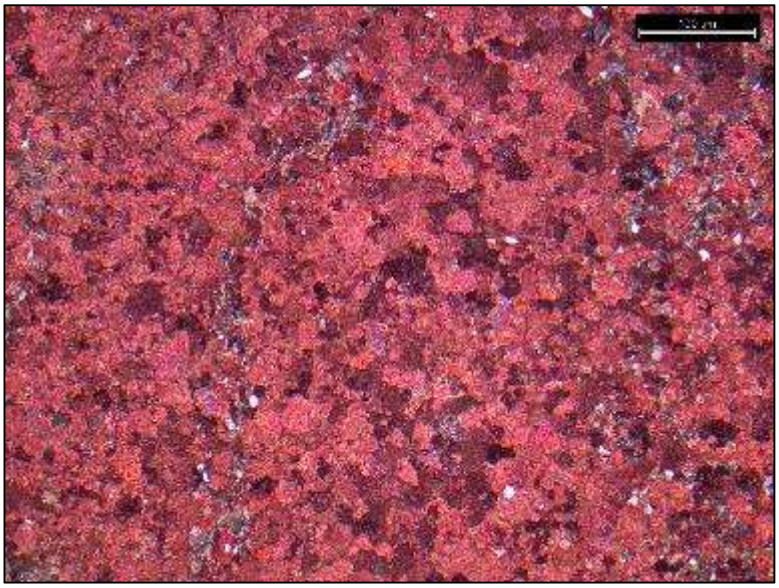

Petrographic Observations:
4X, cross polars, stained. Recrystallized calcite. Some dolomite cementation in fractures and pore spaces? Some quartz grains – undulose extinction. Some fractures filled with quartz cementation. Birefringence in a few grains, grains are sub-angular and range in size from 1 hash mark to 5 hash marks. 95% recrystallized calcite, 4% quartz, 1% dolomite.

KL-GVP-059A/6SH-005 (Profile III)
Note: Later separated into KL-GVP-059-A/6SH-005 & KL-GVP-059-B/6SH-006
Gypsum w/ Quartz & Microcrystalline Dolomite

Hand Sample:

Field Observations:
Top layer with black – has alternating black and white layers on a mm scale. Fairly compact bench.

KL-GVP-059A
This Section: 4X, plain light, stained.

Thin Section: 4X, cross polars, stained.

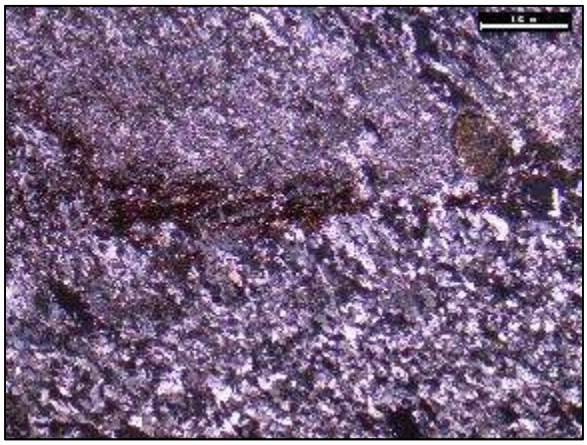

Petrographic Observations:
KL-GVP-059-A: Gypsum, chalcedony, chert. Very few grains display birefringence and some are rhombohedral. Microcrystalline dolomite. No direction indicator, but laminae are visible. Grain size ranges from .5 hash marks to 10 hash marks. 85% gypsum, 10% chalcedony, 3% microcrystalline dolomite, 2% chert.

KL-GVP-059-B

Thin Section: 4X, plain light, stained.

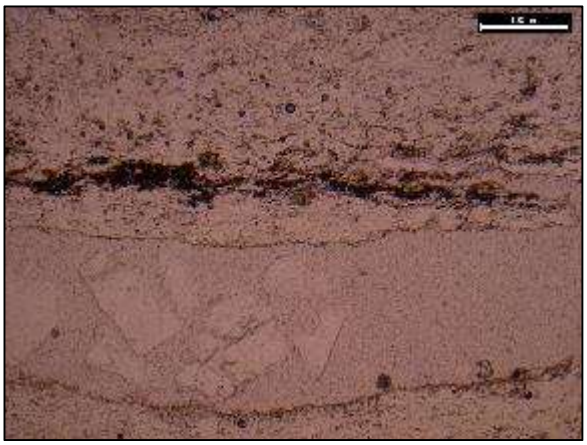

Thin Section: 4X, cross polars, stained.

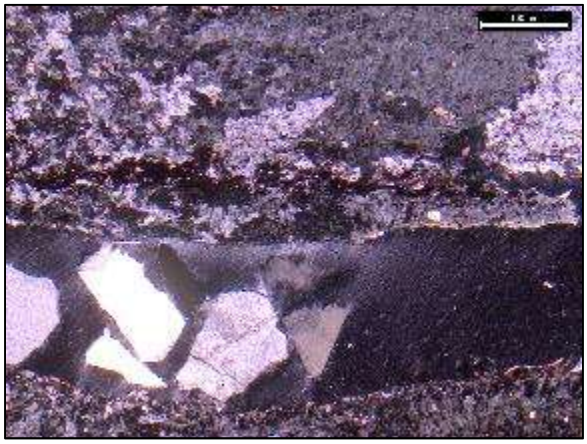

KL-GVP-059B: Gypsum, chalcedony, chert. Very few grains display birefringence and some are rhombohedral – dolomite. Laminae are visible. Some fractures are filled with quartz – undulose extinction. Grain size ranges from .5 hash marks to 15 hash marks. 85% gypsum, 10% chalcedony, 3% microcrystalline dolomite, 2% chert.

KL-GVP-060/6SH-017 (Profile III)
Gypsum w/ Coarse Rhombohedral Dolomite

Hand Sample:

Field Observations:

KL-GVP-060
Thin Section: 4X, plain light, stained.

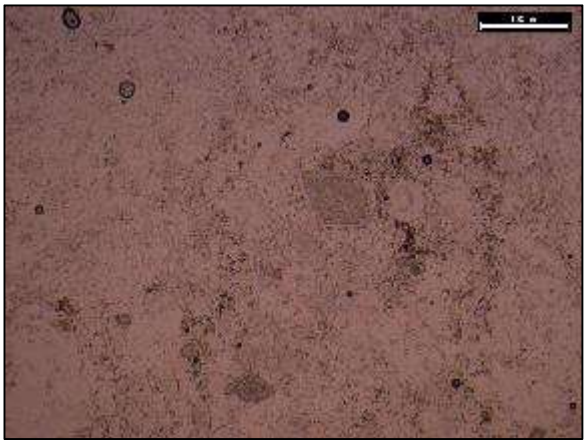

Thin Section: 4X, cross polars, stained.

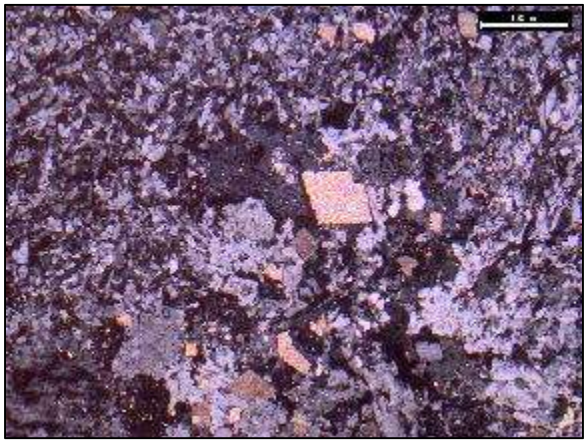

Petrographic Observations:
Gypsum – grain size ranges from 1 – 3 hash marks. A few quartz grains – undulose extinction. Some grains display birefringence. A few coarse rhombohedral dolomite crystals, which are just starting to get corroded by the sulfates in the gypsum – these range in size from 1-7 hash marks. 94% gypsum, 5% recrystallized dolomite, 1% quartz.

KL-GVP-061/6SH-018 (Profile III)
Gypsum w/ Coarse Rhombohedral Dolomite

Hand Sample:

Field Observations:
White and black layers 10-15 cm thick, mostly heterogeneous gypsum. Ranges from white to white and black layers – measles spots within the black layers. Sporatic, delayed reaction to HCl – black layers.

Thin Section:

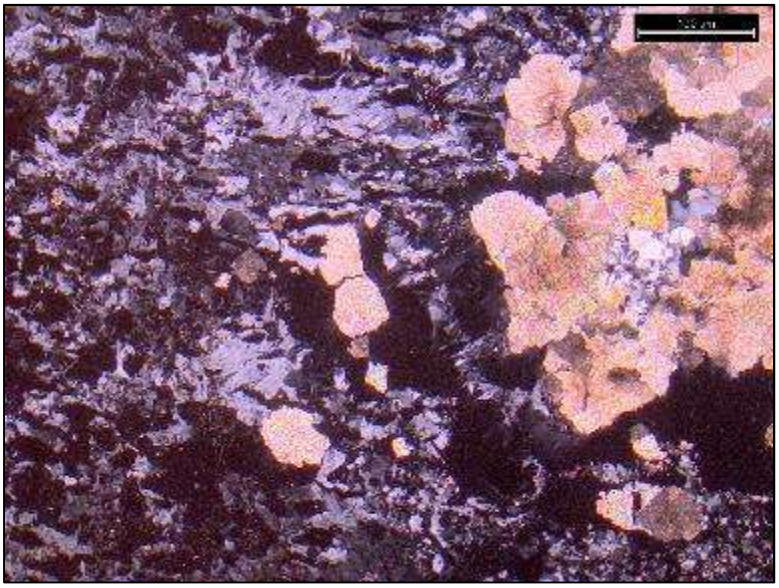

Petrographic Observations:
4X, cross polars, stained. Coarse dolomite rhombs, just starting to get corroded by the sulfate in gypsum. Dolomite halo ghosts seen in plain light – shows sweeping extinction – baroque dolomite – signature of hydrothermal fluids – may have replaced coarser dolomite due to planar edges (only slightly curved) – could be late diagenesis. Gypsum is later than the baroque dolomite. Grains range in size from 2-7 hash marks. 75% gypsum, 25% recrystallized dolomite.

KL-GVP-062/6SH-019 (Profile III)
Gypsum w/ Dolomite

Hand Sample:

Field Observations:
White gypsum, convoluted layers – mm scale, weathered to a reddish brown color, no reaction with HCl. Basal bench is more strongly weathered.

Thin Section:

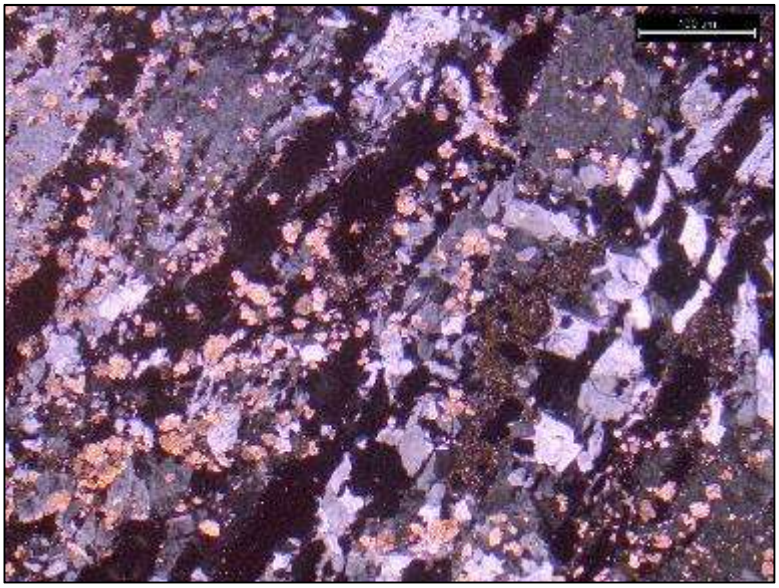

Petrographic Observations:
4X, cross polars, stained. Small dolomite crystals with corroded edges (caused by the sulfates in gypsum). Gypsum is late stage. A few quartz grains. Dolomite is very fine-grained material, which range in size from 1-3 hash marks. 85% gypsum, 14% recrystallized dolomite, 1% quartz.

KL-GVP-063/6SH-020 (Profile III)
Gypsum w/ Dolomite

Billet:

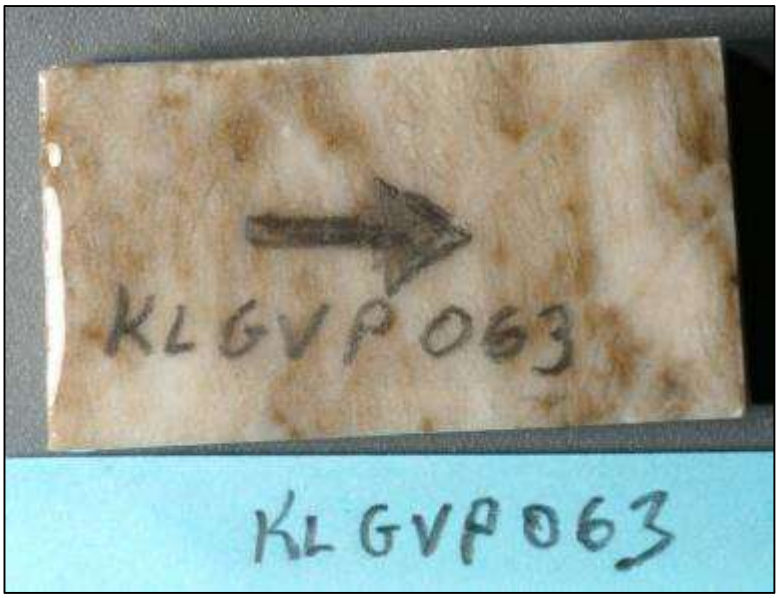

Field Observations:
White gypsum with black layers – some reddish convolute layers. Small, fine layers at top of bench. No reaction with HCl.

Thin Section:

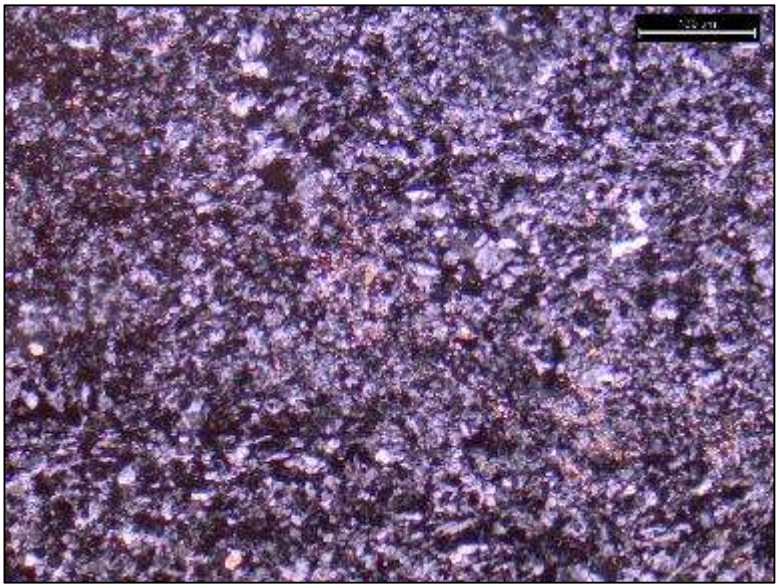

Petrographic Observations:
4X, plain light, stained. Majority of sample is gypsum with very few remnants of dolomite – these grains are very small with a few up to the 1 hash mark size. 95% gypsum, 5% microcrystalline dolomite.

KL-GVP-064/6SH-021 (Profile III)
Primary & Replacement Calcite/Anhydrite/Crackle Breccia w/ Residual Hydrocarbons

Billet:

Field Observations:
Fresh surface is dark gray, almost black, fine-grained carbonate. Petroliferous, strong HCl reaction. Weathers to a tannish color. Breccia at bottom, laminated on top. Pattern on the outside may be breccia.

Thin Section:

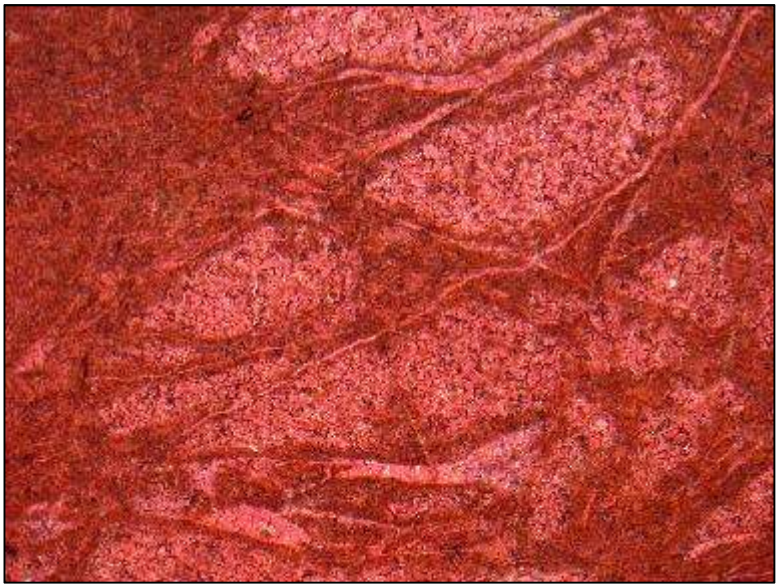

Petrographic Observations:
4X, plain light, stained.
Primary calcite, crackle breccia (branch-like structures) alternated between gypsum & anhydrite, predicated by fluctuating ground water, which was then replaced by carbonate – coarse crystalline calcite. Dark areas between grains are likely residual hydrocarbons. A few quartz grains. Avg. grain size ranges from 1-3 hash marks. 96% primary calcite, 4% hydrocarbons.

KL-GVP-065/6SH-022 (Profile III)
Partially Silicified Late stage Calcite

Billet:

Field Observations:
Convolute layering, alternating gray/dark gray/black mm bands – not petroliferous, strong reaction with HCl. Dark gray inside with laminae slightly visible.

Thin Section:

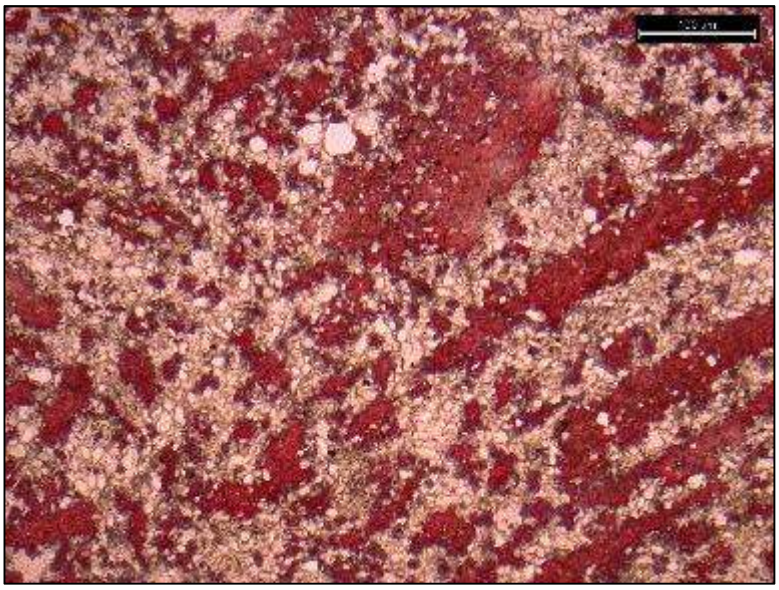

Petrographic Observations:
Partially silicified - full of siliclastics. Calcite (replacement fabric) and gypsum and a few dolomite grains. Calcification and recrystallation are late stage. Some quartz grains – coarse sand grains – (does not have pinkish or bluish edges like dolomite and does not have cleavage like dolomite). Original fabric had quartz detritus. Blackish/grayish bands – gypsum with sweeping extinction. Coarse calcite then came in – replacing the gypsum, but some gypsum remains. Dirty caprock – siliclastic detridal material in the evaporate – could have iron oxide and maybe iron sulfides. Overlapping textures. Grain size ranges from 1-4 hash marks with a few slightly larger quartz grains. 50% quartz, 37% calcite, 10% gypsum, 3% iron oxide.

KL-GVP-066/6SH-023 (Profile III)
Microcrystalline Dolomite w/ Poikilotopic Calcite & Coarse Iron-Rich Baroque Dolomite

Billet:

Field Observations:
Greenish/tan/orange weathered surface, strongly brecciated. Fresh surface: light gray with orange patches. Reaction with HCl.

Thin Section:

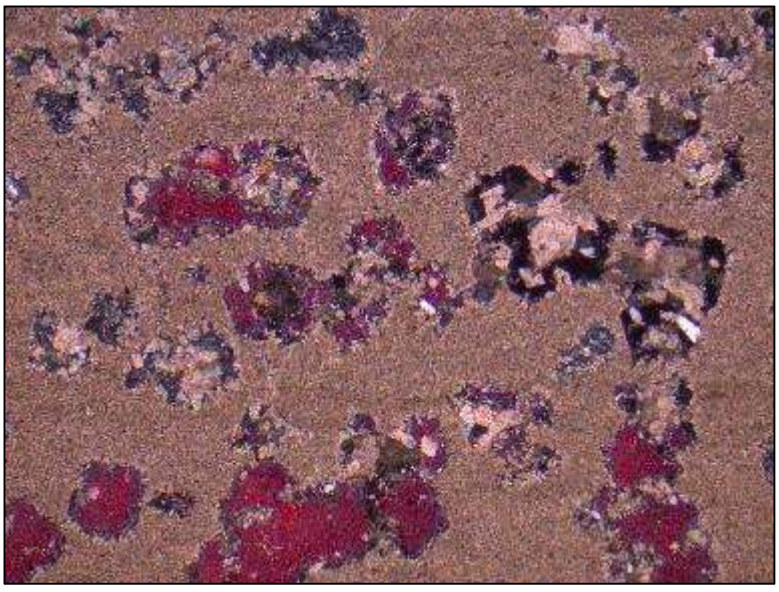

Petrographic Observations:
4X, cross polars, stained. Microcrystalline primary tan dolomite. Coarse baroque dolomite precipitated at a later stage. Late stage poikilotopic calcite is red. Purple mineral is Fe-rich calcite. Blue mineral is an iron rich dolomite with macroscopic crystals. 79.5% microcrystalline dolomite, 4% calcite, 6% Fe rich calcite, 2% Fe dolomite, .5% quartz.

KL-GVP-067/6SH-024 (Profile III)
Recrystallized Dolomite w/ Siliclastics

Billet:

Field Observations:
Orange/tan weathered surface. Light gray & orange inside. Little reaction with HCl. Brecciated with round clasts.

Thin Section:

Petrographic Observations:
4X, plain light, stained. Recrystallized dolomite – coarsely crystalline. Lots of siliclastics. Detrital quartz – edges of grains are irregular. Carbonate has corroded quartz grains – possibly due to halo brines. This dolomite does not have the characteristic rhombohedral shape. 70% recrystallized dolomite, 25% quartz, 5% calcite.

KL-GVP-070/6SH-025 (Profile III)
Microcrystalline Dolomite w/ Poikilotopic Calcite & Coarse Iron-Rich Baroque Dolomite

Billet:

Field Observations:
Brownish/tan weathered surface. Dark gray fresh surface, recrystallized. Delayed reaction with HCl. Petroliferous.

Thin Section:

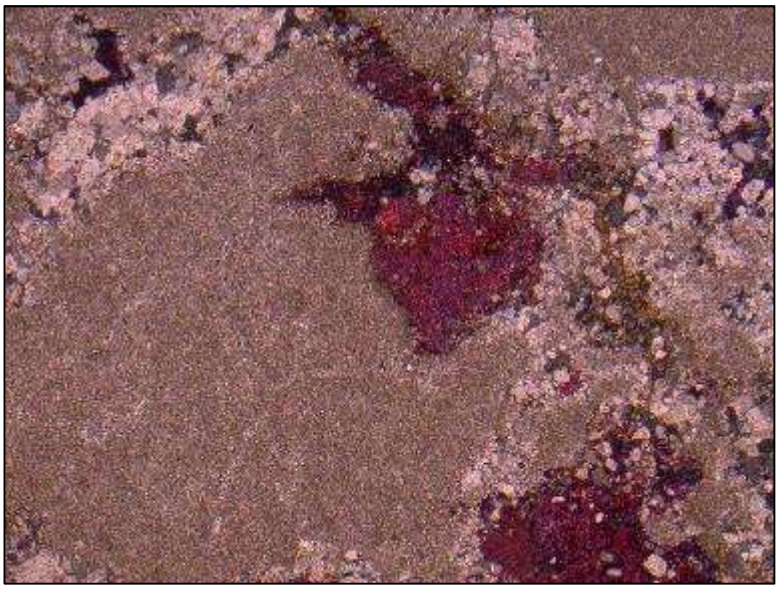

Petrographic Observations:
4X, cross polars, stained. Coarse crystalline replacement dolomite. Poikilotopic calcite – later than dolomite. Baroque dolomite is dirty and ghosty – sweeping extinction w/ curved crystal faces. Blue dolomite cement w/ nice crystal faces filling the voids. Late stage silification – chert infill. Complex diagenetic history: 1) dirty baroque, microspar, recrystallized dolomite, 2) Fe-rich dolomite w/ chert, 3) chert infill, 4) Fe-rich poikilotopic calcite. 62% microcrystalline dolomite, 20% recrystallized dolomite, 10% calcite, 5% Fe rich dolomite, 3% chert.

KL-GVP-071/6SH-026 (Profile III)
Recrystallized and Iron Rich Dolomite

Billet:

Field Observations:
Weathered surface is reddish/tan/orange, fresh surface is dark gray with some calcite – orange, red, and green. Slight reaction with HCl.

Thin Section:

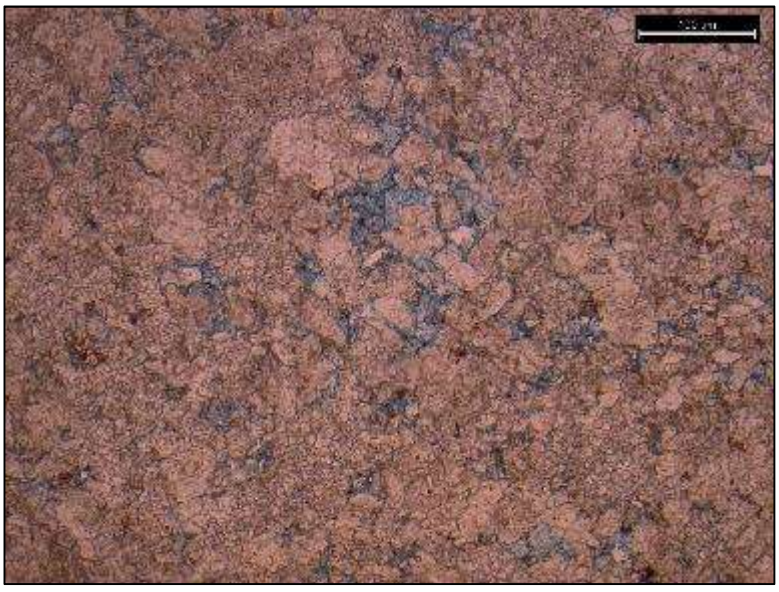

Petrographic Observations:
4X, plain light, stained.
Iron-rich dolomite (blue) – occurred after standard dolomitization – majority is recrystallized (secondary) dolomite, & is coarse grained. A few completely black opaque grains – could be residual pyrite – iron sulfide. * Could also have siderite, anchorite, or Fe2 carbonate. 75% recrystallized dolomite, 23% recrystallized Fe-rich dolomite, 2% residual pyrite – iron sulfide.

KL-GVP-072/6SH-027 (Profile III)
Recrystallized Calcite w/ Quartz

Hand Sample:

Field Observations:
1mm – 1cm layers – thickens upward. Weathered surface is tannish/reddish, very strong reaction with HCl.

Thin Section:

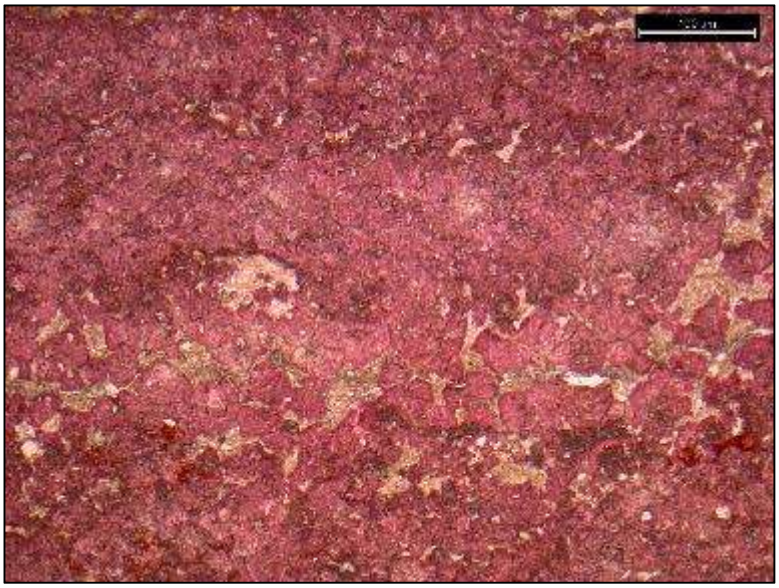

Petrographic Observations:
4X, plain light, stained. Recrystallized calcite with a few quartz crystals. Laminae. Birefringence in a few grains. 93% recrystallized calcite, 5% quartz, 2% residual iron pyrite – iron sulfide (opaque).

KL-GVP-073/6SH-037 (Profile III)
Recrystallized Calcite w/ Quartz

Billet:

Field Observations:
Weathered surface is bluish gray with red on top. This could be a hinge. Many fine laminations. Strong HCl reaction. Fractures filled with calcite. Massive dominant band. Fresh surface is light gray to light tan. A few crystals are visible. Not petroliferous.

Thin Section:

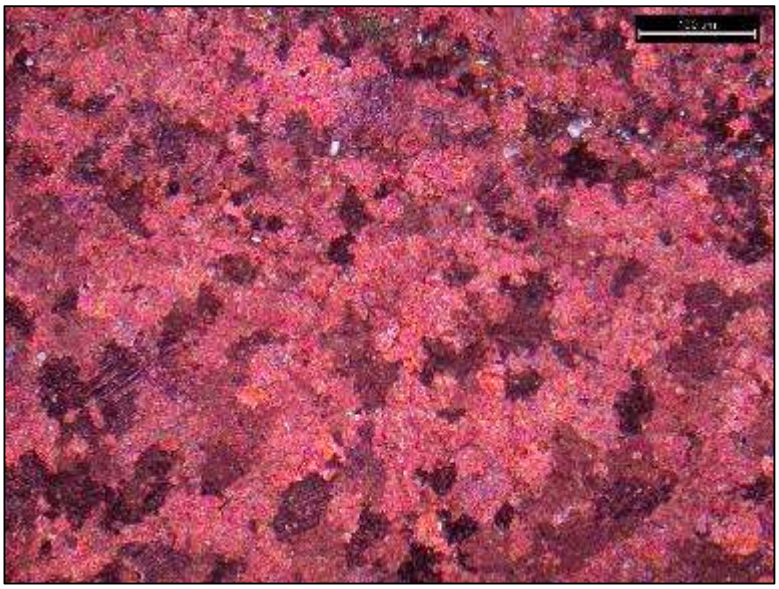

Petrographic Observations:
4X, cross polars, stained.
Mostly calcite with a few quartz grains. A few grains display cross-hatching. One fracture is filled w/ a greenish/brown mineral (in plain light) – not gypsum – probably silicified, but it is not clear – could be residual iron oxide. Some quartz grains in this fracture – matrix in fracture is black in cross-polars. A few grains display birefringence. Purple – Fe- rich calcite. Grain size ranges from 1 hash mark to 1mm. 95% recrystallized calcite, 3% quartz, 2% residual iron oxide – iron sulfate.

KL-GVP-074/6SH-028 (Profile III)
Recrystallized Calcite w/ Quartz

Billet:

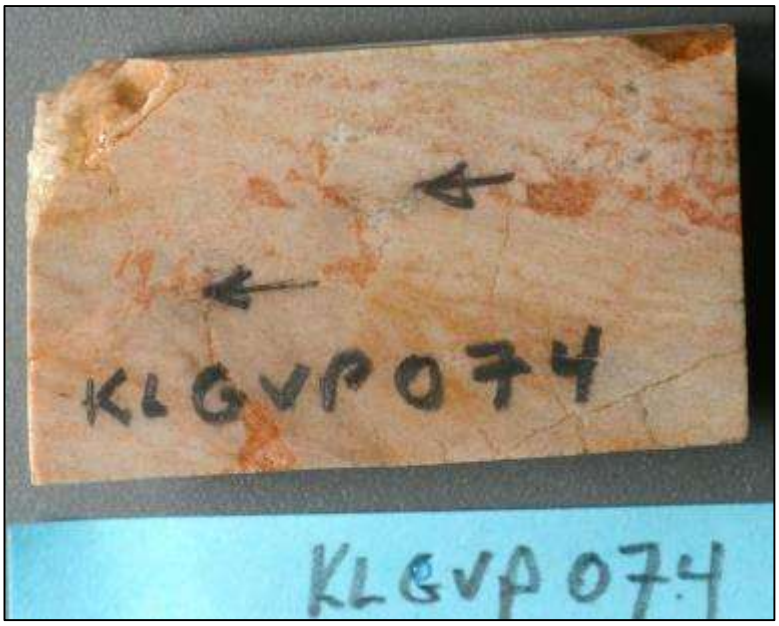

Field Observations:
Conchita Member, not petroliferous, fresh surface is light gray to light tan. A few crystals are visible.

Thin Section:

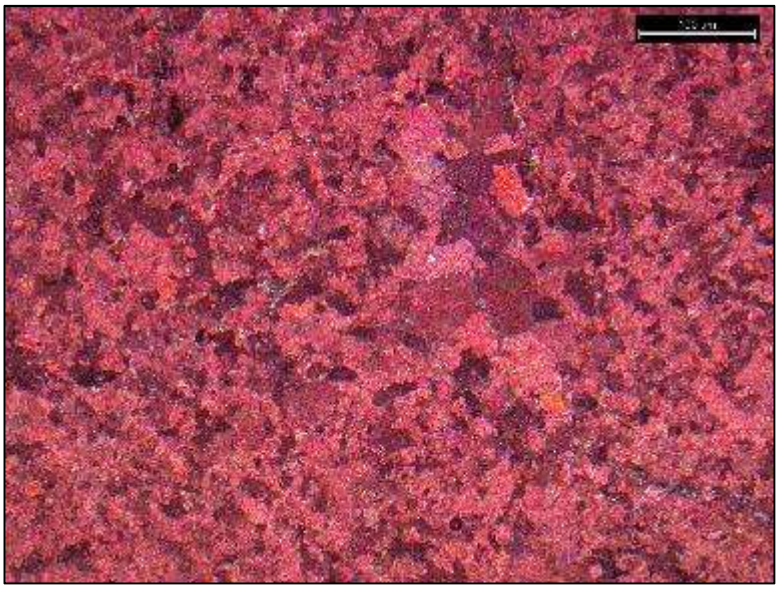

Petrographic Observations:
4X, cross polars, stained.
A few quartz grains – undulose extinction, mostly calcite with a few chalcedony grains. Sub angular grains, some cross-hatching, some rim cementation – not dolomite, small, greenish crystals and possible stylolite. 98% recrystallized calcite, 2% quartz/chalcedony.

KL-GVP-076/6SH-029 (Profile III)
Recrystallized Calcite w/ Quartz

Billet:

Field Observations:
Weathered surface is medium to dark gray. Fresh surface is dark gray to light gray with purple bands & recrystallized. Top is spongy and deeply weathered. Body is not as weathered.

Thin Section

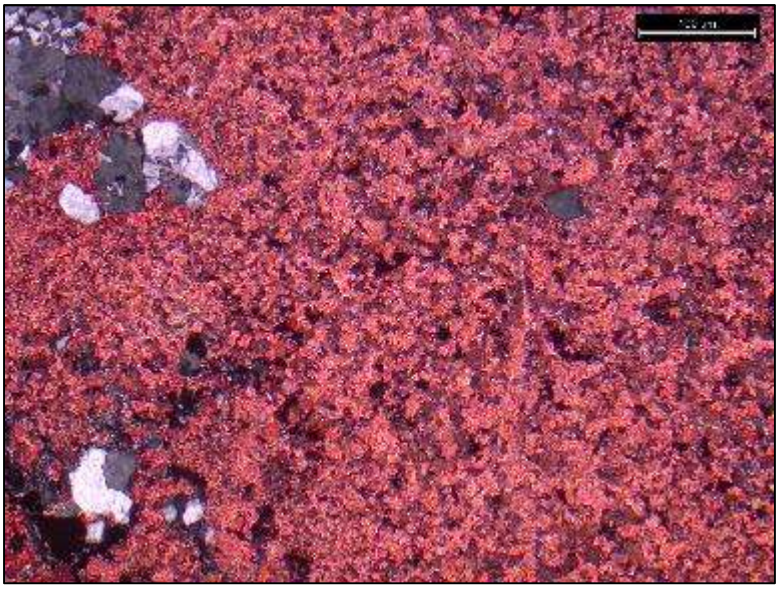

Petrographic Observations:
4X, cross polars, stained. Mostly calcite w/ quartz grains – some are big – undulose extinction, some cross-hatching, black matrix under cross-polars – clear under plain light, birefringence in some grains, fine to medium grained, sub angular grains. One area towards the edge with the 6SH-029 etching may be secondary dolomite, which displays nonmimetic replacement fabric. 95% recrystallized calcite, 5% quartz.

KL-GVP-079/6SH-030 (Profile III)
Microcrystalline Dolomite w/ Calcite

Billet

Field Observations:
Weathered surface is greenish/tan/with purple. Fresh surface is dark gray and petroliferous. Reacts with HCl.

Thin Section:

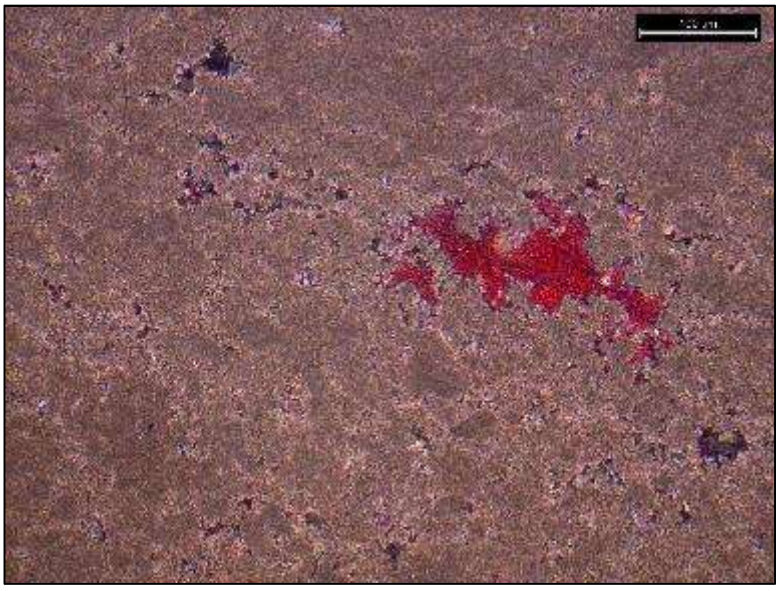

Petrographic Observations:
4X, cross polars, stained. Some quartz grains – undulose extinction. Tannish/gray, fine-grained – microcrystalline dolomite. Some blue is apparent indicating the presence of iron. 87.5% microcrystalline dolomite, 10% calcite, 2% Fe rich calcite, .5% quartz.

KL-GVP-081/6SH-031 (Profile III)
Banded Microcrystalline Dolomite w/ Calcite & Quartz

Billet:

Field Observations:
Weathered surface is karst-like and tan/greenish with laminae visible outside and slightly inside – some dark purple. Fresh surface is dark gray, petroliferous and reacts to HCl.

Thin Section:

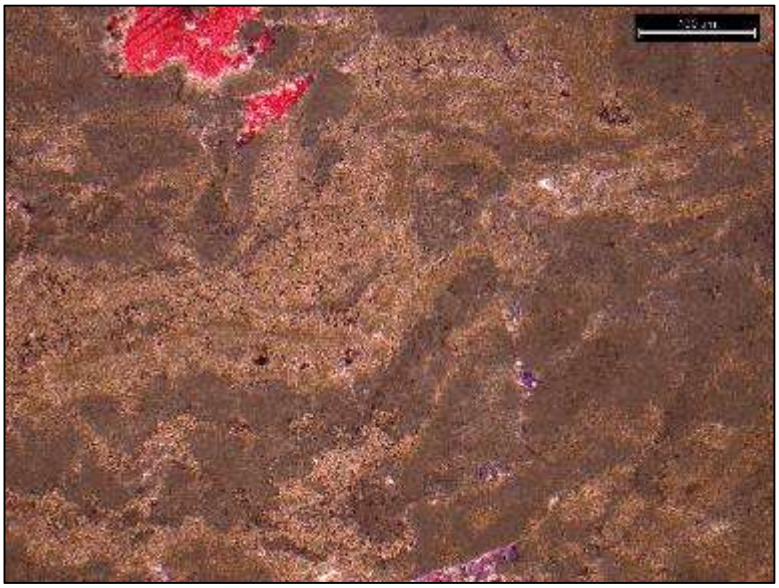

Petrographic Observations:
4X, plain light, stained Microcrystalline & rhombic, micritic, banded dolomite. Late stage, coarse crystalline, Poikilotopic calcite – unit extinction. Typically indicative of a high temperature burial environment. 89% microcrystalline dolomite, 8% calcite, 2% iron rich calcite, 1% quartz.

KL-GVP-083A/6SH-032 (Profile III)
Microcrystalline Dolomite w/ Calcite & Quartz

Field Observations:
KL-GVP-083B: Tannish green karst-like. Weathered surface with laminae are visible. Slightly petroliferous. Fresh surface is reddish/purple and reacts to HCl. Top layer is dark gray inside & petroliferous.

Note: Samples later separated into KL-GVP-083A & KL-GVP-083B

Billet:

Thin Section:

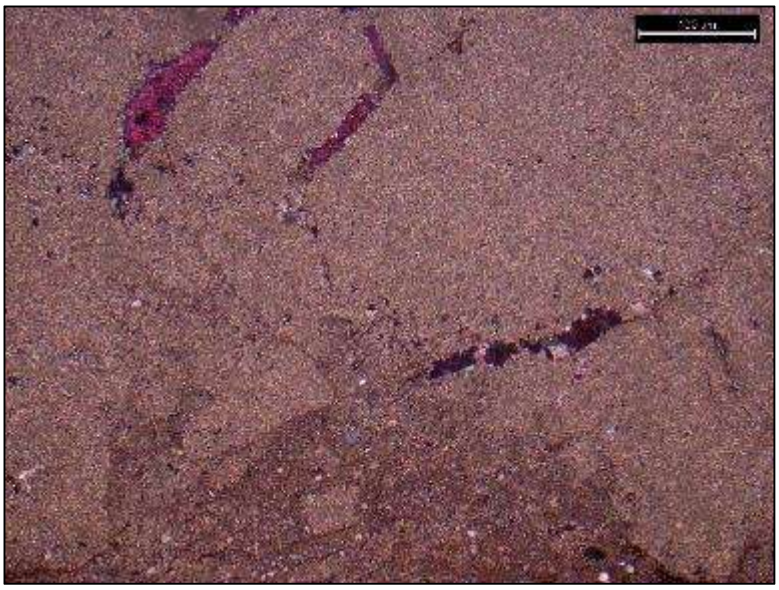

Petrographic Observations:
4X, cross polars, stained.
KL-GVP-083A: Fractures filled with calcite cement, high birefringence in parts. Quartz grains – undulose extinction. Some fractures are filled with quartz cement. Tannish/gray fine-grained material – 95% microcrystalline dolomite, 4% calcite, 1% quartz.

KL-GVP-083B/6SH-007 (Profile III)
Microcrystalline Dolomite w/ Calcite & Quartz

Billet:

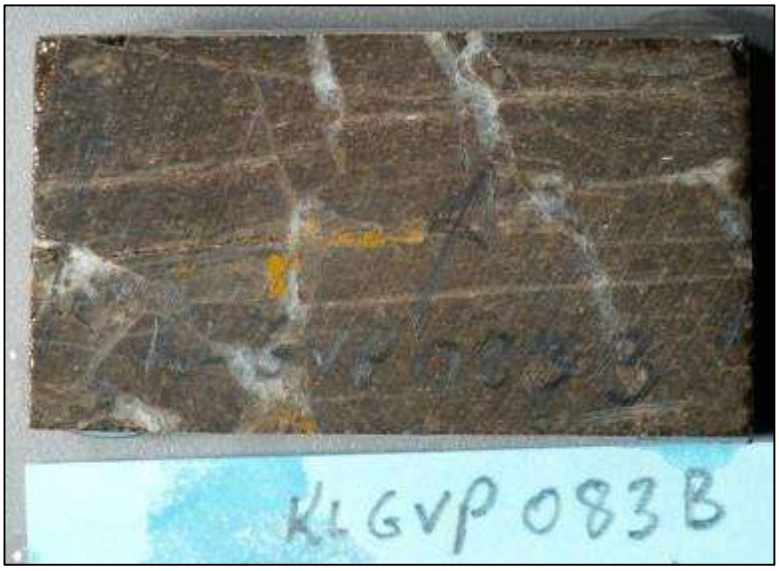

Field Observations:
Tannish/greenish karst. Weathered surface with laminae visible, slightly petroliferous. Fresh surface is reddish/purple and reacts to HCl. Top layer is dark gray inside.

Thin Sections:

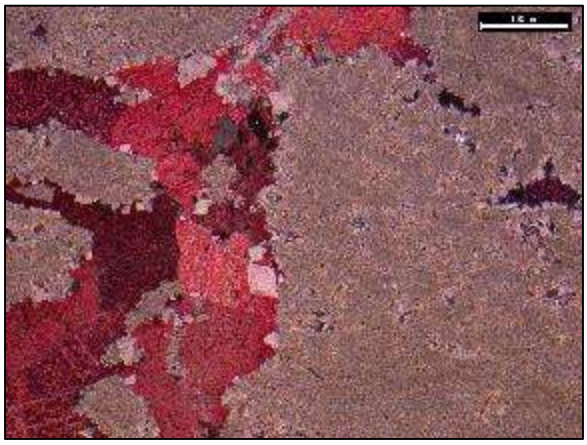

Petrographic Observations:
4X, cross polars, stained. Tannish, microcrystalline primary dolomite. Fractures filled with chalcedony (almost looks like a wood-grain structure), quartz, calcite and a few rhombohedral dolomite crystals. A few grains display birefringence. Cross-hatching is apparent in a few grains. 87% microcrystalline dolomite, 10% calcite, 2% chalcedony, 1% quartz.

KL-GVP-084/6SH-033 (Profile III)
Microcrystalline Dolomite w/ Calcite & Quartz

Billet:

Field Observations:
Greenish/tan weathered surface. Fresh surface is grayish, laminated and brecciated. No reaction with HCl. Possibly a small boudinage.

Thin Section

Petrographic Observations:
4X, cross polars, stained. Some secondary dolomite recrystallization in and around calcite cements – could be dissolution – probably not de-dolomitization. Tannish/gray, fine-grained microcrystalline dolomite. A few small quartz grains. Most fractures filled with calcite. 84% microcrystalline dolomite, 9% calcite, 5% recrystallized dolomite, 1% quartz, 1% residual pyrite – iron sulfide.

KL-GVP-086/6SH-034 (Profile III)
Microcrystalline Dolomite w/ Calcite & Quartz

Billet:

Field Observations:
Weathered surface is reddish/purple/gray laminated and brecciated. Fresh surface is purplish/gray. Strong HCl reaction. Welded together with sandstone.

Thin Section:

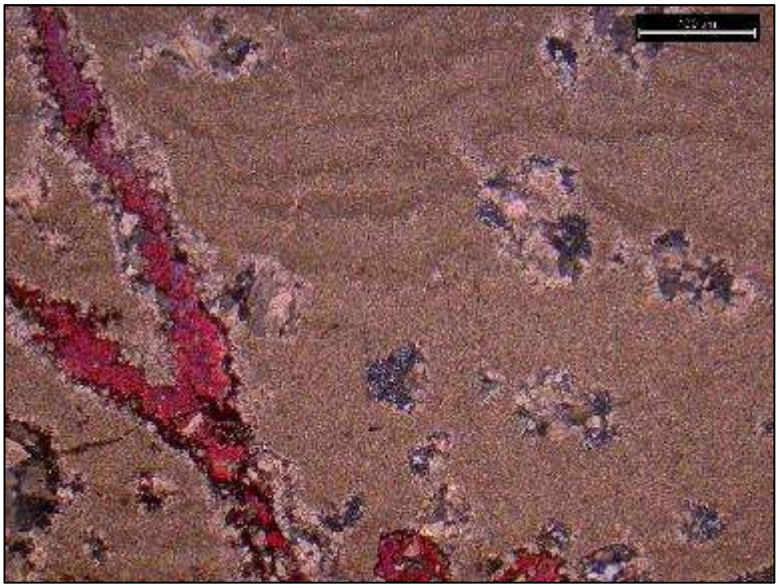

Petrographic Observations:
4X, cross polars, stained. Angular – sub angular calcite, w/ quartz grains – sand grains – undulose extinction, chert, some birefringence. Microcrystalline dolomite, Fe-rich dolomite and Fe-rich calcite. 77% microcrystalline dolomite, 10 % recrystallized, Fe-rich dolomite, 8% Fe-rich calcite, 4% chert, 1% quartz.

KL-GVP-087/6SH-036 (Profile III)
Primary & Replacement Calcite/Anhydrite/Crackle Breccia w/ Residual Hydrocarbons

Billet:

Field Observations:
Mary Jane messy sample.

Thin Section:

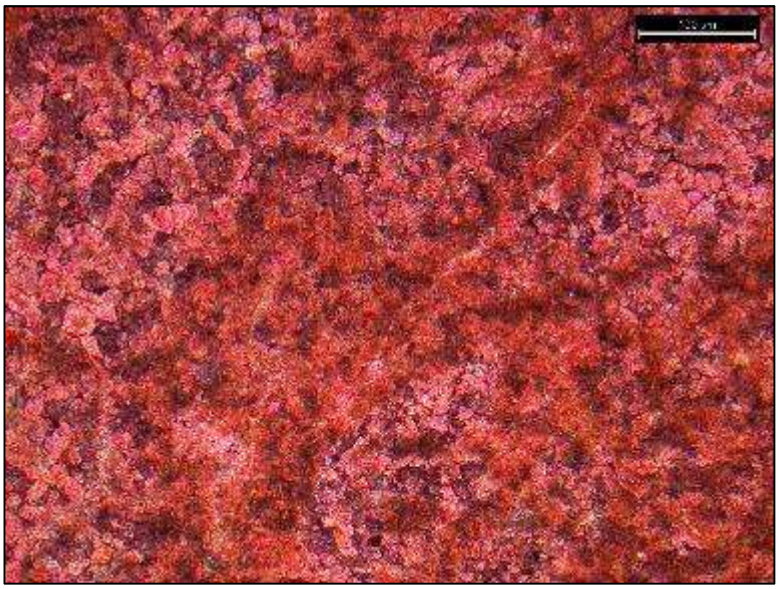

Petrographic Observations:
4X, cross polars, stained. (Primary?) calcite, crackle breccia (branch-like structures) alternated between gypsum & anhydrite, predicated by fluctuating ground water, which was then replaced by carbonate – coarse crystalline calcite. Dark areas between grains are likely residual hydrocarbons. A few quartz grains. Avg. grain size ranges from 1 hash marks – 1mm. 97% calcite, 3% hydrocarbons.

VITA

Kevin M. Lerer was born and raised in Dallas, Texas. He graduated from the Episcopal School of Dallas High School in 1986, where he competed as a four-sport varsity athlete. During this time, he also achieved the rank of Eagle Scout. In May of 1990, Mr. Lerer graduated from Southern Methodist University with a B.A. degree in History and a minor in Geology. Upon graduation, he worked in London, England for a year and then in Alaska for a year, returning to his home town to work in commercial construction as a project manager, in the steel industry as an operations director, and he also started his own successful advertising, marketing and branding company.

After recognizing a change in direction would be beneficial, Mr. Lerer enrolled in the graduate program at the University of Texas at El Paso in 2015, in order to pursue a Master of Science degree in geology. While a graduate student, he maintained a nearly 4.0 GPA, was an active member in the Institute of Tectonic Studies, worked as both a research and teaching assistant and was a member of a National Science Foundation exploration team, which evaluated mantle motion and absolute plate motion models of the Rurutu hotspot in the South Pacific.

Email: kevinlerer1886@gmail.com

This thesis was typed by the author, Kevin Lerer.